Higher-order networks

An introduction to simplicial complexes
Lesson V:

LTCC Course

13 March 2023

Ginestra Bianconi

School of Mathematical Sciences, Queen Mary University of London
The Alan Turing Institute

Higher-order structure and dynamics

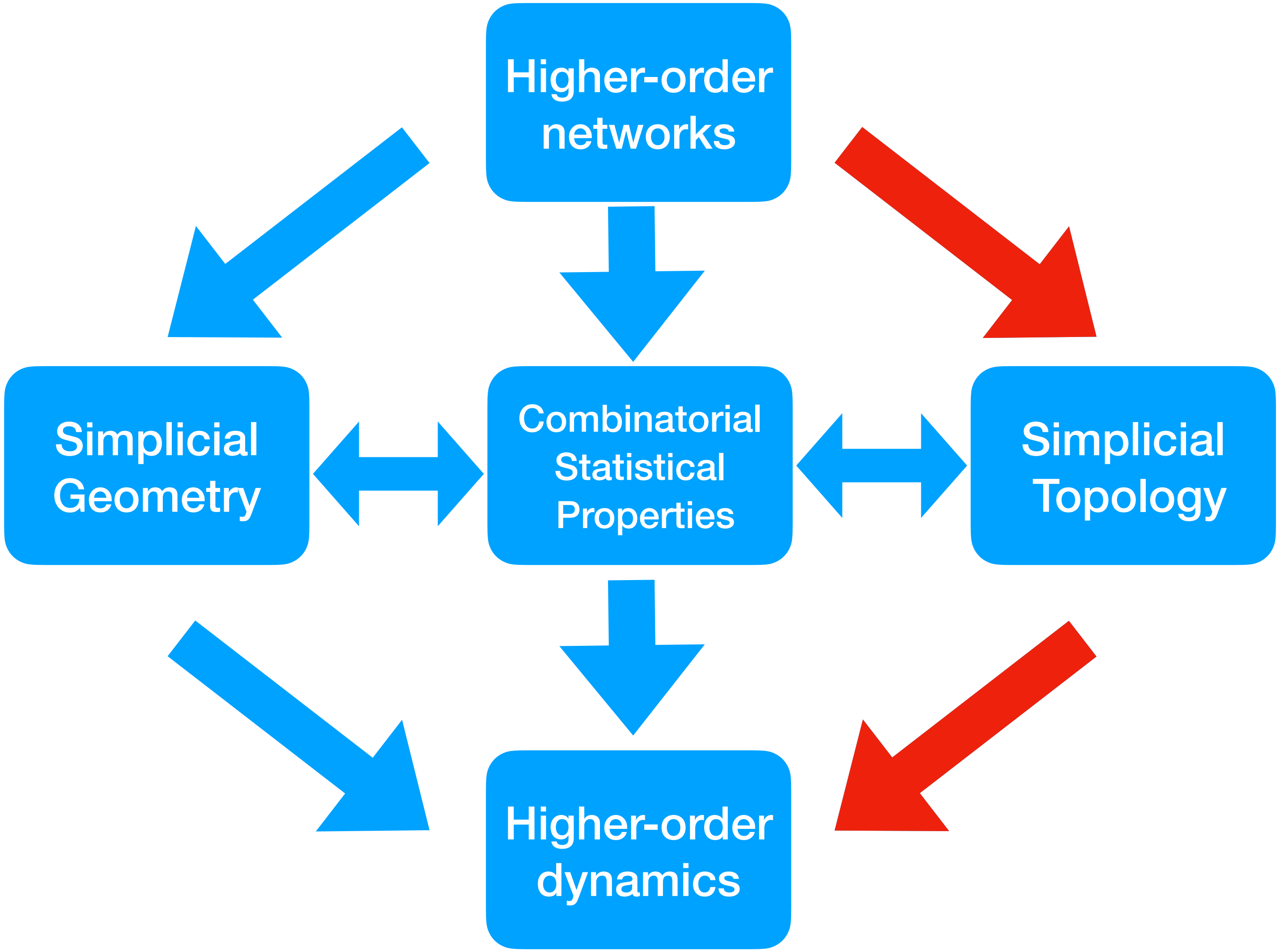

Lesson Va:
Dirac operator and dynamics of topological signals

- **Dirac operator**
    - **On graphs**
    - **On simplicial complexes**
- **Higher-order dynamics of topological signals driven by the Dirac operator**
    - **Dirac synchronisation**
    - **Dirac signal processing**
- **Topological Dirac equation on lattices**

Dirac legacy

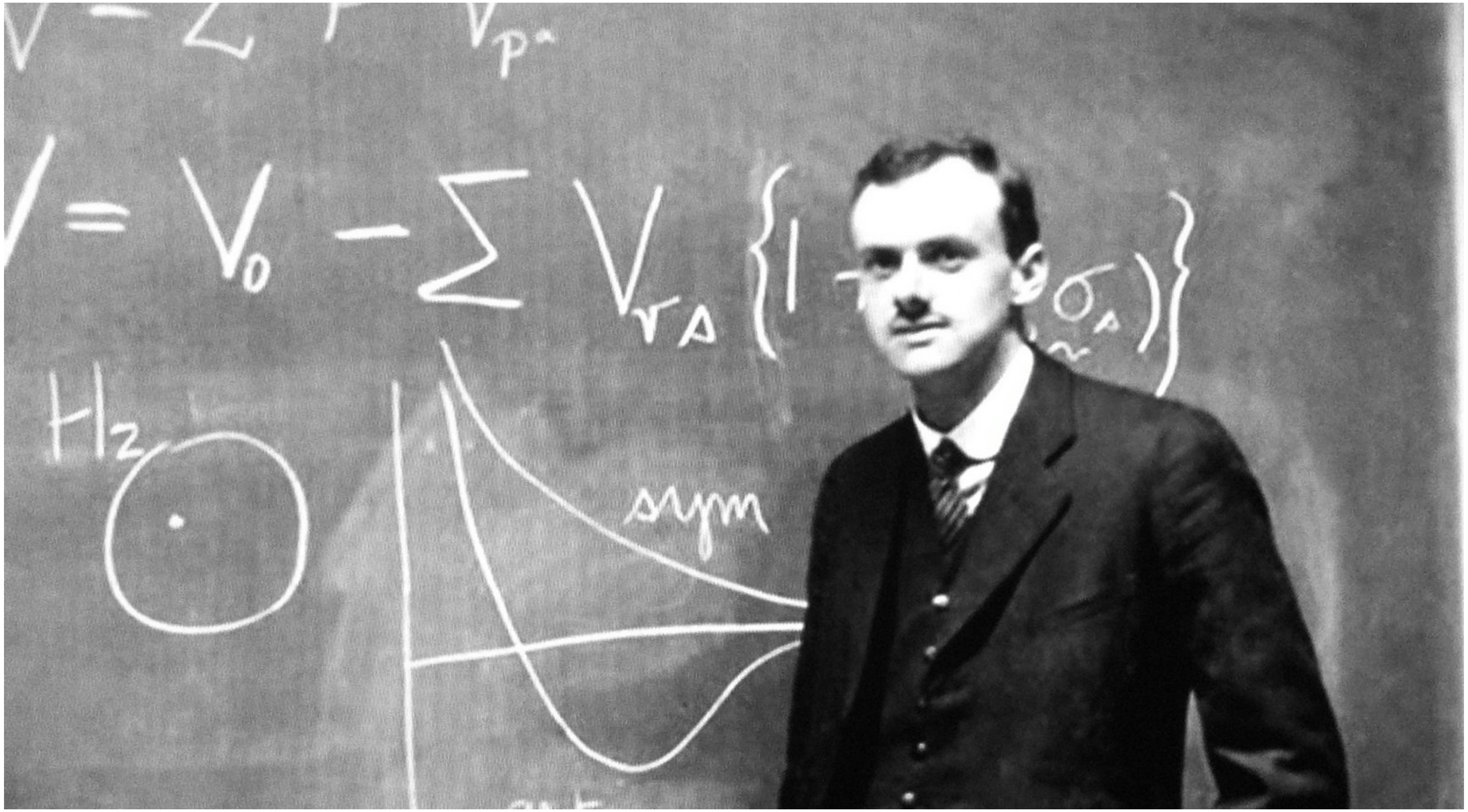

Dirac operator on graphs: References

Davies, E.B., 1993. Analysis on graphs and noncommutative geometry. Journal of functional analysis, 111(2), pp.398-430.

Post, O., 2009, August. First order approach and index theorems for discrete and metric graphs. In *Annales Henri Poincaré* (Vol. 10, No. 5, pp. 823-866). SP Birkhäuser Verlag Basel.

Lloyd, S., Garnerone, S. and Zanardi, P., 2016. Quantum algorithms for topological and geometric analysis of data. *Nature communications*, *7*(1), pp.1-7.

G. Bianconi, Topological Dirac equation on networks and simplicial complexes JPhys Complexity (2021)

G. Bianconi, Dirac gauge theory for topological spinors in 3+ 1 dimensional networks. *arXiv preprint arXiv:2212.05621* (2022).

Topological spinor

- Consider a graph $G = (V, E)$ with $N = |V|$ nodes and $L = |E|$ edges
- The graph Laplacian defines diffusion from nodes to nodes through edges
- The one down Hodge Laplacian defines diffusion for edges to edges through nodes

The Dirac operator allows to couple the topological signals associated to nodes and edges of the graph.

Topological spinor

The spinor is defined on both nodes and edges of a graph $G = (V, E)$

as $\mathbf{\Psi} = \chi \oplus \psi \in C^0 \oplus C^1$ or equivalently

$$\mathbf{\Psi} = \begin{pmatrix} \boldsymbol{\chi} \\ \boldsymbol{\psi} \end{pmatrix}$$

with

- $\boldsymbol{\chi}$ defined on nodes, i.e. $\chi \in C_0$
- $\boldsymbol{\psi}$ defined on edges, i.e. $\psi \in C^1$

Exterior derivative and its dual

- The exterior derivative $d : C^0 \to C^1$ is defined as

$$(d\chi)_{e=[i,j]} = \chi_j - \chi_i \quad \textbf{gradient}$$

- It adjoint operator $d^* : C^1 \to C^0$ is defined as

$$(d^*\psi)_i = \sum_{e \in E_i^+} \psi_e - \sum_{e \in E_i^-} \psi_e \quad \textbf{divergence}$$

Hodge Laplacians of a graph

The graph Laplacian and the 1st order Laplacian are defined as

$L_0 = d^*d$ (graph Laplacian) $L_1 = dd^*$ (1st order Laplacian)

Properties:

A. The Laplacians L_0, L_1 are semi-definite positive and isospectral

B. dim ker$L_n = \beta_n$ where β_n indicates the nth Betti number.

In a connected network $\beta_0 = 1, \beta_1 = L - (N - 1)$

Co-boundary matrix

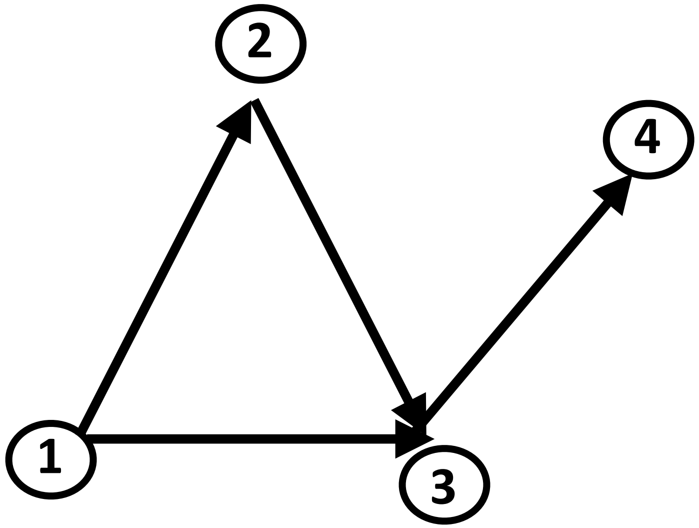

$\bar{\mathbf{B}}_{[1]}$ Discrete gradient

$\bar{\mathbf{B}}_{[1]}^{\dagger}$ Discrete divergence

Coboundary matrix

$\bar{\mathbf{B}}_{[1]}$ is a $L \times N$ matrix of elements

$$\bar{\mathbf{B}}_{[1]}(\ell, i) = \begin{cases} 1 \textbf{ if } \ell = [j, i] \\ -1 \textbf{ if } \ell = [i, j] \\ 0 \textbf{ otherwise} \end{cases}$$

The discrete gradient can be represented by the coboundary matrix $\bar{\mathbf{B}}_{[1]}$

Hodge Laplacians

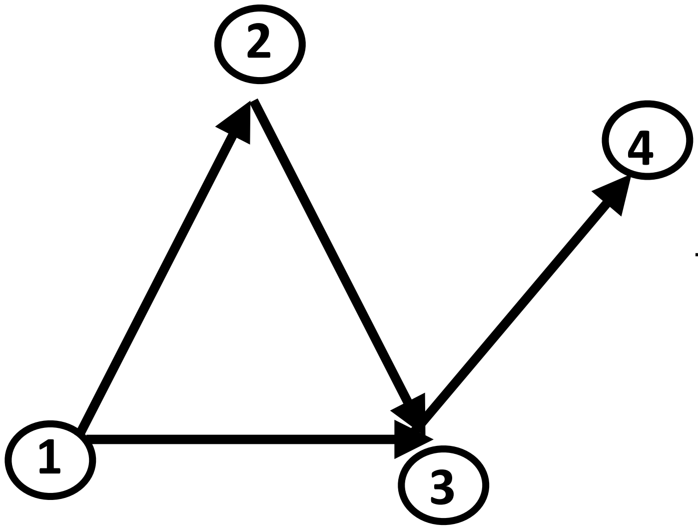

Hodge Laplacians

The Hodge Laplacians describe diffusion

from n-simplices to n-simplices through (n-1) and (n+1) simplices:

for a graph we have

$$\mathbf{L}_{[0]} = \bar{\mathbf{B}}^{\dagger}_{[1]}\bar{\mathbf{B}}_{[1]} \qquad \mathbf{L}_{[1]} = \bar{\mathbf{B}}_{[1]}\bar{\mathbf{B}}^{\dagger}_{[1]}$$

Basic definition of the Dirac operator on graphs

The Dirac operator in its simplest form

is the self-adjoint operator $D : C^0 \oplus C^1 \to C^0 \oplus C^1$ defined as

$$\boxed{D = d + d^*}$$

satisfying

$$D(\chi \oplus \psi) = (d + d^*)(\chi \oplus \psi) = (d^*\psi) \oplus (d\chi)$$

Exterior derivation and its adjoint on a graph

The exterior derivative and its adjoint

$$d = \begin{pmatrix} \mathbf{0} & \mathbf{0} \\ \bar{\mathbf{B}}_{[1]} & \mathbf{0} \end{pmatrix} \qquad d^* = \begin{pmatrix} \mathbf{0} & \bar{\mathbf{B}}_{[1]}^\dagger \\ \mathbf{0} & \mathbf{0} \end{pmatrix}$$

act on a topological spinor

$$\boldsymbol{\Psi} = \begin{pmatrix} \boldsymbol{\chi} \\ \boldsymbol{\psi} \end{pmatrix}$$

Dirac operator on a graph

Exterior divergence

$$d = \begin{pmatrix} \mathbf{0} & \mathbf{0} \\ \bar{\mathbf{B}}_{[1]} & \mathbf{0} \end{pmatrix} \qquad d^* = \begin{pmatrix} \mathbf{0} & \bar{\mathbf{B}}_{[1]}^{\dagger} \\ \mathbf{0} & \mathbf{0} \end{pmatrix}$$

Dirac operator is a self-adjoint operator

$$D = d + d^*$$

Dirac operator on graph

Dirac operator on a graph

$$\mathbf{D} = \begin{pmatrix} \mathbf{0} & \bar{\mathbf{B}}^{\dagger}_{[1]} \\ \bar{\mathbf{B}}_{[1]} & \mathbf{0} \end{pmatrix}$$

Action of the Dirac operator on the topological spinor

$$\mathbf{D}\boldsymbol{\Psi} = \begin{pmatrix} \mathbf{0} & \bar{\mathbf{B}}^{\dagger}_{[1]} \\ \bar{\mathbf{B}}_{[1]} & \mathbf{0} \end{pmatrix} \begin{pmatrix} \chi \\ \psi \end{pmatrix} = \begin{pmatrix} \bar{\mathbf{B}}^{\dagger}_{[1]}\psi \\ \bar{\mathbf{B}}_{[1]}\chi \end{pmatrix}$$

The Dirac as the square-root of the Laplacian

The Dirac operator
can be interpreted as the
“square-root” of the Laplacian

$$\mathbf{D} = \begin{pmatrix} 0 & \bar{\mathbf{B}}_{[1]}^{\dagger} \\ \bar{\mathbf{B}}_{[1]} & 0 \end{pmatrix}, \qquad \mathbf{D}^2 = \mathscr{L} = \begin{pmatrix} \mathbf{L}_{[0]} & \mathbf{0} \\ \mathbf{0} & \mathbf{L}_{[1]} \end{pmatrix}$$

The non-zero eigenvalues of the Dirac operator
are the square root of the non-zero eigenvalues of the graph Laplacian.

The spectrum of the Dirac operator

Since $\mathbf{D}^2 = \mathscr{L} = \begin{pmatrix} \mathbf{L}_{[0]} & \mathbf{0} \\ \mathbf{0} & \mathbf{L}_{[1]} \end{pmatrix}$ and $\mathbf{L}_{[0]}, \mathbf{L}_{[1]}$ are isospectral, it follows that:

Spectrum: For every positive eigenvalue μ of $\mathbf{L}_{[0]}$ there is one positive and one negative eigenvalue λ of the Dirac operator $\mathbf{D}$ with

$$\lambda = \pm\sqrt{\mu}$$

Chirality

Let us define $\gamma_0 = \begin{pmatrix} \mathbf{1} & \mathbf{0} \\ \mathbf{0} & -\mathbf{1} \end{pmatrix}$

obeying the anti commutator relation $\{\mathbf{D}, \gamma_0\} = \mathbf{0}$

- **Chirality**:If $\boldsymbol{\Psi} = (\chi, \psi)^\top$ is an eigenvector of the Dirac operator with eigenvalue λ, i.e. if $\mathbf{D}\boldsymbol{\Psi} = \lambda\boldsymbol{\Psi}$ then $\gamma_0\boldsymbol{\Psi} = (\chi, -\psi)^\top$ is an eigenvector of $\mathbf{D}$ with eigenvalue $-\lambda$

- Indeed from the anti-commutator relation it follows that $\mathbf{D}\gamma_0\boldsymbol{\Psi} = -\gamma_0\mathbf{D}\boldsymbol{\Psi} = -\lambda\gamma_0\boldsymbol{\Psi}$

Eigenvectors of the Dirac operator

- It follows that the matrix of eigenvectors of the Dirac operator can be expressed as

$$\mathbf{\Phi} = \begin{pmatrix} \mathbf{U}^{[1]} & \mathbf{U}^{[1]} & \mathbf{U}_0^{harm} & \mathbf{0} \\ \mathbf{V}^{[1]} & -\mathbf{V}^{[1]} & \mathbf{0} & \mathbf{U}_1^{harm} \end{pmatrix}$$

- where $\mathbf{U}^{[1]}, \mathbf{V}^{[1]}$ Indicates the right and left singular vector of the coboundary operator and $\mathbf{U}_0^{harm}, \mathbf{U}_1^{harm}$ are the matrices of the harmonic eigenvectors of $\mathbf{L}_{[0]}, \mathbf{L}_{[1]}$ respectively.

Index of the Dirac operator

The index of the Dirac operator D is given

by the Euler number χ_E of the graph

$$\text{ind}\, D = \text{dim ker}\, d - \text{dim ker}\, d^* = \chi_E$$

Indeed

$$\text{ind}\, D = \chi_E = N - L$$

Introducing an algebra

Dirac operator on a network can be enriched by an algebra

$$\mathbf{D} = \begin{pmatrix} \mathbf{0} & b^* \bar{\mathbf{B}}_{[1]}^{\dagger} \\ b \bar{\mathbf{B}}_{[1]} & \mathbf{0} \end{pmatrix}$$

with $b \in \mathbb{C}, \quad |b| = 1$

Topological spinor

On a network we consider the topological spinor

$$\mathbf{\Psi} = \begin{pmatrix} \boldsymbol{\chi} \\ \boldsymbol{\psi} \end{pmatrix}$$

Characterising the dynamical state of the topological signals of the network, being a vector with a block structure formed by a 0-cochain and a 1-cochain

$$\boldsymbol{\chi} = \begin{pmatrix} \chi_1 \\ \chi_2 \\ \vdots \\ \chi_N \end{pmatrix}, \quad \boldsymbol{\psi} = \begin{pmatrix} \psi_{\ell_1} \\ \psi_{\ell_2} \\ \vdots \\ \psi_{\ell_L} \end{pmatrix}.$$

Topological Dirac equation

The topological Dirac equation is then given by

$$i\partial_t \boldsymbol{\Psi} = \mathscr{H}\boldsymbol{\Psi}$$

with Hamiltonian

$$\mathscr{H} = \mathbf{D} + m\boldsymbol{\beta}$$

Where $\boldsymbol{\beta} = \begin{pmatrix} \mathbf{1} & \mathbf{0} \\ \mathbf{0} & -\mathbf{1} \end{pmatrix}$ leading to the anti-commutator $\{\mathbf{D}, \boldsymbol{\beta}\} = \mathbf{0}$

Energy Eigenstates

The energy eigenstates satisfy $E\boldsymbol{\Psi} = \mathscr{H}\boldsymbol{\Psi}$ which leads to

$$E\boldsymbol{\chi} = b^*\bar{\mathbf{B}}^\dagger\boldsymbol{\psi} + m\boldsymbol{\chi},$$
$$E\boldsymbol{\psi} = b\bar{\mathbf{B}}\boldsymbol{\chi} - m\boldsymbol{\psi}$$

It follows that $\boldsymbol{\chi}, \boldsymbol{\psi}$ are respectively the right and left eigenvectors of $\bar{\mathbf{B}}$ with eigenvalue λ

and that the dispersion relation is relativistic $E^2 = |\lambda|^2 + m^2$,

i.e. the energy values are given by $E = \pm\sqrt{|\lambda|^2 + m^2}$

Sketch of the derivation

The eigenvalue problem $E\boldsymbol{\Psi} = \mathscr{H}\boldsymbol{\Psi}$ is equivalent to

$$E\boldsymbol{\chi} = b^*\bar{\mathbf{B}}^\dagger\boldsymbol{\psi} + m\boldsymbol{\chi},$$
$$E\boldsymbol{\psi} = b\bar{\mathbf{B}}\boldsymbol{\chi} - m\boldsymbol{\psi}$$

Let us re-order obtaining

$$(E-m)\boldsymbol{\chi} = b^*\bar{\mathbf{B}}^\dagger\boldsymbol{\psi},$$
$$(E+m)\boldsymbol{\psi} = b\bar{\mathbf{B}}\boldsymbol{\chi}$$

Therefore

$$(E-m)(E+m)\boldsymbol{\chi} = \bar{\mathbf{B}}^\dagger\bar{\mathbf{B}}\boldsymbol{\chi} = \mathbf{L}_{[0]}\boldsymbol{\chi},$$
$$(E+m)(E-m)\boldsymbol{\psi} = \bar{\mathbf{B}}\bar{\mathbf{B}}^\dagger\boldsymbol{\psi} = \mathbf{L}_{[1]}^{down}\boldsymbol{\psi}$$

$\longrightarrow$ This implies $E^2 = m^2 + |\lambda|^2$

Matter-Antimatter asymmetry and homology

For $E^2 > m^2$ there is symmetry between positive energy eigenstates and negative energy eigenstates.

However the symmetry between positive energy states and negative energy states breaks down for $|E| = m$

The states at energy states at $E = m$ are localised on nodes and they have a degeneracy given by the Betti number β_0

The energy states $E = -m$ are localised on links and they have a degeneracy given by the Betti number β_1

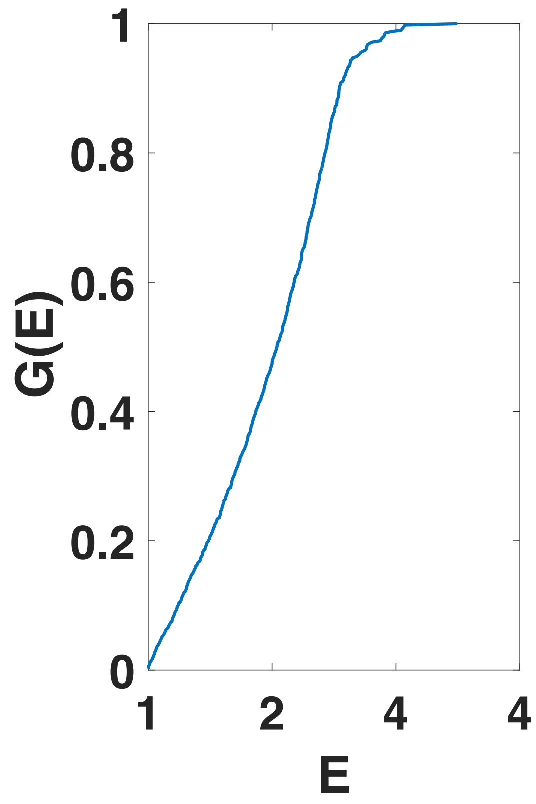

Density of states

Eigenvectors of the Dirac operator on real networks

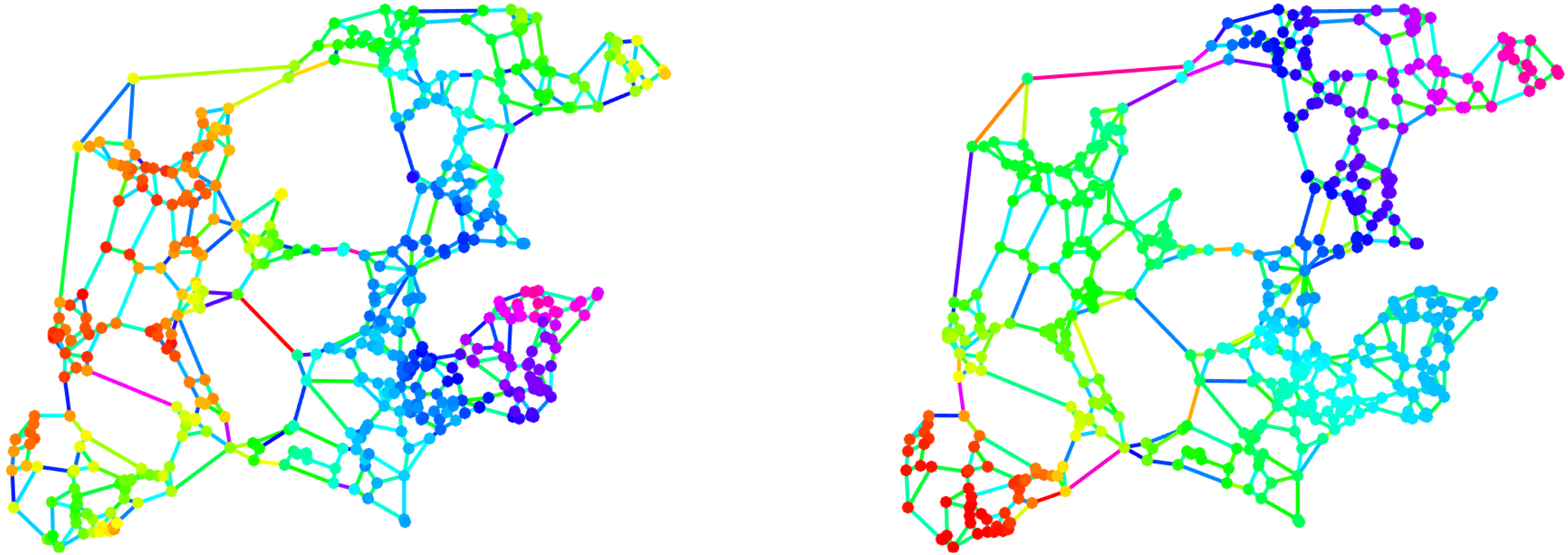

Eigenvectors of the Dirac Operator on real networks

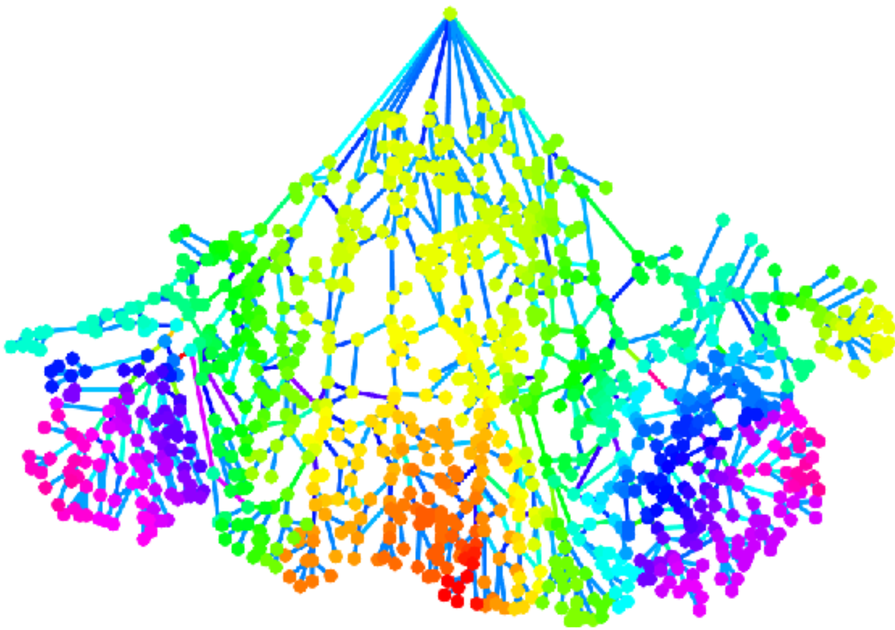

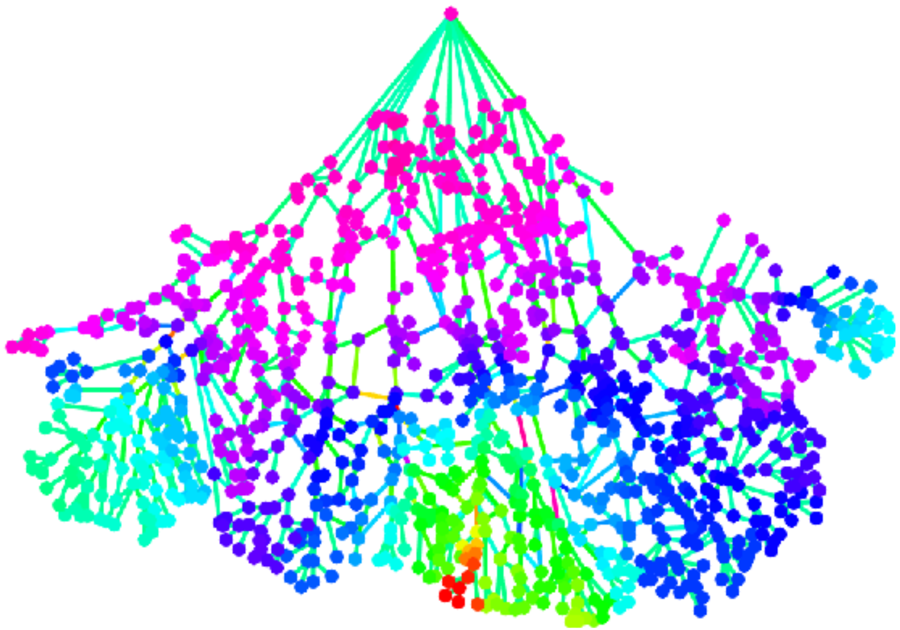

Metric matrices

We introduce the metric matrices:

- $\mathbf{G}_0 = e^{\mathbf{A}_0}$ metric on the nodes, indicating a $N \times N$ matrix
- $\mathbf{G}_1 = e^{\mathbf{A}_1}$ metric on the undirected edges, indicating a $L \times L$ matrix

Typically the metric matrices are taken real and diagonal

Indicating distances or affinity weights in applied topology

Weighted Dirac operator on a network

$$\hat{\mathbf{D}} = \begin{pmatrix} \mathbf{0} & b^* \bar{\mathbf{B}}^*_{[1]} \\ b \bar{\mathbf{B}}_{[1]} & \mathbf{0} \end{pmatrix}$$

with $b \in \mathbb{C}, \ |b| = 1$ **and** $\bar{\mathbf{B}}^*_{[1]} = \mathbf{G}_0 \bar{\mathbf{B}}^\top_{[1]} \mathbf{G}_1^{-1}$

$$\hat{\mathbf{D}}^2 = \mathscr{L} = \begin{pmatrix} \hat{\mathbf{L}}_{[0]} & \mathbf{0} \\ \mathbf{0} & \hat{\mathbf{L}}_{[1]} \end{pmatrix}$$

with

$$\hat{\mathbf{L}}_{[0]} = \bar{\mathbf{B}}^*_1 \bar{\mathbf{B}}_1, \hat{\mathbf{L}}_{[1]} = \bar{\mathbf{B}}_1 \bar{\mathbf{B}}^*_1$$

F. Baccini, F. Geraci and G. Bianconi (2022)

Normalised Dirac operator

If the matrix $\mathbf{G}_1^{-1}$,$\mathbf{G}_0^{-1}$ are the diagonal matrices with elements

$$\mathbf{G}_1^{-1}(\ell,\ell) = w_\ell/2$$
$$\mathbf{G}_0^{-1}(i,i) = \sum_{\ell \in E_i} w_\ell$$

The weighted Dirac operator is also called normalised Dirac operator and has eigenvalues bounded in absolute value by one $|\lambda| \leq 1$

F. Baccini, F. Geraci and G. Bianconi (2022)

The Dirac operator for treating dynamics of topological signals

Topological signals

Simplicial complexes and networks can sustain dynamical variables (signals) not only defined on nodes but also defined on higher order simplices these signals are called *topological signals*

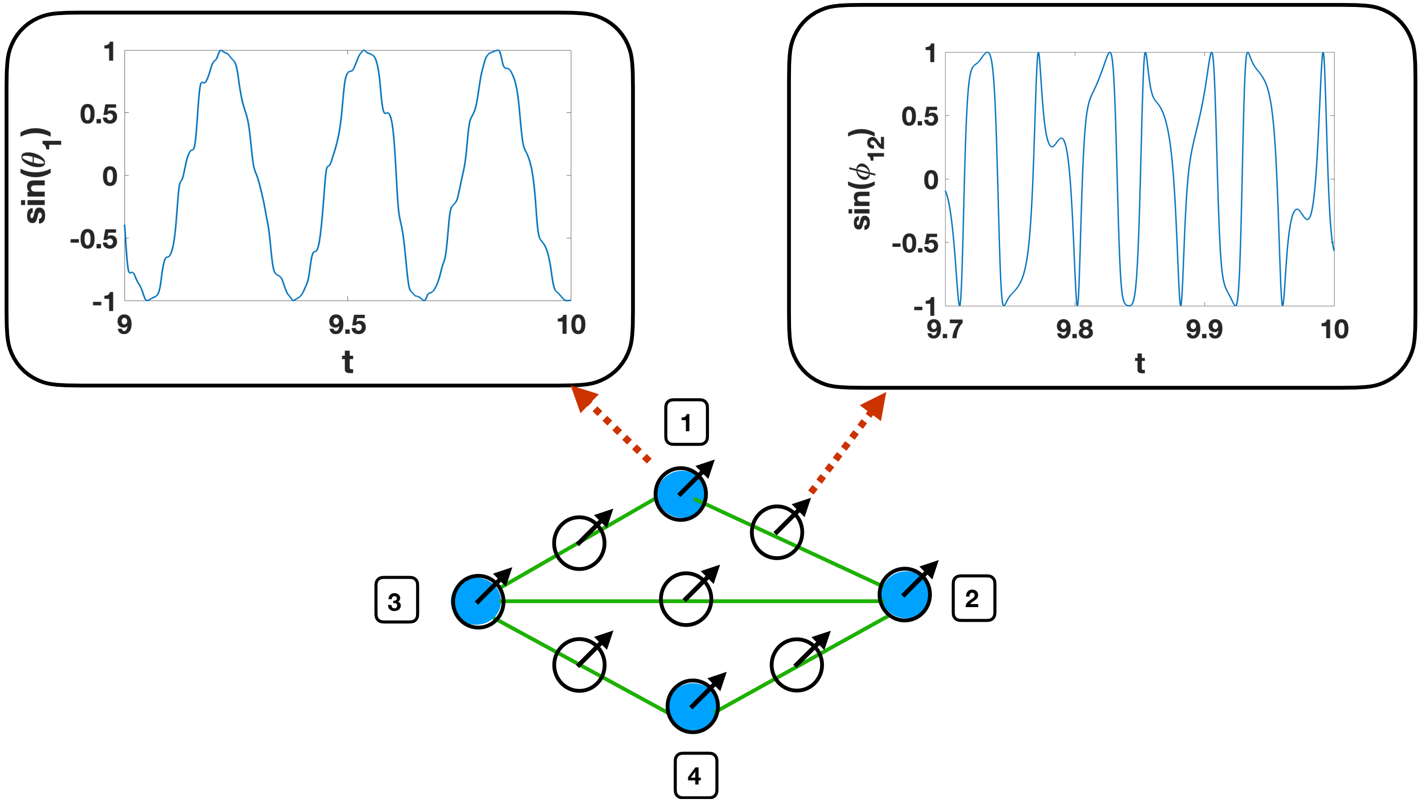

Topological signals

- Citations in a collaboration network
- Speed of wind at given locations
- Currents at given locations in the ocean
- Fluxes in biological transportation networks
- Synaptic signal
- Edge signals in the brain

Topological signals
are co-chains or vector fields

Kuramoto model on a network

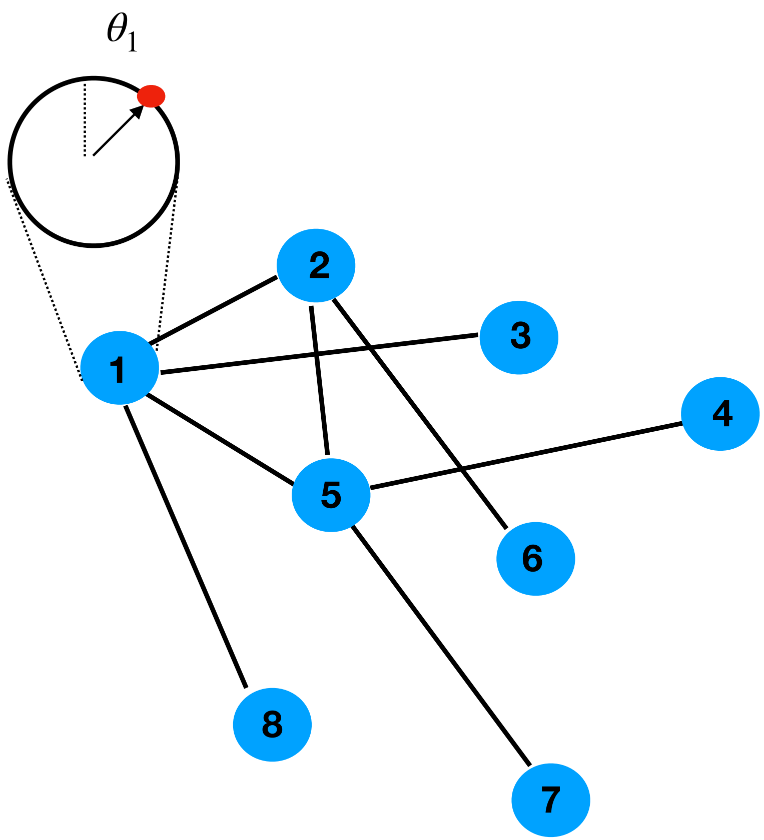

The Kuramoto model

$$\dot{\theta}_r = \omega_r + \sigma \sum_{j=1}^{N} a_{rj} \sin\left(\theta_j - \theta_r\right)$$

With $\omega \sim \mathcal{N}(\Omega, 1)$

describes synchronization of node phases of $\sigma > \sigma_c$

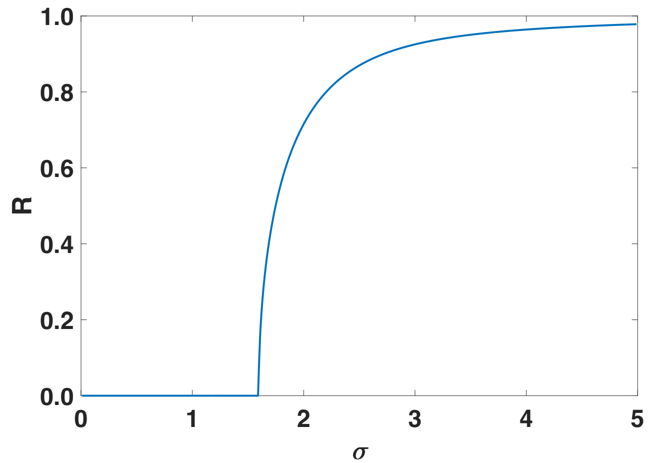

Order parameter

$$R = \frac{1}{N}\left|\sum_{r=1}^{N} e^{i\theta_r}\right|$$

In the Standard Kuramoto model
the free dynamics
of the synchronised state
is uniform over the whole
(connected) network

The Topological Kuramoto model

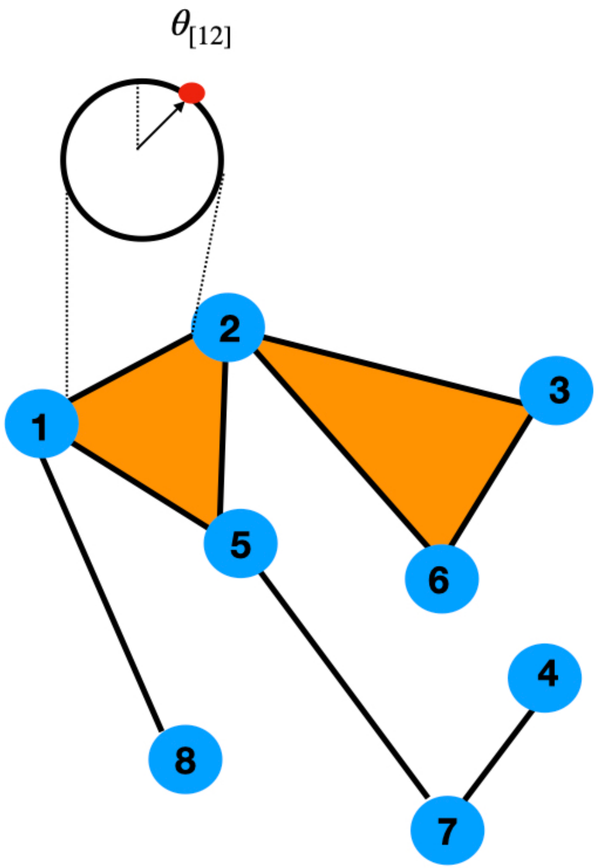

How to define
the Topological Kuramoto model
coupling higher dimensional
topological signals?

Topological Kuramoto model

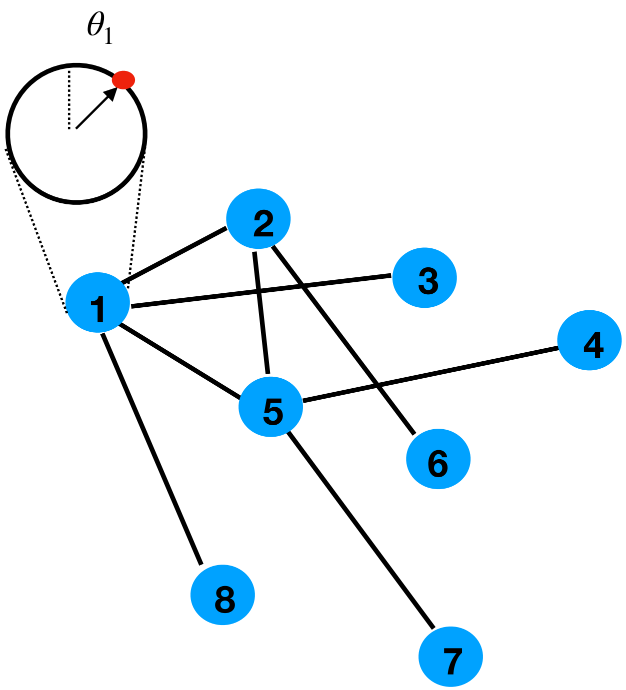

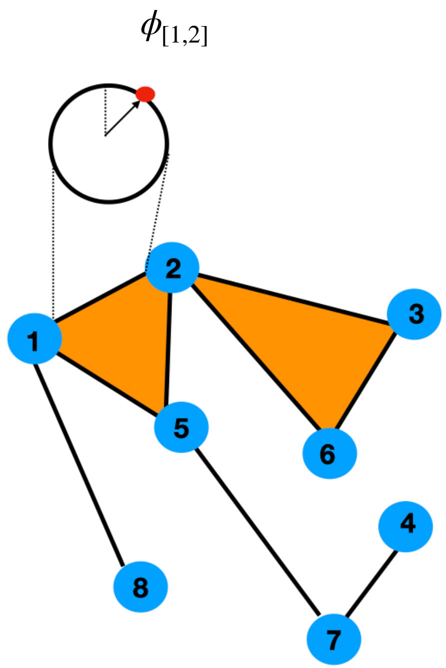

Standard Kuramoto model

$$\dot{\boldsymbol{\theta}} = \boldsymbol{\omega} - \sigma \mathbf{B}_{[1]} \sin \mathbf{B}_{[1]}^{\top} \boldsymbol{\theta}$$

Topological Higher-order Kuramoto model

$$\dot{\boldsymbol{\phi}} = \hat{\boldsymbol{\omega}} - \sigma \mathbf{B}_{[n+1]} \sin \mathbf{B}_{[n+1]}^{\top} \boldsymbol{\phi} - \sigma \mathbf{B}_{[n]}^{\top} \sin \mathbf{B}_{[n]} \boldsymbol{\phi},$$

A. P. Millan, J.J. Torres and G. Bianconi PRL (2020)

The Topological Kuramoto Model

In the Topological Kuramoto model the free dynamics of the synchronized state
is localised on the
n-dimensional holes

$$\frac{d\langle \mathbf{u}_{harm}, \boldsymbol{\phi} \rangle}{dt} = \langle \mathbf{u}_{harm}, \hat{\boldsymbol{\omega}} \rangle$$

The free dynamics is localised on harmonic components

Linearized Dynamics

The linearized dynamics is dictated by the Hodge-Laplacian

$$\dot{\boldsymbol{\phi}} = \hat{\boldsymbol{\omega}} - \sigma \mathbf{L}_{[n]} \boldsymbol{\phi},$$

The harmonic component of the signal oscillates freely

$$\dot{\boldsymbol{\phi}}_{harmonic} = \hat{\boldsymbol{\omega}}_{harmonic}$$

The other modes freeze asymptotically in time as they obey

$$\dot{\boldsymbol{\phi}}_{\mu} = \hat{\boldsymbol{\omega}}_{\mu} - \mu \boldsymbol{\phi}_{\mu}$$

Where $\mu \neq 0$ indicates the eigenvalue of the Hodge Laplacian

Linearised Dynamics

The linearised dynamics is dictated by the graph

$$\dot{\boldsymbol{\phi}} = \hat{\boldsymbol{\omega}} - \sigma \mathbf{L}_{[n]} \boldsymbol{\phi} \,.$$

The phases and the intrinsic frequencies can be decomposed in the basis of the eigenvectors of the graph Laplacian

$$\boldsymbol{\phi}(t) = \sum_{\mu} c_{\mu}(t) \mathbf{u}_{\mu}$$

$$\hat{\boldsymbol{\omega}} = \sum_{\mu} \hat{\omega}_{\mu} \mathbf{u}_{\mu}$$

The dynamical equation in this basis reduce to

$$\dot{c}_{\mu} = \hat{\omega}_{\mu} - \sigma \mu c_{\mu}$$

Linearised Dynamics (continuation)

The dynamical equations

$$\dot{c}_\mu = \hat{\omega}_\mu - \sigma\mu c_\mu$$

have solution

$$c_{harm}(t) = c_{harm}(0) + \hat{\omega}_{harm} t$$

$$c_\mu(t) = \frac{\hat{\omega}_\mu}{\sigma\mu}\left(1 - e^{-\sigma\mu t}\right) + c_\mu(0) e^{-\sigma\mu t}$$

Therefore the harmonic mode undergoes an unperturbed motion,

while the non-harmonic modes are freezing with time.

Topological Kuramoto model on a graph

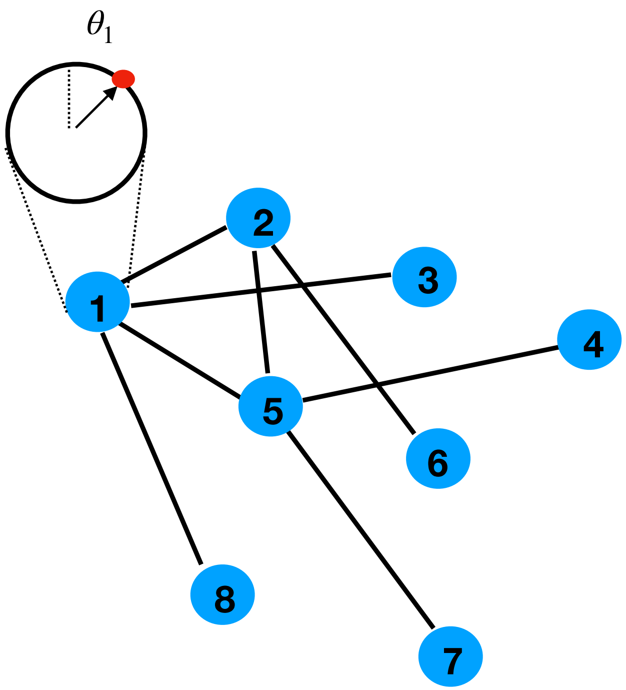

Standard Kuramoto model

$$\dot{\boldsymbol{\theta}} = \boldsymbol{\omega} - \sigma \mathbf{B}_{[1]} \sin \mathbf{B}_{[1]}^{\top} \boldsymbol{\theta}$$

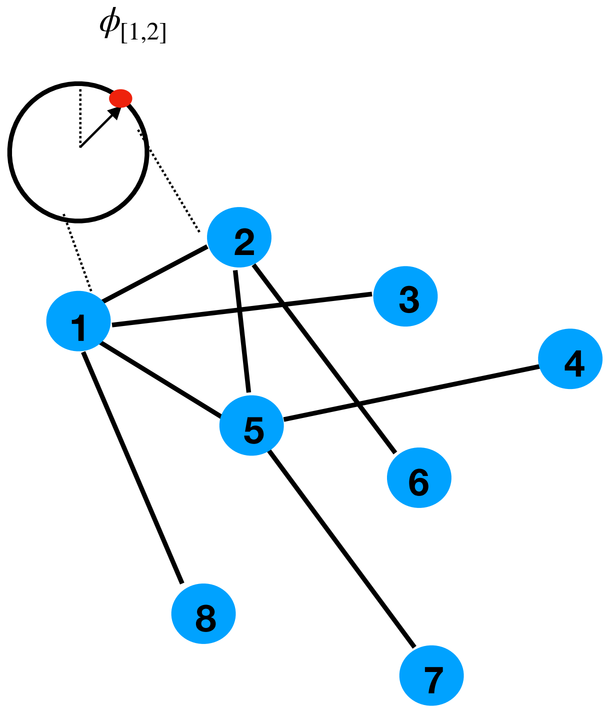

Topological Higher-order Kuramoto model

$$\dot{\boldsymbol{\phi}} = \hat{\boldsymbol{\omega}} - \sigma \mathbf{B}_{[1]}^{\top} \sin \mathbf{B}_{[1]} \boldsymbol{\phi},$$

A. P. Millan, J.J. Torres and G. Bianconi PRL (2020)

Topological Kuramoto model on a graph

Let us define the vectors

$$\mathbf{\Phi} = \begin{pmatrix} \boldsymbol{\theta} \\ \boldsymbol{\phi} \end{pmatrix}, \quad \mathbf{\Omega} = \begin{pmatrix} \boldsymbol{\omega} \\ \hat{\boldsymbol{\omega}} \end{pmatrix},$$

Then the node and edge based topological Kuramoto model can be written in terms of the Dirac operator as

$$\dot{\boldsymbol{\theta}} = \boldsymbol{\omega} - \sigma \bar{\mathbf{B}}_{[1]}^{\top} \sin \bar{\mathbf{B}}_{[1]} \boldsymbol{\theta}$$

$$\dot{\boldsymbol{\phi}} = \hat{\boldsymbol{\omega}} - \sigma \bar{\mathbf{B}}_{[1]} \sin \bar{\mathbf{B}}_{[1]}^{\top} \boldsymbol{\phi},$$

$$\Rightarrow \quad \dot{\mathbf{\Phi}} = \mathbf{\Omega} - \sigma \mathbf{D} \sin \mathbf{D} \mathbf{\Phi}$$

Topological Kuramoto model on a graph

Let us define the vectors

$$\mathbf{\Phi} = \begin{pmatrix} \boldsymbol{\theta} \\ \boldsymbol{\phi} \end{pmatrix}, \quad \mathbf{\Omega} = \begin{pmatrix} \boldsymbol{\omega} \\ \hat{\boldsymbol{\omega}} \end{pmatrix},$$

Then the node and edge based normalised topological Kuramoto model can be written in terms of the **normalised Dirac operator** as

$$\dot{\boldsymbol{\theta}} = \boldsymbol{\omega} - \sigma \bar{\mathbf{B}}_{[1]}^{\top} \sin \bar{\mathbf{B}}_{[1]} \boldsymbol{\theta}$$

$$\dot{\boldsymbol{\phi}} = \hat{\boldsymbol{\omega}} - \sigma \bar{\mathbf{B}}_{[1]} \sin \bar{\mathbf{B}}_{[1]}^{*} \boldsymbol{\phi},$$

$$\Longrightarrow \quad \dot{\mathbf{\Phi}} = \mathbf{\Omega} - \sigma \hat{\mathbf{D}} \sin \hat{\mathbf{D}} \mathbf{\Phi}$$

Dirac Synchronization

Dirac Synchronization allows to couple locally

and topologically signals defined on nodes and links.

Dirac synchronisation obeys

$$\dot{\boldsymbol{\Phi}} = \boldsymbol{\Omega} - \sigma \hat{\mathbf{D}} \sin((\hat{\mathbf{D}} - \gamma_0 z \hat{\mathbf{D}}^2)\boldsymbol{\Phi})$$

For the node topological signal we introduce a phase lag depending on the edge signal and vice versa for the edge signal we introduce a phase lag depending on the node signal

L. Calmon, J. Restrepo, J.J. Torres and G. Bianconi (2022)

Dirac Synchronization is explosive

Dirac synchronisation obeys

$$\dot{\mathbf{\Phi}} = \mathbf{\Omega} - \sigma\hat{\mathbf{D}}\sin((\hat{\mathbf{D}} - \gamma_0 z\hat{\mathbf{D}}^2)\mathbf{\Phi})$$

- **Node and links signals are entangled.** The order parameters depend on linear combinations of nodes and link signals
- **The synchronization transition is discontinuous**

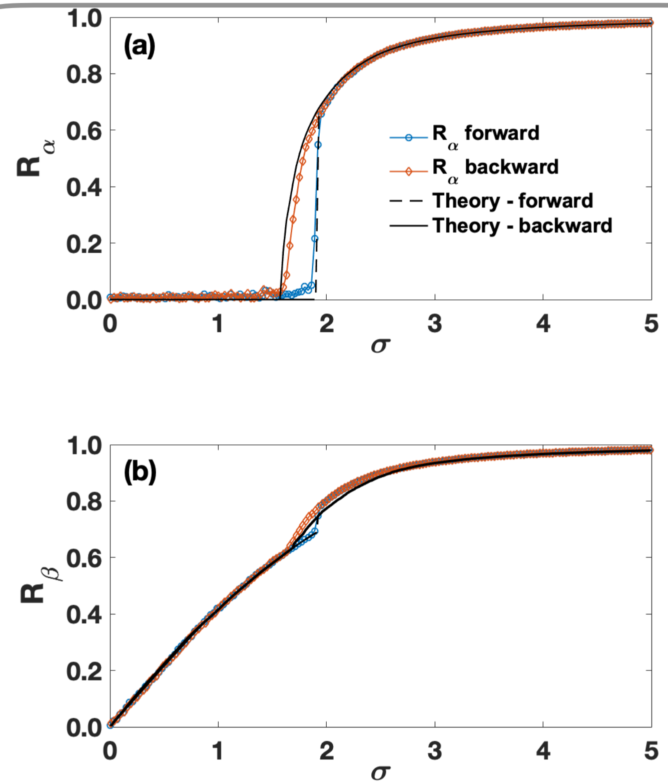

L. Calmon, J. Restrepo, J.J. Torres and G. Bianconi (2022)

Dependence on z

The phase diagram can display not only a forward but also a backward discontinuous transition as a function of z

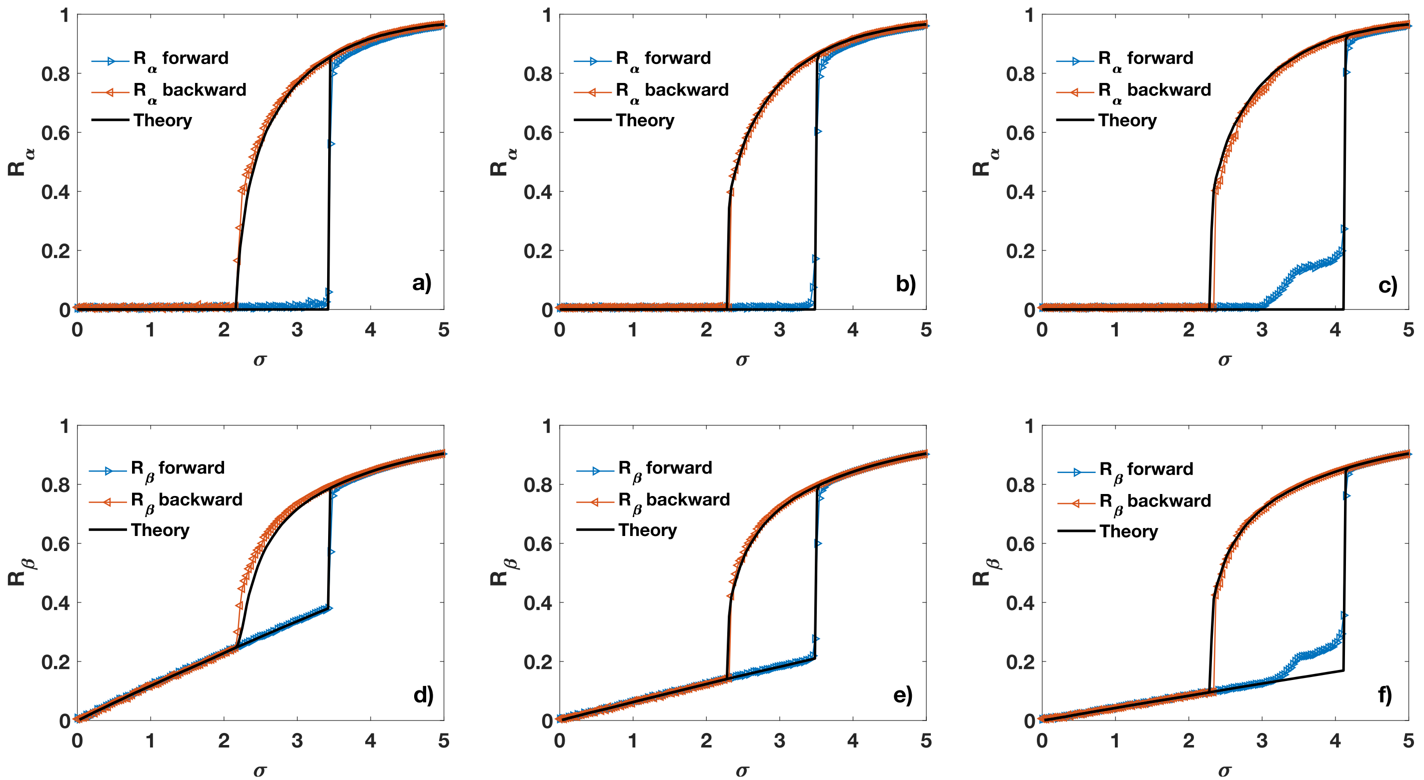

Linearised Dynamics

The linearised dynamics is dictated by the Dirac operator

$$\dot{\mathbf{\Phi}} = \mathbf{\Omega} - \sigma(\hat{\mathbf{D}}^2 + z\boldsymbol{\gamma}\hat{\mathbf{D}}^3)\mathbf{\Phi},$$

Let us now decompose $\mathbf{\Phi}, \mathbf{\Omega}$ on the eigenvectors of the Dirac operator $\mathbf{W}_\lambda$ obtaining

$$\mathbf{\Phi} = \sum_\lambda c_\lambda \boldsymbol{W}_\lambda \quad \mathbf{\Omega} = \sum_\lambda \omega_\lambda \boldsymbol{W}_\lambda$$

Linearised Dynamics

The harmonic component of the signal oscillates freely

$$\dot{c}_{harmonic} = \hat{\mathbf{\Omega}}_{harmonic}$$

The other modes freeze asymptotically **at a stable focu**s in time and obey

$$\begin{pmatrix} \dot{c}_\lambda \\ \dot{c}_{-\lambda} \end{pmatrix} = \begin{pmatrix} \omega_\lambda \\ \omega_{-\lambda} \end{pmatrix} - \sigma \begin{pmatrix} \lambda^2 & z\lambda^3 \\ -z\lambda^3 & \lambda^2 \end{pmatrix} \begin{pmatrix} c_\lambda \\ c_{-\lambda} \end{pmatrix}$$

Where $\lambda \neq 0$ indicates a positive eigenvalue of the Dirac operator

Linearised Dynamics (continuation)

The dynamical equation for the harmonic mode

has solution

$$c_{harm}(t) = c_{harm}(0) + \omega_{harm} t$$

Therefore the harmonic modes

undergo an unperturbed motion

Linearised Dynamics (continuation)

The dynamical equation for the other modes

has solution

$$\begin{pmatrix} c_\lambda(t) \\ c_{-\lambda}(t) \end{pmatrix} = A(t)\begin{pmatrix} 1 \\ -\mathrm{i} \end{pmatrix} + B(t)\begin{pmatrix} 1 \\ \mathrm{i} \end{pmatrix}$$

with

$$A(t) = \frac{\omega_\lambda + \mathrm{i}\omega_{-\lambda}}{2\sigma(\lambda^2 + \mathrm{iz}\lambda^3)}\left(1 - e^{-\sigma(\lambda + \mathrm{iz}\lambda^3)\mathrm{t}}\right) + A(0)e^{-\sigma(\lambda + \mathrm{iz}\lambda^3)\mathrm{t}}$$

$$B(t) = \frac{\omega_\lambda - \mathrm{i}\omega_{-\lambda}}{2\sigma(\lambda^2 + \mathrm{iz}\lambda^3)}\left(1 - e^{-\sigma(\lambda - \mathrm{iz}\lambda^3)\mathrm{t}}\right) + B(0)e^{-\sigma(\lambda - \mathrm{iz}\lambda^3)\mathrm{t}}$$

Therefore while the non-harmonic modes display a stable focus.

Dirac Synchronization is rhythmic

One of the two complex order parameters develops spontaneous low frequency rhythms

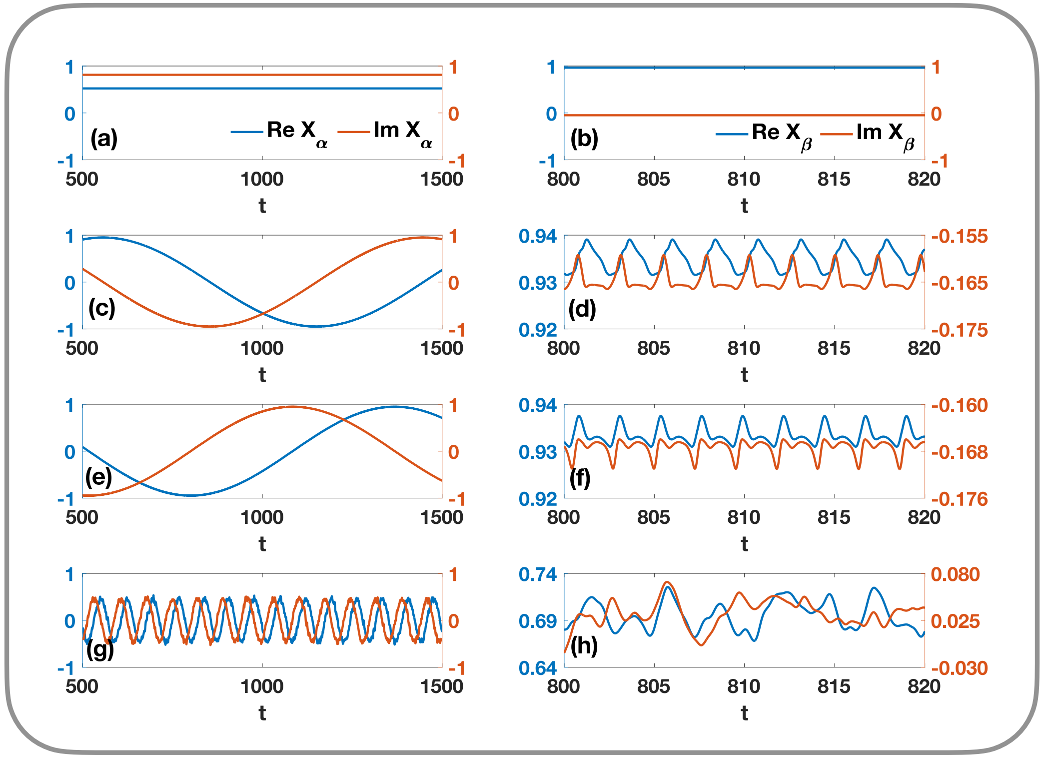

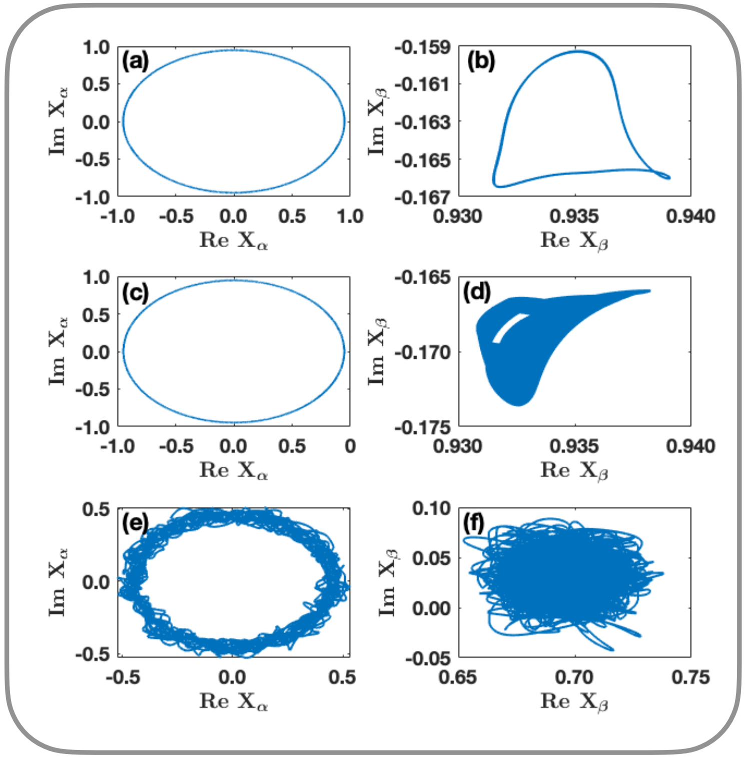

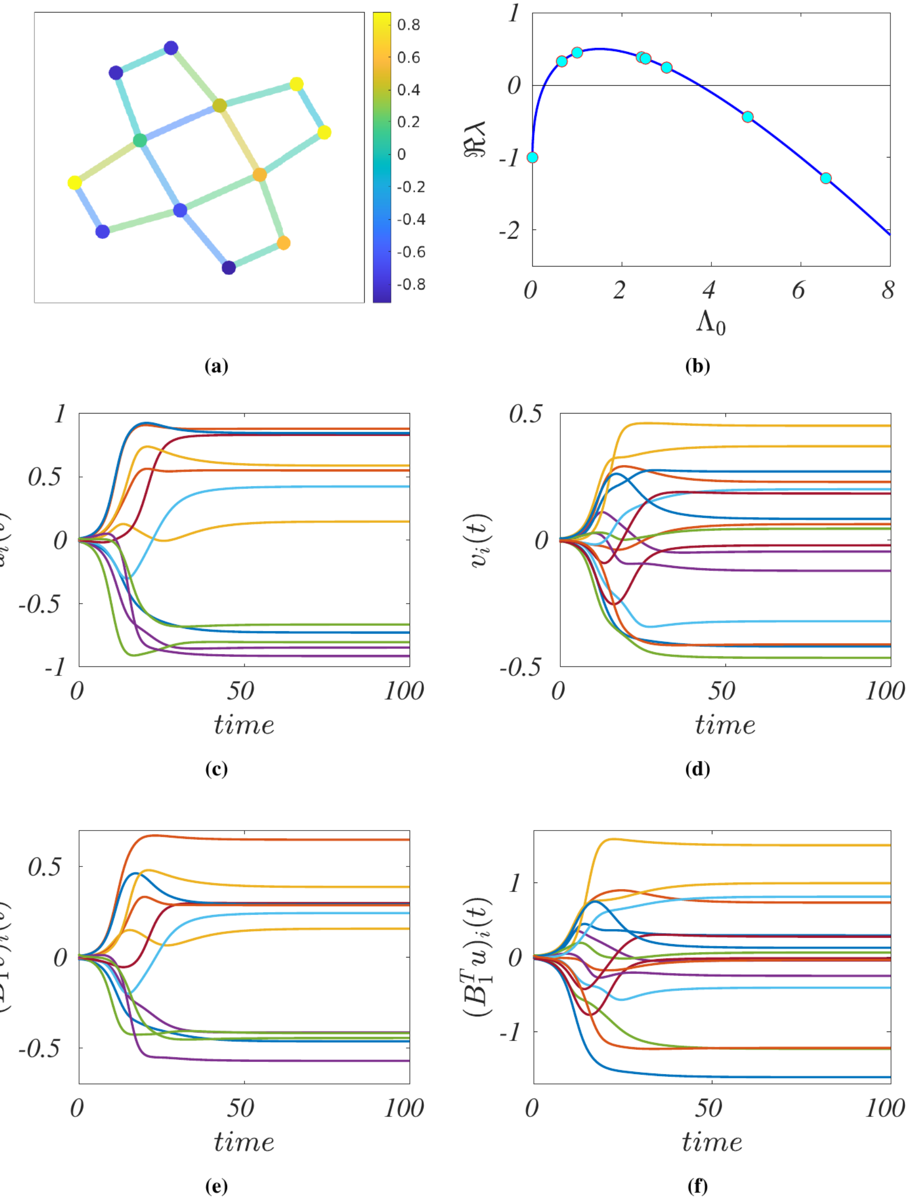

Dirac Turing patterns

Defining $\boldsymbol{\Psi} = (\boldsymbol{\theta}, \boldsymbol{\phi})^{\top}$ describing topological signals on nodes and links and the reaction diffusion dynamics

$$\dot{\boldsymbol{\Phi}} = F(\boldsymbol{\Phi}, \mathbf{D}\boldsymbol{\Phi}) - \gamma \mathbf{D}\boldsymbol{\Phi},$$

Turing patterns on nodes and links can set in provided suitable topological and dynamical conditions.

Giambagli et al. (2022)

Dirac Turing patterns

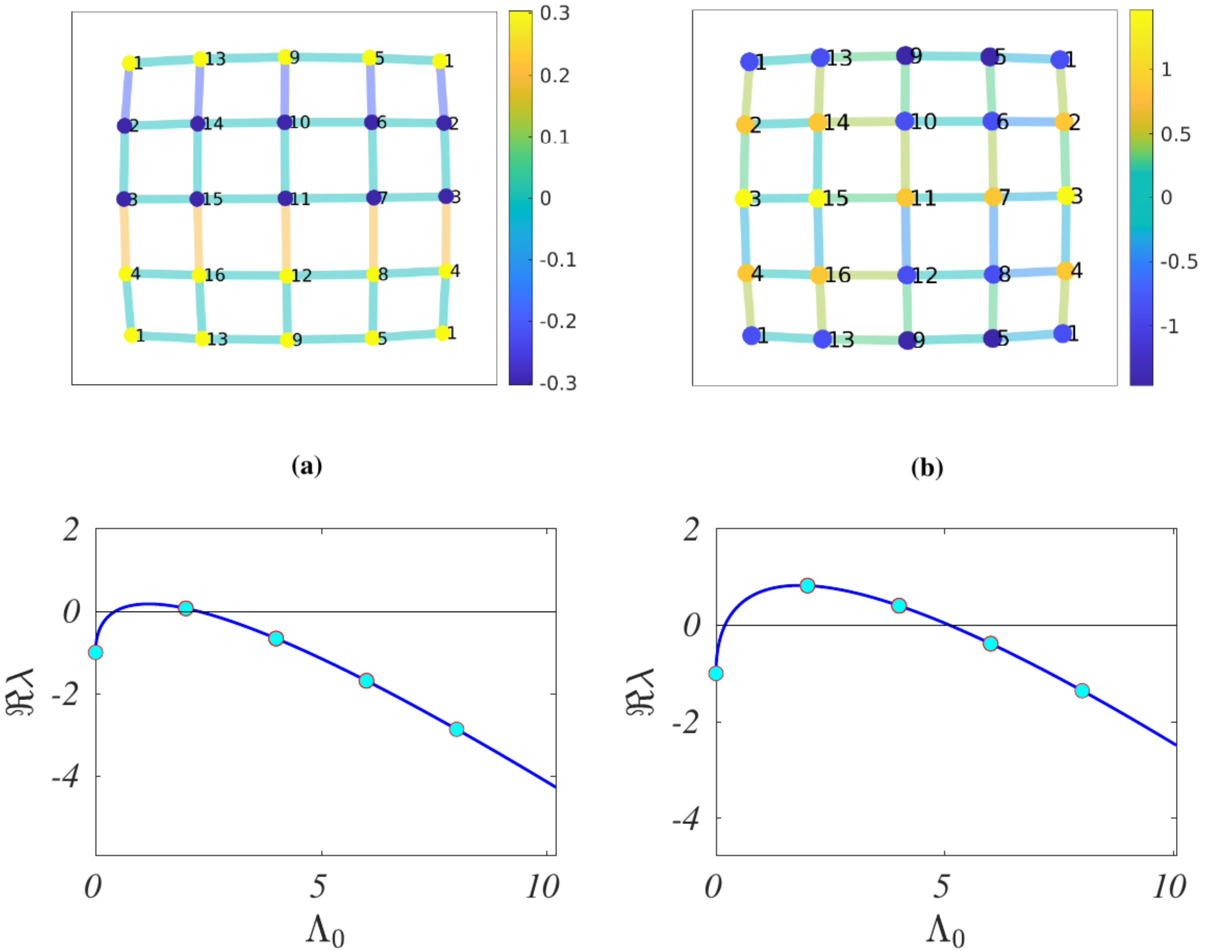

- Hypercubic tessellations of d-dimensional torus admit Turing patterns on any dimension

- The figure show Turing patterns on nodes and links on a 2D Torus.

The Dirac operator on simplicial complexes

The Dirac operator on simplicial complexes

The Dirac operator allows
to study interacting topological signals of different dimensions
coexisting in the same network topology

Dirac operator

$$\mathbf{D} = \begin{pmatrix} 0 & \bar{\mathbf{B}}_1^\dagger & 0 \\ \bar{\mathbf{B}}_1 & 0 & \bar{\mathbf{B}}_2^\dagger \\ 0 & \bar{\mathbf{B}}_2 & 0 \end{pmatrix},$$

Topological signal "spinor"

$$\mathbf{s} = \begin{pmatrix} \mathbf{s}_0 \\ \mathbf{s}_1 \\ \mathbf{s}_2 \end{pmatrix}$$

$\mathbf{s}_0$ Node signal

$\mathbf{s}_1$ Link signal

$\mathbf{s}_2$ Triangle signal

The action of the Dirac operator

The Dirac operator allows cross-talking between signals of different dimension

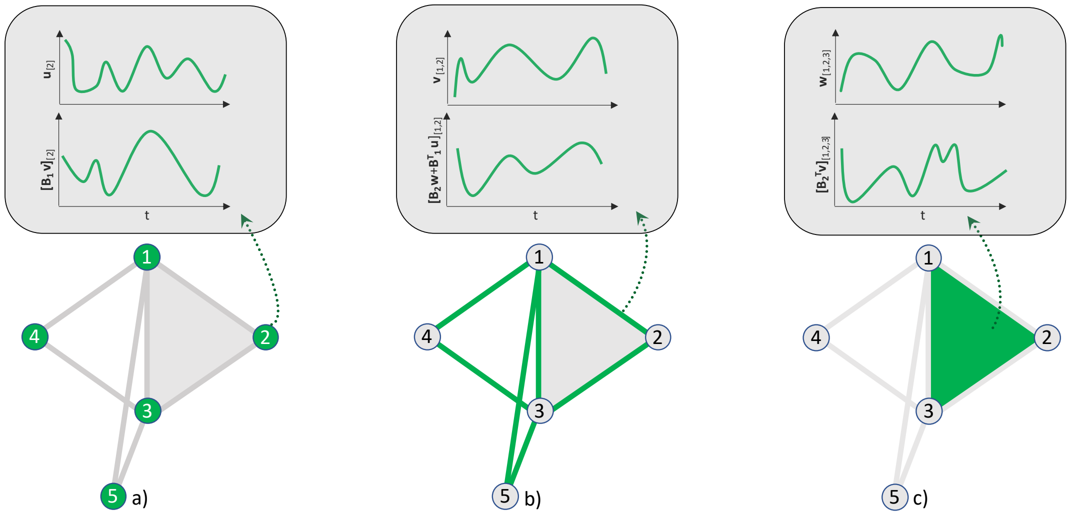

$$\mathbf{D} = \begin{pmatrix} 0 & \bar{\mathbf{B}}_1^\dagger & 0 \\ \bar{\mathbf{B}}_1 & 0 & \bar{\mathbf{B}}_2^\dagger \\ 0 & \bar{\mathbf{B}}_2 & 0 \end{pmatrix}, \text{ acts on } \mathbf{s} = \begin{pmatrix} \mathbf{s}_0 \\ \mathbf{s}_1 \\ \mathbf{s}_2 \end{pmatrix} \quad \rightarrow \quad \mathbf{Ds} = \begin{pmatrix} \bar{\mathbf{B}}_1^\dagger \mathbf{s}_1 \\ \bar{\mathbf{B}}_1 \mathbf{s}_0 + \bar{\mathbf{B}}_1^\dagger \mathbf{s}_2 \\ \bar{\mathbf{B}}_2 \mathbf{s}_1 \end{pmatrix}$$

Dirac decomposition

$$\mathbf{D} = \mathbf{D}_{[1]} + \mathbf{D}_{[2]}$$

Here

$\mathbf{D}_{[1]}$ only couples node and link signals and

$\mathbf{D}_{[2]}$only couples link and triangle signals

$$\mathbf{D}_{[1]} = \begin{pmatrix} 0 & \bar{\mathbf{B}}_1 & 0 \\ \bar{\mathbf{B}}_1^\top & 0 & 0 \\ 0 & 0 & 0 \end{pmatrix} \quad \mathbf{D}_{[2]} = \begin{pmatrix} 0 & 0 & 0 \\ 0 & 0 & \bar{\mathbf{B}}_2 \\ 0 & \bar{\mathbf{B}}_2^\top & 0 \end{pmatrix}$$

$$\mathbf{D}_{[1]}^2 = \mathscr{L}_{[1]} = \begin{pmatrix} \mathbf{L}_{[0]} & \mathbf{0} & \mathbf{0} \\ \mathbf{0} & \mathbf{L}_{[1]}^{down} & \mathbf{0} \\ \mathbf{0} & \mathbf{0} & \mathbf{0} \end{pmatrix} \quad \mathbf{D}_{[2]}^2 = \mathscr{L}_{[2]} = \begin{pmatrix} \mathbf{0} & \mathbf{0} & \mathbf{0} \\ \mathbf{0} & \mathbf{L}_{[1]}^{up} & \mathbf{0} \\ \mathbf{0} & \mathbf{0} & \mathbf{L}_{[2]}^{down} \end{pmatrix}$$

Dirac decomposition

Every topological signal can be decomposed in a unique way thanks to the Dirac decomposition

$$\mathbb{R}^{D_S} = \mathrm{im}(\mathbf{D}_{[1]}) \oplus \mathrm{ker}(\mathbf{D}) \oplus \mathrm{im}(\mathbf{D}_{[2]})$$

therefore every signals defined on nodes, links and triangles can be decomposed in a unique way as

$$\mathbf{s} = \mathbf{s}^{[1]} + \mathbf{s}^{[2]} + \mathbf{s}^{harm}$$

With

$$\mathbf{s}^{[1]} = \mathbf{D}_{[1]}\mathbf{D}_{[1]}^{+}\mathbf{s}$$

$$\mathbf{s}^{[2]} = \mathbf{D}_{[2]}\mathbf{D}_{[2]}^{+}\mathbf{s}$$

Eigenvalues of the Dirac operator

Due to the Dirac decomposition
the eigenvalues of the Dirac operator $\mathbf{D}$
are the direct sum
of the non-zero eigenvalues
of $\mathbf{D}_{[1]}$ and of $\mathbf{D}_{[2]}$
plus the zero eigenvalue
with degeneracy $\beta_0 + \beta_1 + \beta_2$

Eigenvectors of the Dirac operator

Due to the Dirac decomposition

the eigenvectors of the Dirac operator $\mathbf{D}$

are the eigenvectors

corresponding to non-zero eigenvalues

of $\mathbf{D}_{[1]}$ or of $\mathbf{D}_{[2]}$

r the harmonic eigenvectors of $\mathbf{D}$

$$\mathbf{\Phi} = \begin{pmatrix} \mathbf{\Phi}^{[1]} & \mathbf{\Phi}^{[2]} & \mathbf{\Phi}^{harm} \end{pmatrix}$$

With $\mathbf{\Phi}^{[1]}$ localised on nodes and links and

$\mathbf{\Phi}^{[2]}$ localised on links and triangles

Eigenvalues of $\mathbf{D}_{[n]}$

The eigenstates of $\mathbf{D}_{[n]}$ satisfy

$$\mu \mathbf{s} = \mathbf{D}_{[n]} \mathbf{s}$$

with $\mathbf{s} = (\mathbf{s}_0, \mathbf{s}_1, \mathbf{s}_2)^\top$ which leads to

$$\mu \mathbf{s}_{n-1} = \mathbf{B}_n \mathbf{s}_n$$
$$\mu \mathbf{s}_n = \mathbf{B}_n^\top \mathbf{s}_{n-1}$$

It follows that $\mathbf{s}_{n-1}, \mathbf{s}_n$ are respectively the left and right singular vectors of $\mathbf{B}_n$ with eigenvalue λ and $\mu = \pm |\lambda|$

Matter-antimatter symmetry…

For every singular value $\lambda \neq 0$ of $\bar{\mathbf{B}}_{[n]}$

corresponding to the singular vectors $\mathbf{u}_\lambda, \mathbf{v}_\lambda$

the Dirac operator admits

a positive eigenvalue $\mu = |\lambda|$ with eigenvector $\boldsymbol{\phi}_\lambda^{[+]} = \begin{pmatrix} \mathbf{u}_\lambda \\ \mathbf{v}_\lambda \end{pmatrix}$

and

a negative eigenvalue $\mu = -|\lambda|$ with eigenvector $\boldsymbol{\phi}_\lambda^{[-]} = \begin{pmatrix} \mathbf{u}_\lambda \\ -\mathbf{v}_\lambda \end{pmatrix}$

…and its violation

The zero eigenvectors of $\mathbf{D}_{[n]}$

are linear combinations of the zero eigenvectors of $\mathbf{B}_{[n]}$

they can be only localised on n-dimensional

or on (n-1)-dimensional simplices

The degeneracy the zero eigenvalue is given by

the sum of the Betti numbers $\beta_{n-1} + \beta_n$

Eigenvectors or the Dirac operator

In summary the eigenvectors of the Dirac operator

defined on a simplicial complex of dimension 2 have the structure

$$\boldsymbol{\Phi} = \begin{pmatrix} \mathbf{U}^{[1]} & \mathbf{U}^{[1]} & \mathbf{0} & \mathbf{0} & \mathbf{U}_0^{harm} & \mathbf{0} & \mathbf{0} \\ \mathbf{V}^{[1]} & -\mathbf{V}^{[1]} & \mathbf{U}^{[2]} & \mathbf{U}^{[2]} & \mathbf{0} & \mathbf{U}_1^{harm} & \mathbf{0} \\ \mathbf{0} & \mathbf{0} & \mathbf{V}^{[2]} & -\mathbf{V}^{[2]} & \mathbf{0} & \mathbf{0} & \mathbf{U}_2^{harm} \end{pmatrix}$$

Topological Dirac equation on simplicial complexes

- The topological Dirac equation can be extended to simplicial complexes, in the case of zero mass it is given by

$$i\partial_t \boldsymbol{\psi} = \mathbf{D}\boldsymbol{\psi}$$

- It can be shown that thanks to the Hodge decomposition this equation leads to a multi-band spectrum of the energy states.

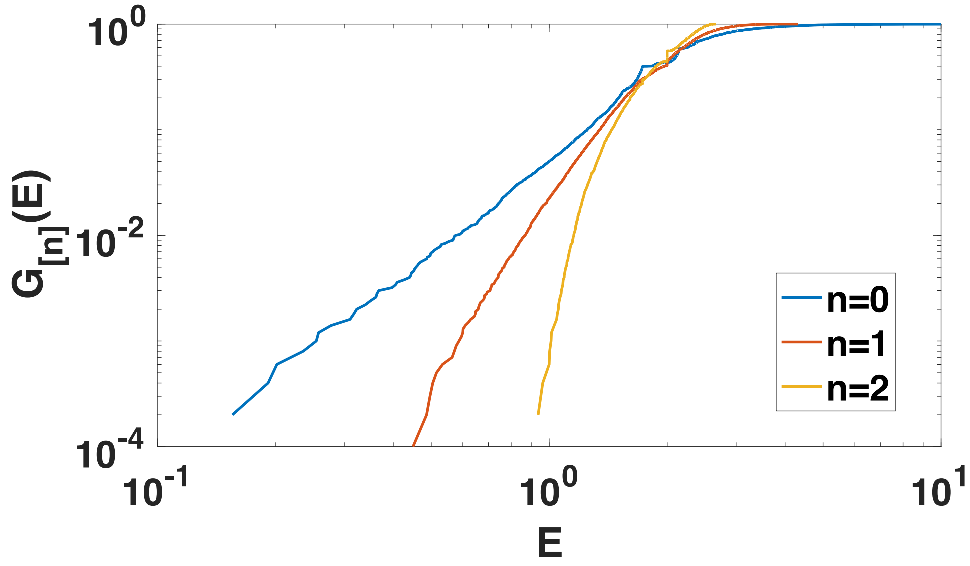

Multi-band eigenspectrum of the Topological Dirac equation on a 3-dimensional NGF

Dirac Signal Processing

Signal Processing with the Hodge Laplacians

Given a **noisy topological signal defined exclusively on a given dimension of the simplicial complex:** $\tilde{\mathbf{s}} = \mathbf{s} + \boldsymbol{\epsilon}$ with $\boldsymbol{\epsilon}$ noise, how can we reconstruct $\mathbf{s}$?

1. By ensuring the reconstructed $\hat{\mathbf{s}}$ is close to $\tilde{\mathbf{s}}$
2. With a regularisation enforced by the Hodge Laplacian

Hodge Laplacian filter: $\hat{\mathbf{s}} =$ argmin $\left\{ ||\tilde{\mathbf{s}} - \hat{\mathbf{s}}||_2^2 + \tau \hat{\mathbf{s}}^T \mathbf{L} \hat{\mathbf{s}} \right\}$

(Barbarossa et. al., 2020, Schaub et al. 2022)

Topological signals of different dimension are processed independently

Edge signals and the Hodge decomposition

The edge signal can be decomposed Into harmonic flow, gradient flow ard curl flow thanks to Hodge decomposition

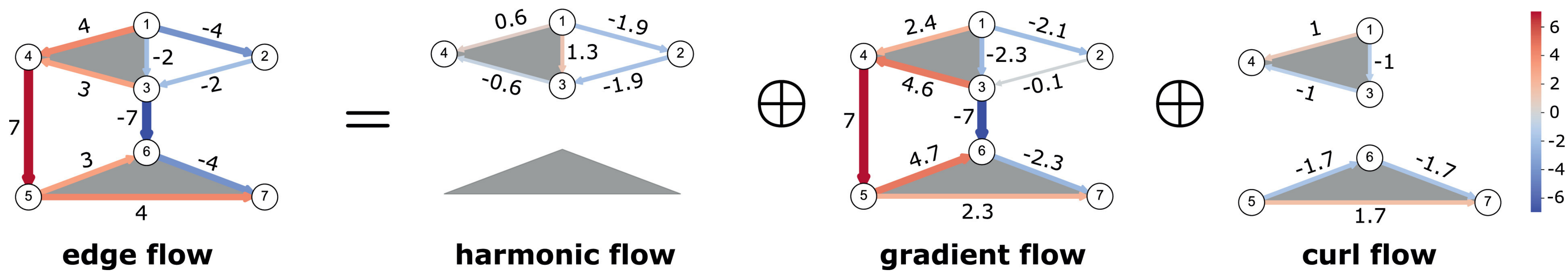

Schaub et al. 2022

Signal Processing with the Hodge Laplacian

Hodge Laplacian filter

$$\hat{\mathbf{s}} = \text{argmin} \left\{ ||\tilde{\mathbf{s}} - \hat{\mathbf{s}}||_2^2 + \tau \hat{\mathbf{s}}^T \mathbf{L} \hat{\mathbf{s}} \right\}$$

has solution

$$\hat{\mathbf{s}} = \left[\mathbf{I} + \tau \mathbf{L}_{[n]}\right]^{-1} \tilde{\mathbf{s}}$$

The Hodge Laplacian filter processes independently the solenoidal and the irrotational components of the signal

It is effective in presenting stable curl flows

Dirac Signal Processing

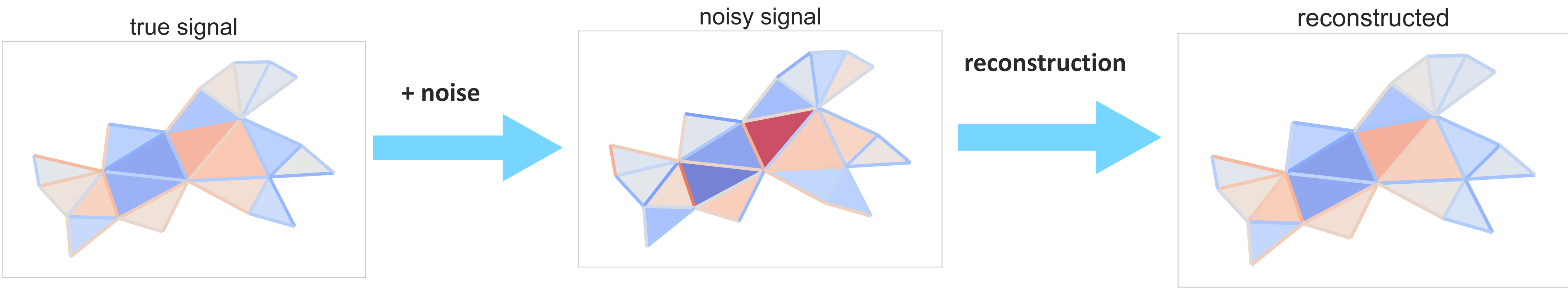

The Dirac operator allows us to filter out nodes and links signals **jointly**

L. Calmon, M. Schaub and G. Bianconi
Dirac signal processing of topological signals
(2023)

Processing with the Dirac operator

Given a **noisy topological signal defined on simplices of different dimension**

$\tilde{\mathbf{s}} = \mathbf{s} + \boldsymbol{\epsilon}$ with $\boldsymbol{\epsilon}$ noise

Joint-filtering with the Dirac:

$$\hat{\mathbf{s}} = \text{argmin} \left\{ ||\tilde{\mathbf{s}} - \hat{\mathbf{s}}||_2^2 + \tau \hat{\mathbf{s}}^T (\mathbf{D} - m\mathbf{I})^2 \, \hat{\mathbf{s}} \right\}$$

$m > 0 \rightarrow$ higher cost negative components

$m < 0 \rightarrow$ higher cost to positive components

Processing with the Dirac operator

Given a **noisy topological signal defined on simplices of different dimension**

$\tilde{\mathbf{s}} = \mathbf{s} + \boldsymbol{\epsilon}$ with $\boldsymbol{\epsilon}$ noise

Joint-filtering with the Dirac:

$$\hat{\mathbf{s}} = \text{argmin} \left\{ ||\tilde{\mathbf{s}} - \hat{\mathbf{s}}||_2^2 + \tau \hat{\mathbf{s}}^T (\mathbf{D} - m\mathbf{I})^2 \hat{\mathbf{s}} \right\}$$

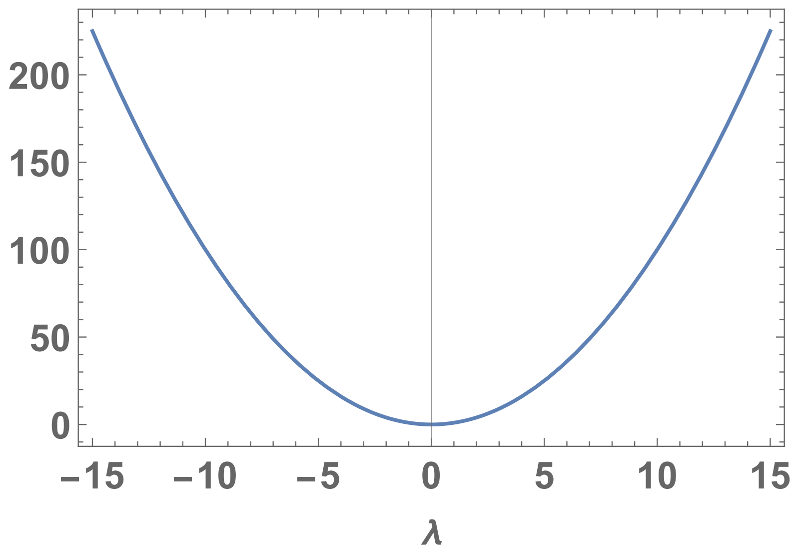

Regularization for $m = 0$

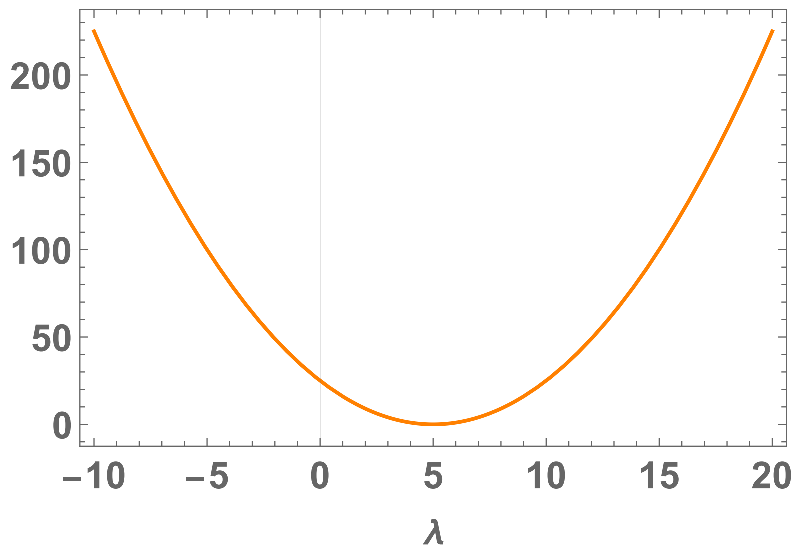

Regularization for $m = 5$

Dirac Signal Processing

Hodge Laplacian filter

$$\hat{\mathbf{s}} = \text{argmin} \left\{ ||\tilde{\mathbf{s}} - \hat{\mathbf{s}}||_2^2 + \tau \hat{\mathbf{s}}^T \left(\mathbf{D} - m\mathbf{I}\right)^2 \hat{\mathbf{s}} \right\}$$

has solution

$$\hat{\mathbf{s}} = \left[\mathbf{I} + \tau(\mathbf{D} - m\mathbf{I})^2\right]^{-1} \tilde{\mathbf{s}}$$

Dirac signal processing is able to jointly filters signal of different dimensions

Interpretation of the parameter m

The parameter m can be interpreted as

$$\boxed{m = \frac{\mathbf{s}^{\top}\mathbf{D}\mathbf{s}}{\mathbf{s}^{\top}\mathbf{s}}}$$

Which allow us to interpret the regularisation as a minimization of the mean square error of the signal around m

The parameter m can be learned from data

Interpretation of the regularisation term

Let us assume the estimated signal is equal to the true signal, i.e. $\hat{\mathbf{s}} = \mathbf{s}$,
Then regularisation term

$\mathscr{R} = \mathbf{s}^\top(\mathbf{D} - m\mathbf{I})^2\mathbf{s}$ with $m = \dfrac{\mathbf{s}^\top\mathbf{D}\mathbf{s}}{\mathbf{s}^\top\mathbf{s}}$ can be written as

$$\frac{1}{\mathbf{s}^\top\mathbf{s}}\mathscr{R} = \frac{1}{\mathbf{s}^\top\mathbf{s}}\left[\mathbf{s}^T\left(\mathbf{D} - \frac{\mathbf{s}^\top\mathbf{D}\mathbf{s}}{\mathbf{s}^\top\mathbf{s}}\mathbf{I}\right)^2\mathbf{s}\right] = \frac{\mathbf{s}^\top\mathbf{D}^2\mathbf{s}}{\mathbf{s}^\top\mathbf{s}} - \left(\frac{\mathbf{s}^\top\mathbf{D}\mathbf{s}}{\mathbf{s}^\top\mathbf{s}}\right)^2$$

The Florentine Families network:

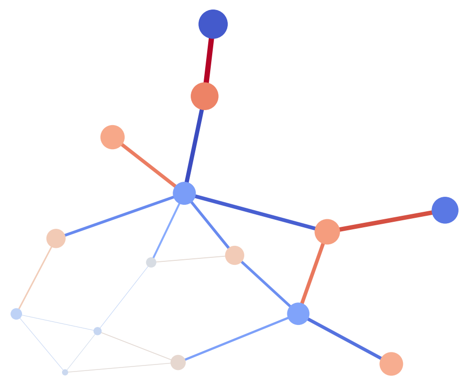

- Simple **network structure**, true signal aligned with an eigenvector of $\mathbf{D}$

Dirac signal processing

$$\hat{\mathbf{s}} = \text{argmin}\left\{ \|\tilde{\mathbf{s}} - \hat{\mathbf{s}}\|_2^2 + \tau \hat{\mathbf{s}}^T \left(\mathbf{D} - m\mathbf{I}\right)^2 \hat{\mathbf{s}} \right\}$$

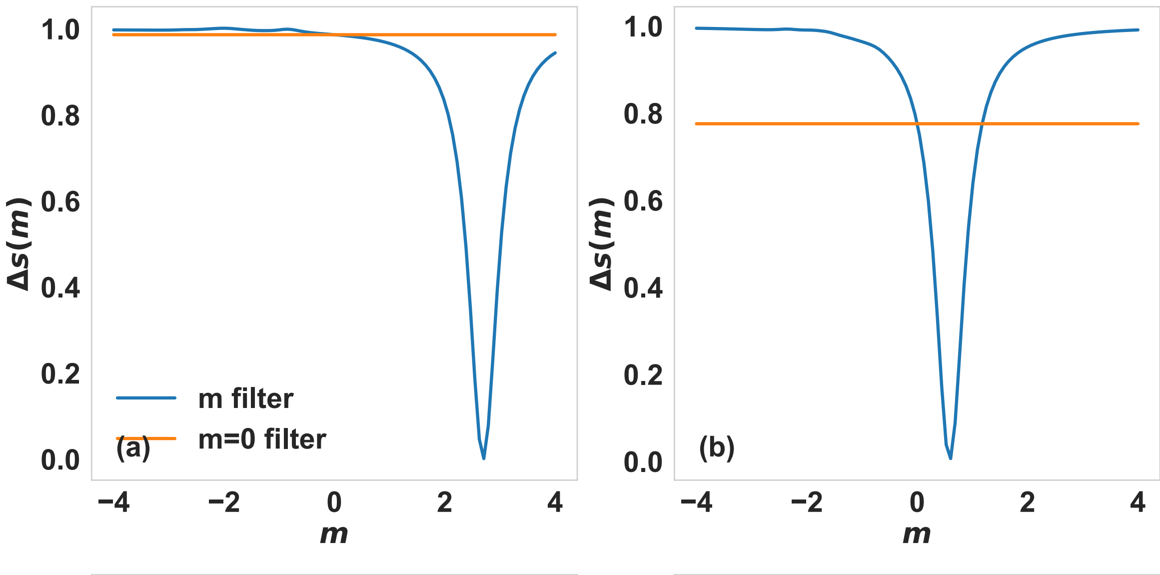

Learning m

$$m = \frac{\mathbf{s}^\top \mathbf{D}\mathbf{s}}{\mathbf{s}^\top \mathbf{s}}$$

Require: Initial guess $\hat{m}_n^{(0)}$, Convergence threshold δ, Learning rate η, Measured data $\tilde{\mathbf{s}}_{[n]}$

$t \leftarrow 0$

$\hat{m}_n(t=0) \leftarrow \hat{m}_n^{(0)}$

while $|\hat{m}_n(t) - \hat{m}_n(t-1)| < \delta$ **do**

$t \leftarrow t+1$

$\hat{\mathbf{s}}_{[n]} \leftarrow [\mathbf{I} + \tau(\mathbf{D}_{[n]} - m_n\mathbf{I})^2]^{-1}\tilde{\mathbf{s}}_{[n]}$

$\hat{m}_n(t+1) \leftarrow (1-\eta)\hat{m}_n(t) + \eta\frac{\hat{\mathbf{s}}_{[n]}^\top \mathbf{D}_{[n]}\hat{\mathbf{s}}_{[n]}}{\hat{\mathbf{s}}_{[n]}^\top \hat{\mathbf{s}}_{[n]}}$

end while

Learning m

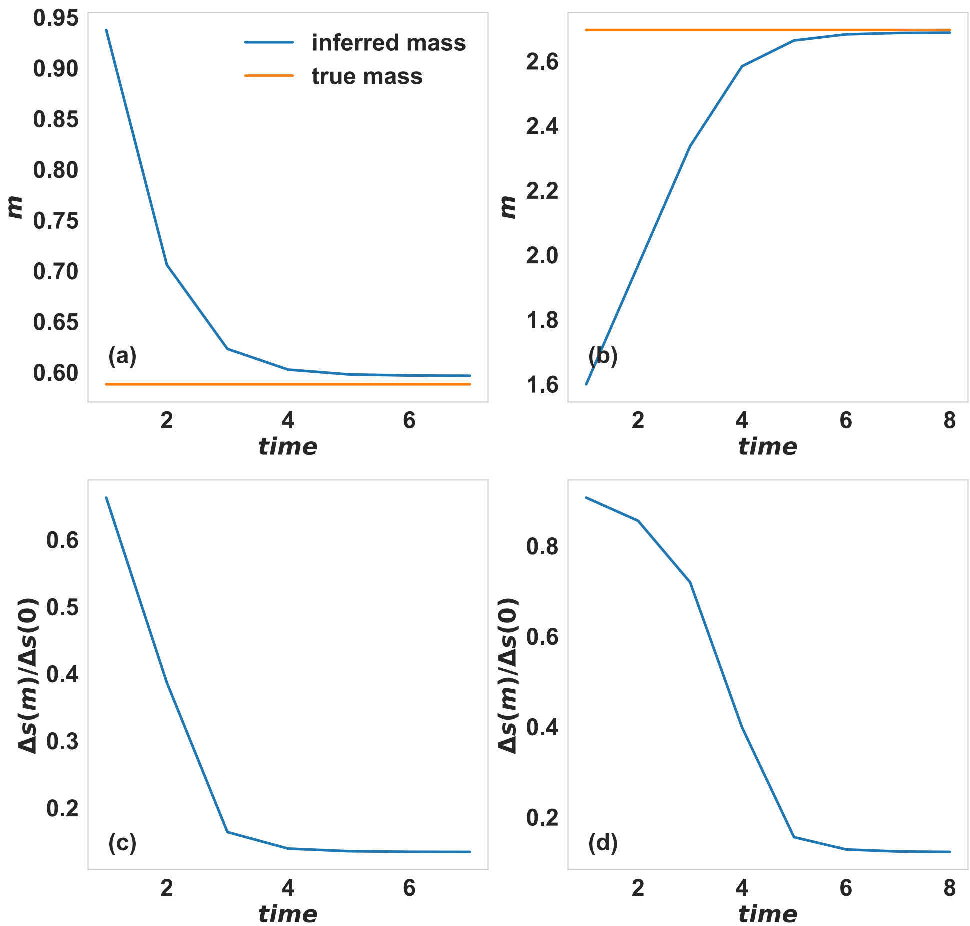

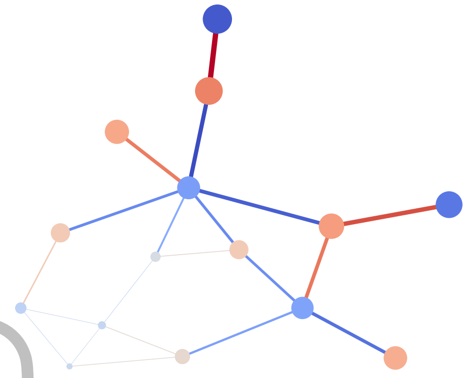

$$\boxed{m = \frac{\mathbf{s}^\top \mathbf{D} \mathbf{s}}{\mathbf{s}^\top \mathbf{s}}}$$

Learning m

Require: Initial guess $\hat{m}_n^{(0)}$, Convergence threshold δ, Learning rate η, Measured data $\tilde{\mathbf{s}}_{[n]}$

$t \leftarrow 0$

$\hat{m}_n(t=0) \leftarrow \hat{m}_n^{(0)}$

while $|\hat{m}_n(t) - \hat{m}_n(t-1)| < \delta$ **do**

$\quad t \leftarrow t+1$

$\quad \hat{\mathbf{s}}_{[n]} \leftarrow [\mathbf{I} + \tau(\mathbf{D}_{[n]} - m_n \mathbf{I})^2]^{-1} \tilde{\mathbf{s}}_{[n]}$

$\quad \hat{m}_n(t+1) \leftarrow (1-\eta)\hat{m}_n(t) + \eta \frac{\hat{\mathbf{s}}_{[n]}^\top \mathbf{D}_{[n]} \hat{\mathbf{s}}_{[n]}}{\hat{\mathbf{s}}_{[n]}^\top \hat{\mathbf{s}}_{[n]}}$

end while

Dirac signal processing on the Network Geometry with Flavor

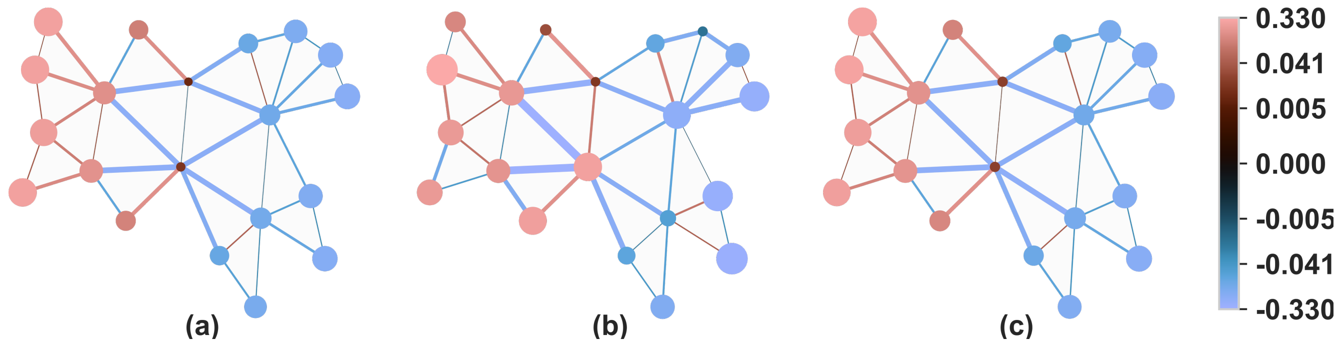

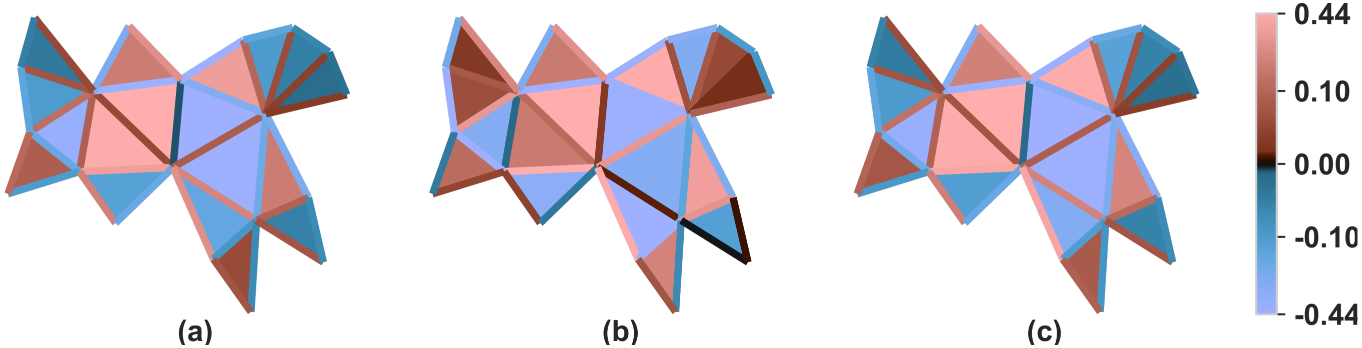

Dirac signal processing on buoys data

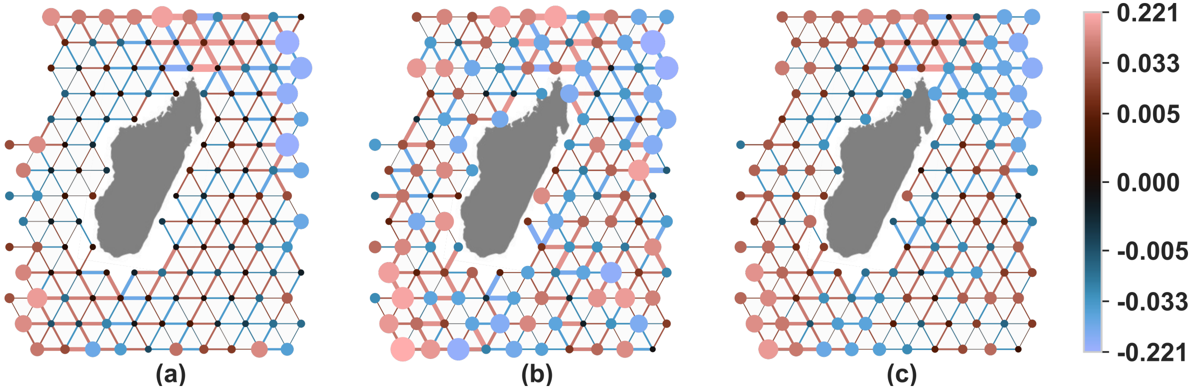

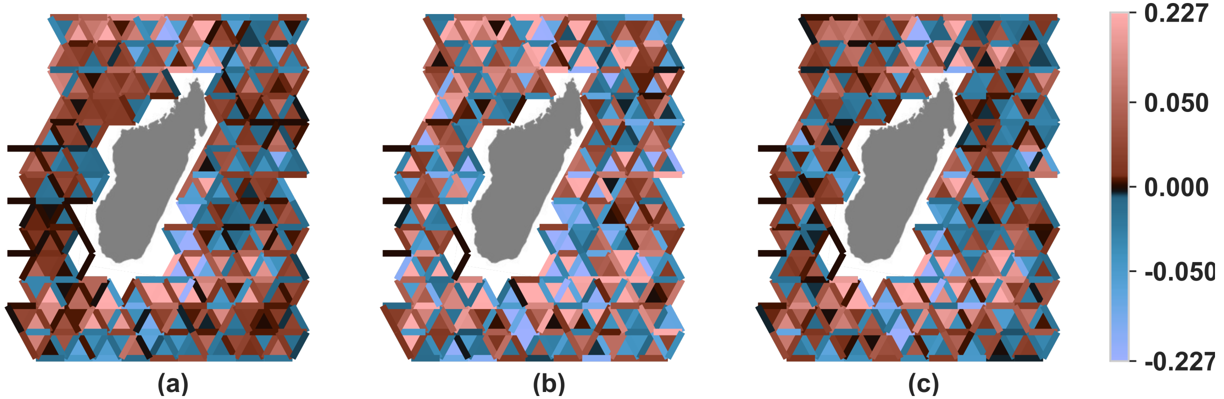

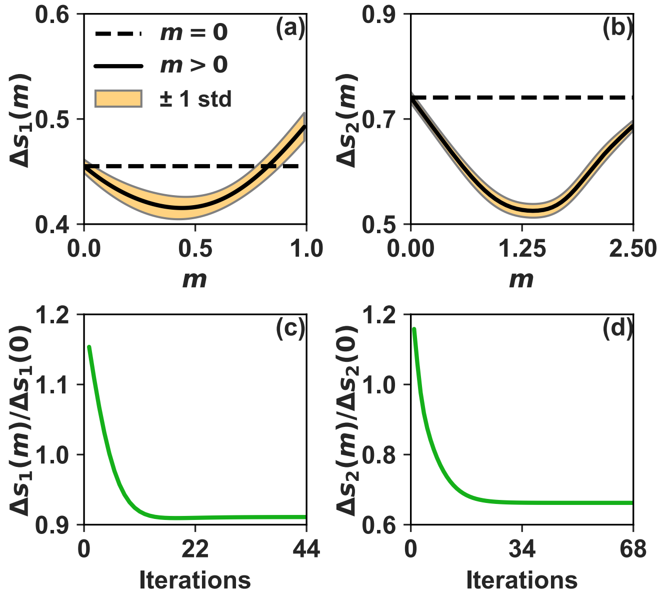

Dirac equation lattices:
combing the Dirac operator with algebra

G. Bianconi,

Topological Dirac equation on networks and simplicial complexes JPhys Complexity (2021)

G.Bianconi,

Dirac gauge theory for topological spinors in 3+ 1 dimensional networks. *arXiv preprint arXiv:2212.05621 (2022)*.

Directional Dirac operator on lattices

On a lattice links have different directions

The Directional Dirac operator induces a
phase rotation of the topological signal depending on the direction of the links

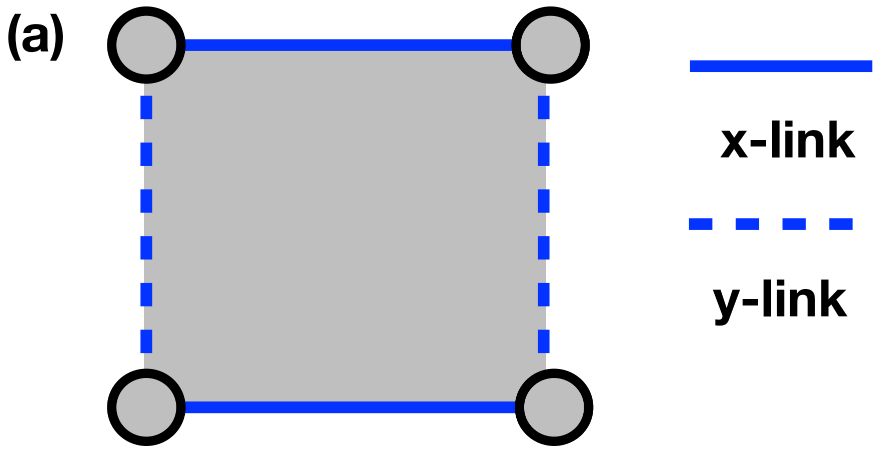

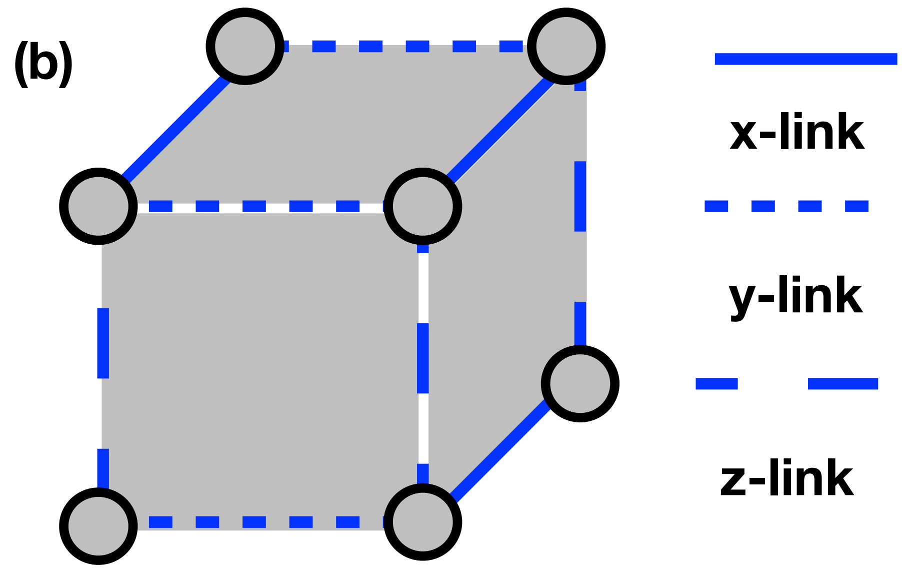

Topological spinor for 3-dimensional lattice

In order to treat every type of link differently

by inducing different rotations of the topological spinor,

in 3-d we need to consider the spinor $\boldsymbol{\Psi}$ formed by two 0-cochains and two 1-cochains, i.e.

$$\boldsymbol{\Psi} = \begin{pmatrix} \boldsymbol{\Phi} \\ \mathbf{X} \end{pmatrix},$$

with

$$\boldsymbol{\Phi} = \begin{pmatrix} \phi^{(1)} \\ \phi^{(2)} \end{pmatrix}, X = \begin{pmatrix} \chi^{(1)} \\ \chi^{(2)} \end{pmatrix}$$

Directional Boundary operators and graph Laplacians on 3-dimensional lattice

We consider directional boundary operators only acting between nodes and w-type links

$$[\mathbf{B}_{(w)}]_{i\ell} = \begin{cases} 1 \text{ if } \ell = [j,i] \text{ and } \ell \text{ is a type } w\text{–link} \\ -1 \text{ if } \ell = [i,j] \text{ and } \ell \text{ is a type } w\text{–link} \\ 0 \text{ otherwise} \end{cases}$$

This allows to define the directional graph Laplacians

$$\mathbf{L}_{(w)} = \mathbf{B}_{(w)}\mathbf{B}_{(w)}^{\top}$$

whose sum gives the graph Laplacian of the network

$$\mathbf{L} = \mathbf{L}_{(x)} + \mathbf{L}_{(y)} + \mathbf{L}_{(z)}$$

Note that on square lattices we have that the directional Laplacian commute

$$[\mathbf{L}_{(w)}, \mathbf{L}_{(w')}] = \mathbf{0}$$

Directional Dirac operators on 3-dimensional lattice

In 3d the Directional Dirac operators are defined as

$$\mathbf{D}_{(w)} = \begin{pmatrix} \mathbf{0} & \mathscr{B}_{(\mathbf{w})} \\ \mathscr{B}^{\dagger}_{(\mathbf{w})} & \mathbf{0} \end{pmatrix}$$

with

$$\mathscr{B}_{(x)} = \boldsymbol{\sigma}_1(\mathbf{B}_{(x)}), \qquad \mathscr{B}_{(y)} = \boldsymbol{\sigma}_2(\mathbf{B}_{(y)}), \qquad \mathscr{B}_{(z)} = \boldsymbol{\sigma}_3(\mathbf{B}_{(z)}),$$

where we make use of the Pauli matrices

$$\boldsymbol{\sigma}_1(\mathbf{F}) = \begin{pmatrix} \mathbf{0} & \mathbf{F} \\ \mathbf{F} & \mathbf{0} \end{pmatrix}, \qquad \boldsymbol{\sigma}_2(\mathbf{F}) = \begin{pmatrix} \mathbf{0} & -i\mathbf{F} \\ i\mathbf{F} & \mathbf{0} \end{pmatrix}, \qquad \boldsymbol{\sigma}_3(\mathbf{F}) = \begin{pmatrix} \mathbf{F} & \mathbf{0} \\ \mathbf{0} & -\mathbf{F} \end{pmatrix}.$$

Topological Dirac equation on 3-dimensional lattice

The Topological Dirac equation in 3d lattice is given by

$$i\partial_t \boldsymbol{\Psi} = (\not{\mathbf{D}} + m\boldsymbol{\beta})\boldsymbol{\Psi}$$

where

$$\not{\mathbf{D}} = \sum_{w \in \{x,y,z\}} \mathbf{D}_{(w)}$$

and

$$\boldsymbol{\beta} = \begin{pmatrix} \mathbf{1} & \mathbf{0} \\ \mathbf{0} & -\mathbf{1} \end{pmatrix}$$

Dispersion relations and anti-commutation relations

The dispersion relation remain relativistic

$$E^2 = m^2 + |\lambda_x|^2 + |\lambda_y|^2 + |\lambda_z|^2$$

with $\lambda_{(w)}$ indicating the eigenvalue of the directional boundary operator $\mathbf{B}_{(w)}$

despite the directional Dirac operators do not commute or anti-commute

$$[\mathbf{D}_{(x)}, \mathbf{D}_{(y)}] = \begin{pmatrix} \mathbf{0} & \mathbf{0} \\ \mathbf{0} & \mathrm{i}\boldsymbol{\sigma}_{\mathrm{z}}(\mathbf{B}_{(\mathrm{x})}\mathbf{B}^{\dagger}_{(\mathrm{y})} + \mathbf{B}_{(\mathrm{y})}\mathbf{B}^{\dagger}_{(\mathrm{x})}) \end{pmatrix} \qquad \{\mathbf{D}_{(x)}, \mathbf{D}_{(y)}\} = \begin{pmatrix} \mathbf{0} & \mathbf{0} \\ \mathbf{0} & \mathrm{i}\boldsymbol{\sigma}_{\mathrm{z}}(\mathbf{B}^{\dagger}_{(\mathrm{x})}\mathbf{B}_{(\mathrm{y})} - \mathbf{B}^{\dagger}_{(\mathrm{y})}\mathbf{B}_{(\mathrm{x})}) \end{pmatrix}$$

The Directional Dirac operator of Multiplex Networks

Multilayer Networks

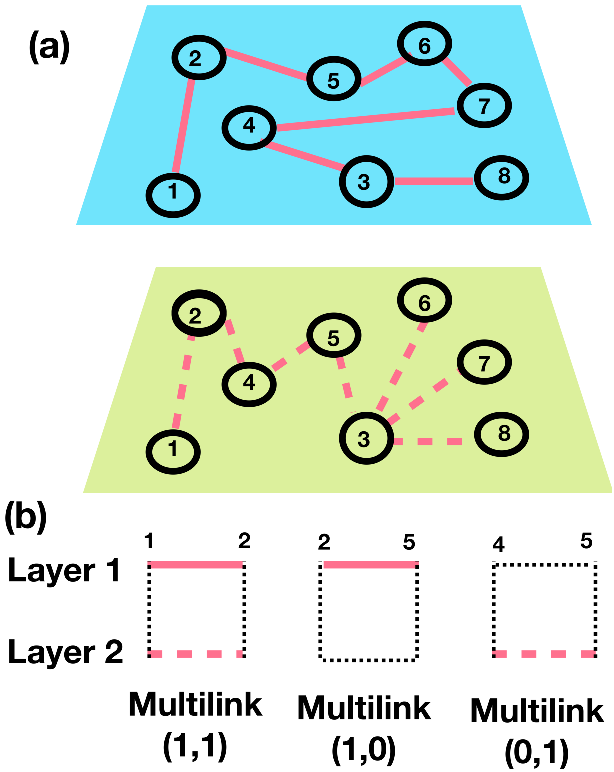

G. Bianconi PRE (2013)

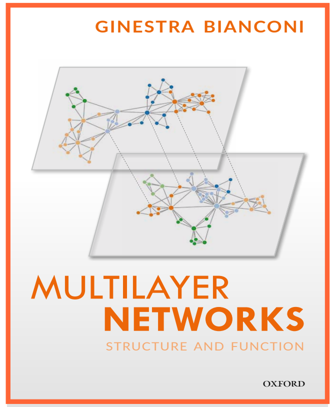

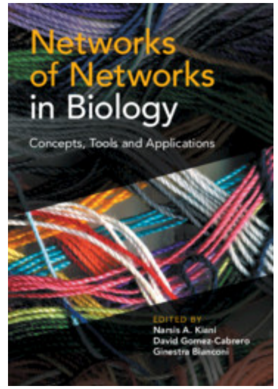

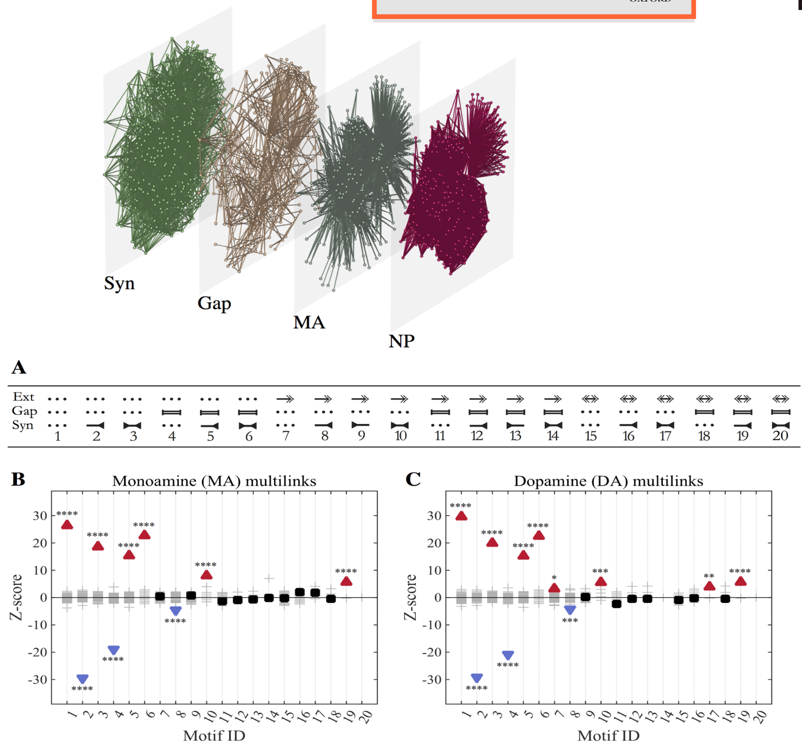

Multilayer connectome of c.elegans, Bentley et al (2016)

Application to multiplex networks

We can "blindly" use the directional Dirac operators of 3d lattices for multiplex networks where one distinguish between different types of multilinks

The dispersion relation is relativistic

$$E^2 = m^2 + \mu$$

With μ indicating the eigenvalue of

$$\mathbf{L} = \mathbf{L}_{(1,0)} + \mathbf{L}_{(0,1)} + \mathbf{L}_{(1,1)}$$

Note however that in practically all multiplex networks the graphical Laplacians do not commute

$$[\mathbf{L}_{\vec{m}}, \mathbf{L}_{\vec{m}'}] \neq \mathbf{0}$$

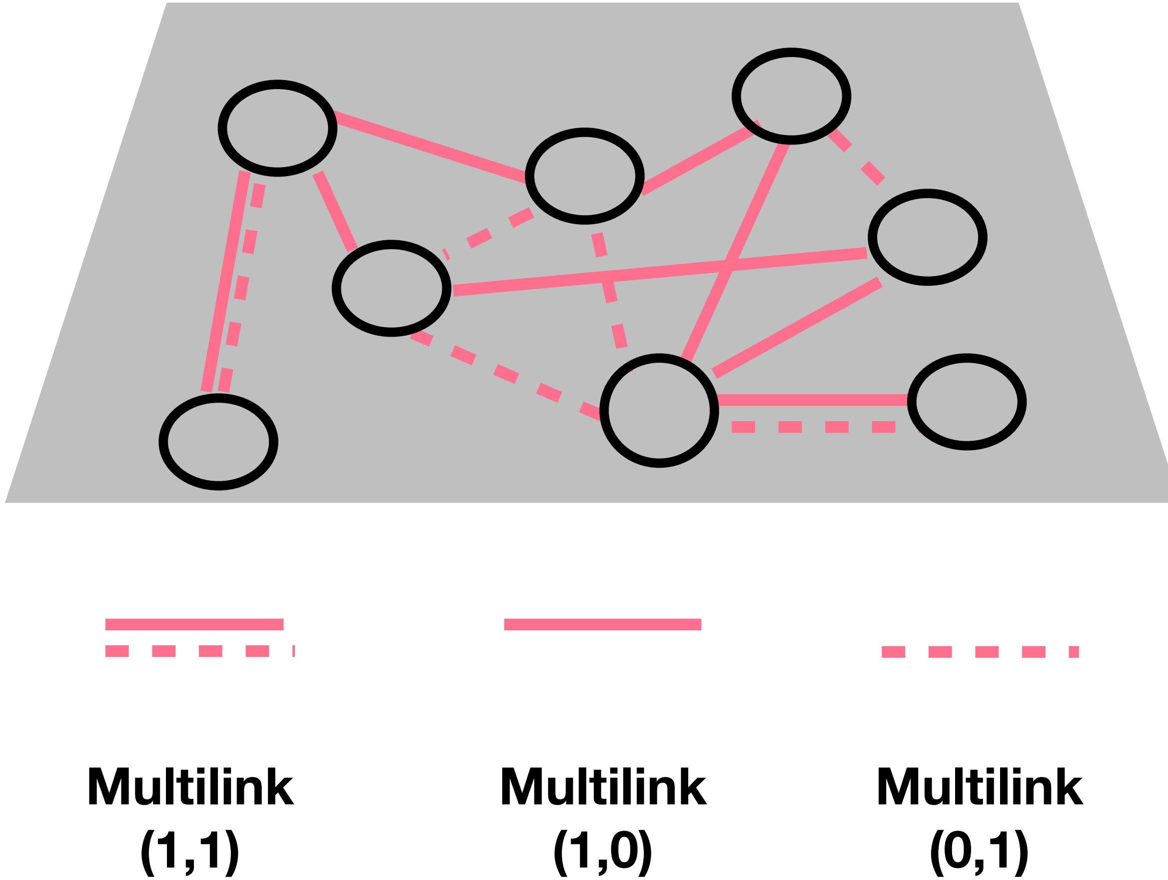

Conclusions

- The Dirac operator can be used to treat topological signals defined on simplices of different dimensions (nodes, links, triangles, etc)
- The Dirac operator is a powerful way to couple dynamics on different dimension including Dirac synchronisation and Dirac Turing patterns
- Dirac signal processing allows to filter simultaneously topological signals on nodes links and triangles
- The Dirac operator can be efficiently combined with a suitable algebra in order to take into account for different directionalities of the links

Lesson Vb:
Effect of geometrical and combinatorial properties of higher-order networks on dynamics

- **Interplay between network geometry and dynamics**
  - **The effect of the spectral dimension on sychronization**
  - **Percolation on hyperbolic geometry**
- **Triadic interactions and triadic percolation**

Higher-order structure and dynamics

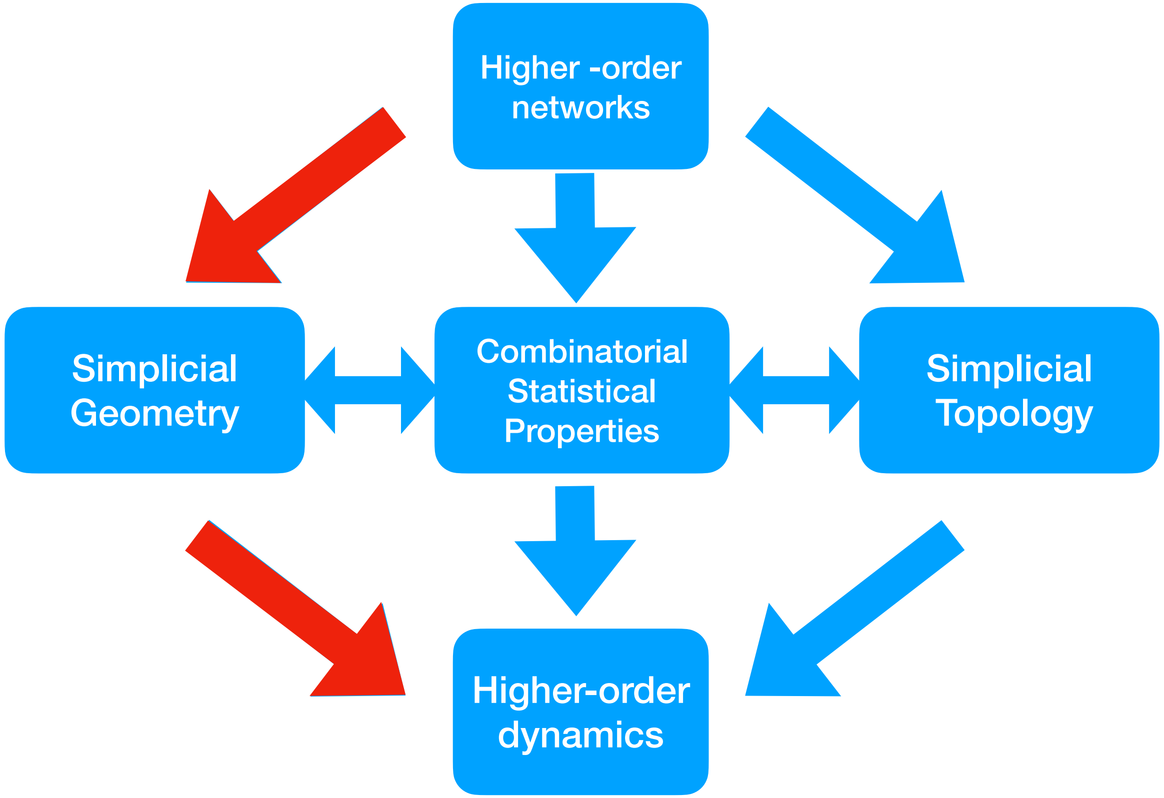

Synchronization
on simplicial complex skeletons
with finite spectral dimension

The role of dimensionality in neuronal dynamics

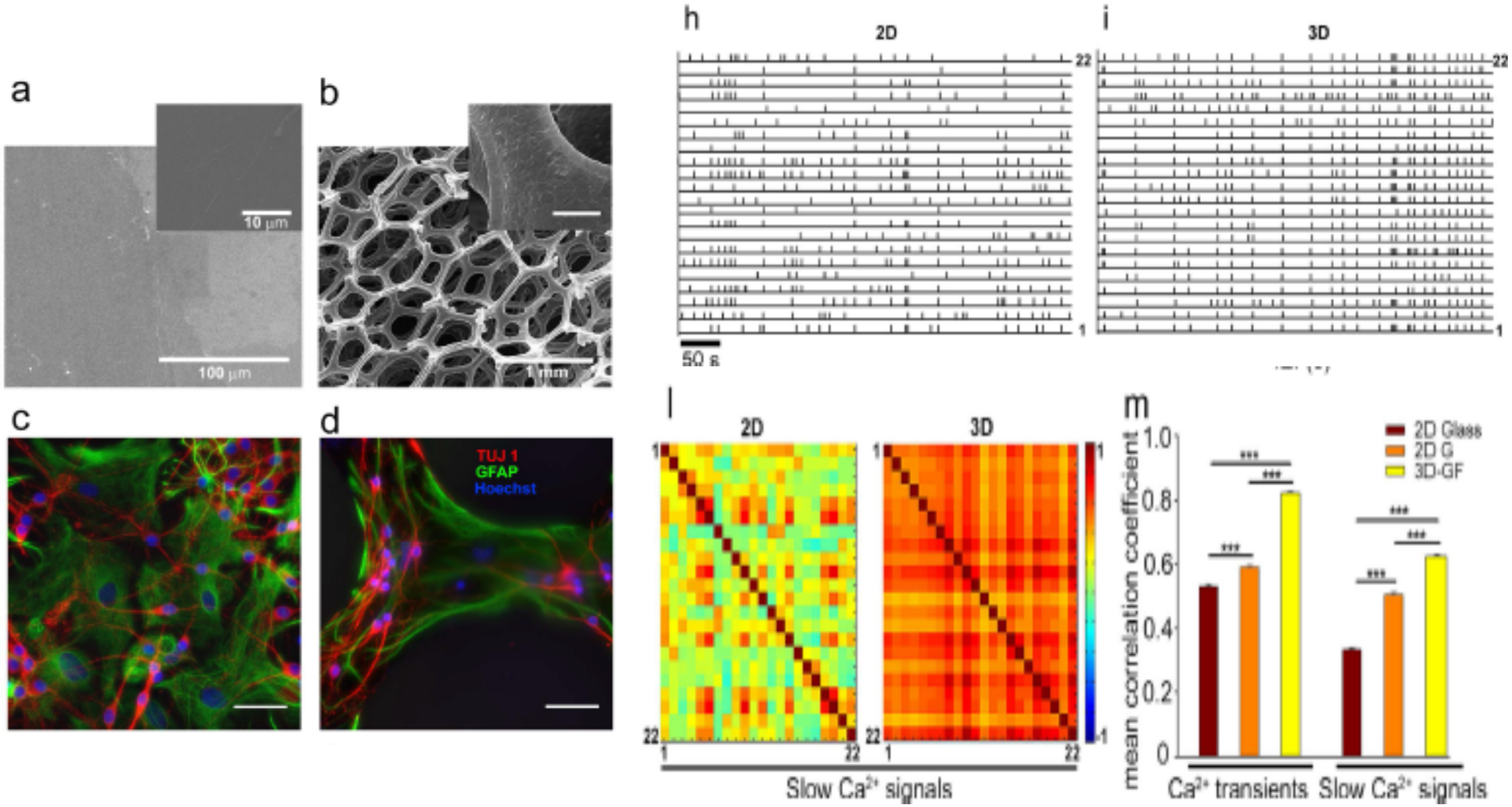

Uloa Severino et al. Scientific Reports (2016)

Kuramoto model on a network

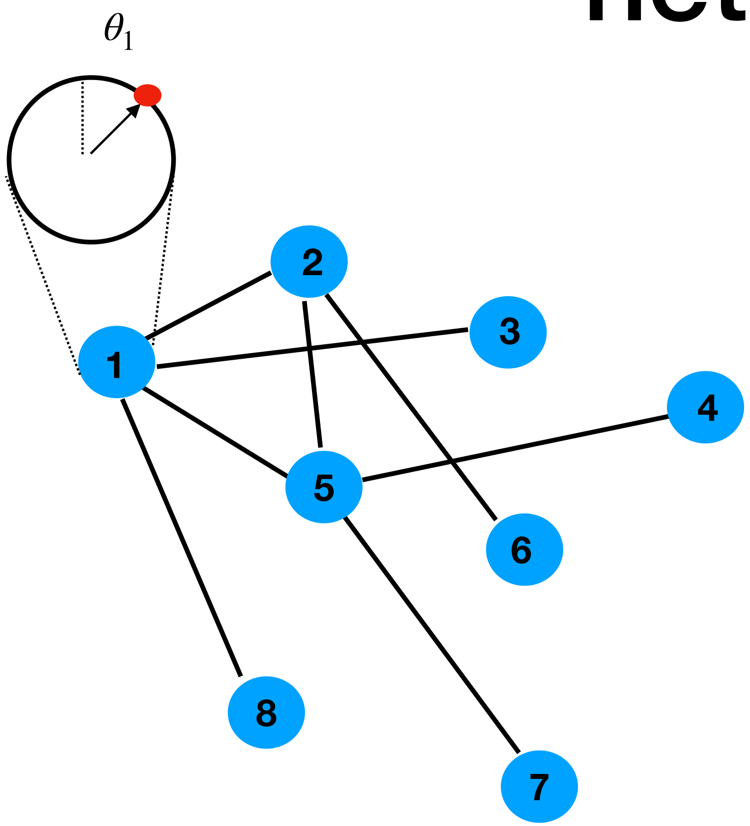

Given a network of N nodes
defined by an adjacency matrix a
we assign to each node a phase obeying

$$\dot{\theta}_i = \omega_i + \sigma \sum_{j=1}^{N} a_{ij} \sin\left(\theta_j - \theta_i\right)$$

where the internal frequencies of the nodes
are drawn randomly from

$$\omega \sim \mathcal{N}(\Omega, 1)$$

and the coupling constant is σ

The oscillators are non-identical

Order parameter for synchronization

We consider the global order parameter R

$$R = \frac{1}{N}\left|\sum_{i=1}^{N} e^{\mathrm{i}\,\theta_i}\right|$$

which indicates the

synchronisation transition such that for

$$|\sigma - \sigma_c| \ll 1$$

$$R = \begin{cases} 0 & \textbf{for } \sigma < \sigma_c \\ c(\sigma - \sigma_c)^{1/2} & \textbf{for } \sigma \geq \sigma_c \end{cases}$$

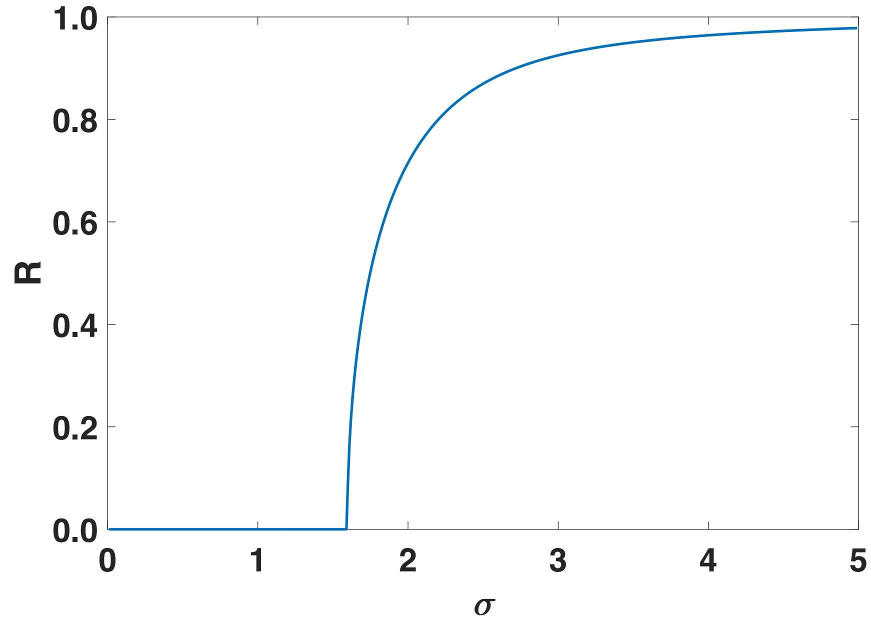

Kuramoto (1975)

Network Geometry with Flavor

Starting from a single d-dimensional simplex

GROWTH :

At every timestep we add a new d-dimensional simplex

(formed by one new node and an existing (d-1)-face).

ATTACHMENT:

The probability that a new node will be connected to a face μ depends on the flavor s=-1,0,1 and is given by

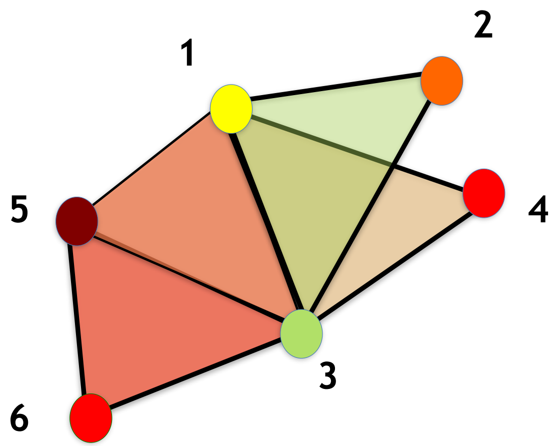

$$\Pi_\alpha^{[s]} = \frac{(1 + sn_\alpha)}{\sum_{\alpha'}(1 + sn_{\alpha'})}$$

Bianconi & Rahmede (2016)

Emergent Hyperbolic geometry

The emergent hidden geometry is the hyperbolic H^d space
Here all the links have equal length

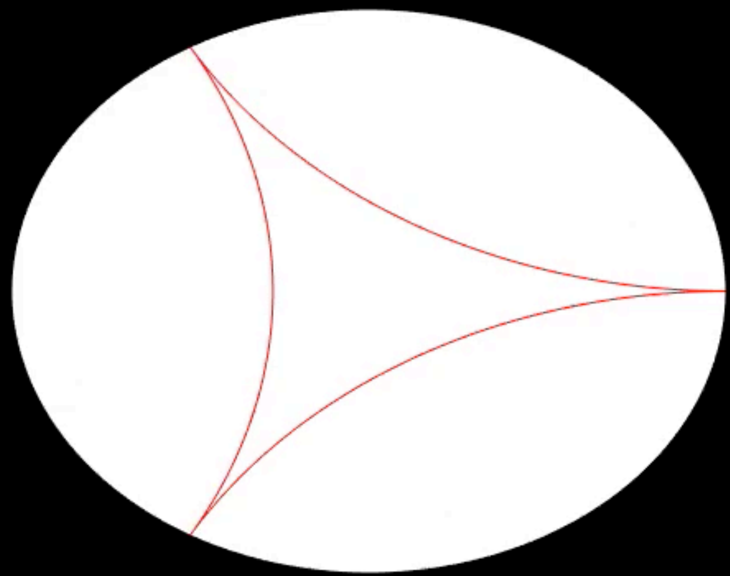

d=2

Emergent hyperbolic geometry

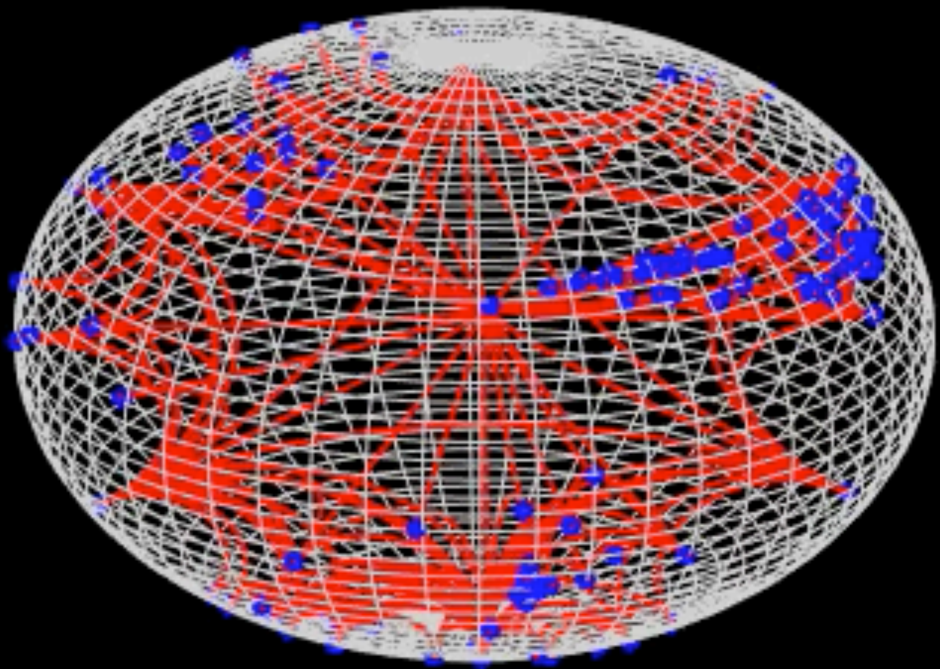

d-dimensional NGF of flavor $s = -1$
can be interpreted as $D = d - 1$ topologies
if we neglect the volume of d-simplices

Spectral dimensions of NGF and s=-1

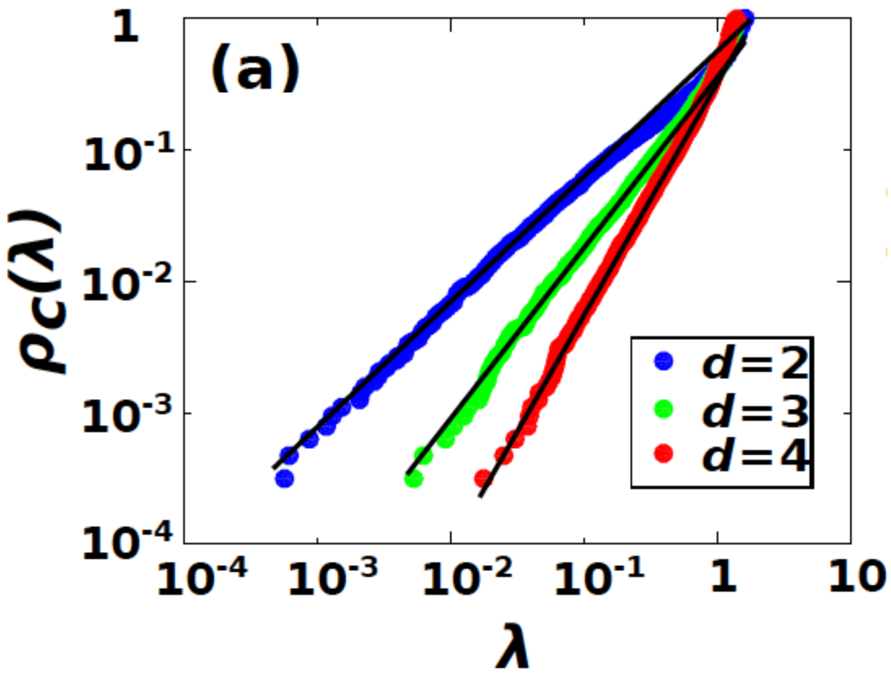

In order to test that these networks have a finite spectral dimension and a density of eigenvalues

$\rho(\lambda) \sim \lambda^{d_S/2-1}$ **for** $\lambda \ll 1$

We consider the cumulative density of eigenvalues

$\rho_c(\lambda) \sim \lambda^{d_S/2}$ **for** $\lambda \ll 1$

NGF have finite spectral dimension with

$d_S \sim d$ **for** $d = 2,3,4$

Millan et al. Sci. Rep. (2018); Millan et al. PRE (2019)

Frustrated synchronisation

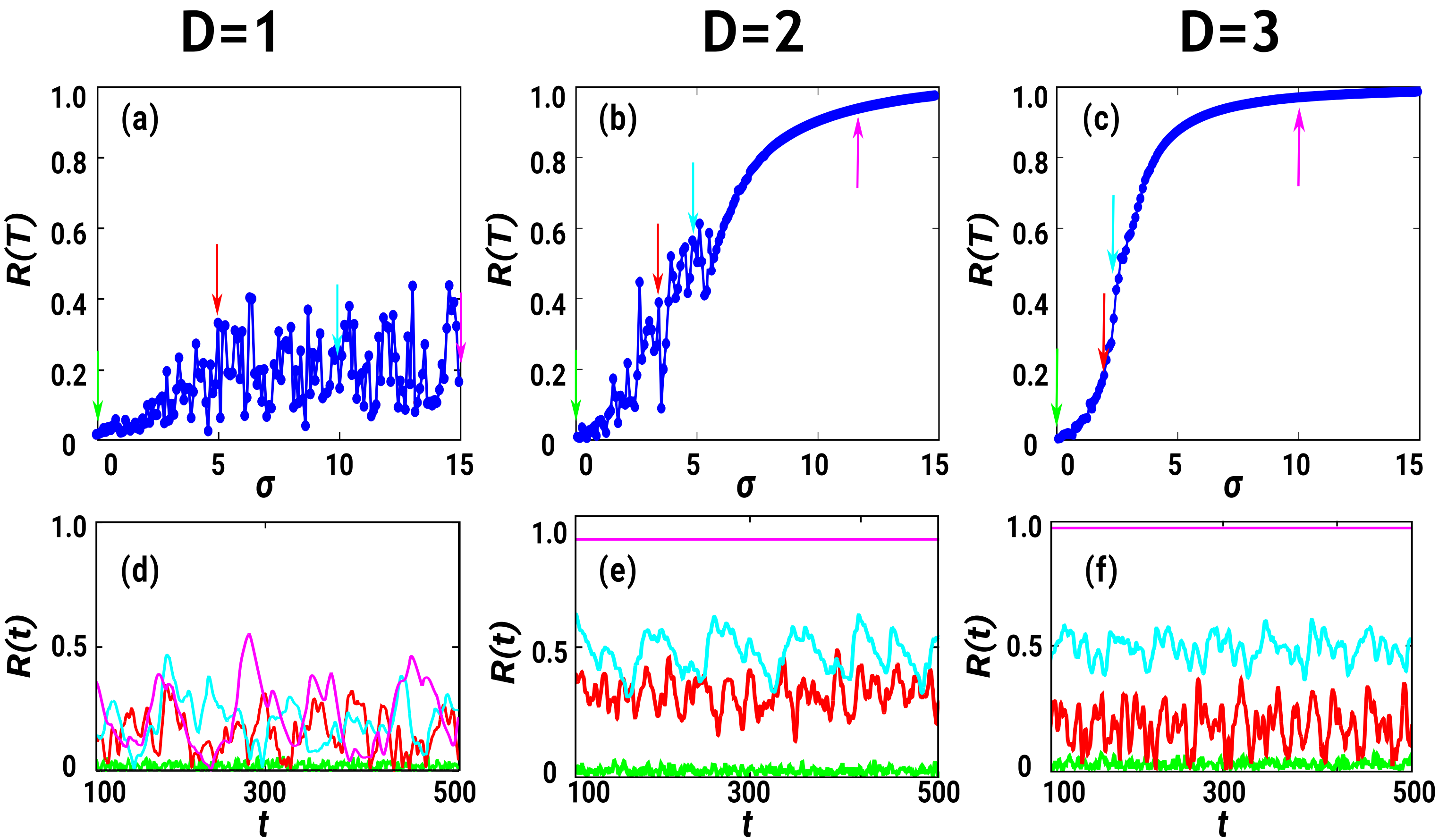

Millan et al. Sci. Rep. (2018); Millan et al. PRE (2019)

Linearized Kuramoto model

The Kuramoto model describes the dynamics of phases that obey

$$\boxed{\dot{\theta}_i = \omega_i + \sigma \sum_{j=1}^{N} a_{ij} \sin\left(\theta_j - \theta_i\right)}$$

Close to the synchronisation transition

when the phases obey

$$\theta_i = \Omega t + \phi_i \quad \textbf{with} \quad \phi_i \ll 1$$

the dynamics can be linearised obtaining the equations

$$\boxed{\dot{\phi}_i \simeq \omega_i - \Omega - \sigma \sum_{j=1}^{N} L_{ij} \phi_j}$$

Fully synchronized phase and the spectral dimension

The synchronized phase is not thermodynamically achieved

for networks with spectral dimension

$$\boxed{d_S \leq 4}$$

In Complex Network Manifolds with D=3 the fully synchronized state is marginally stable

Millan et al. Sci. Rep. (2018); Millan et al. PRE (2019)

Synchronization of different communities

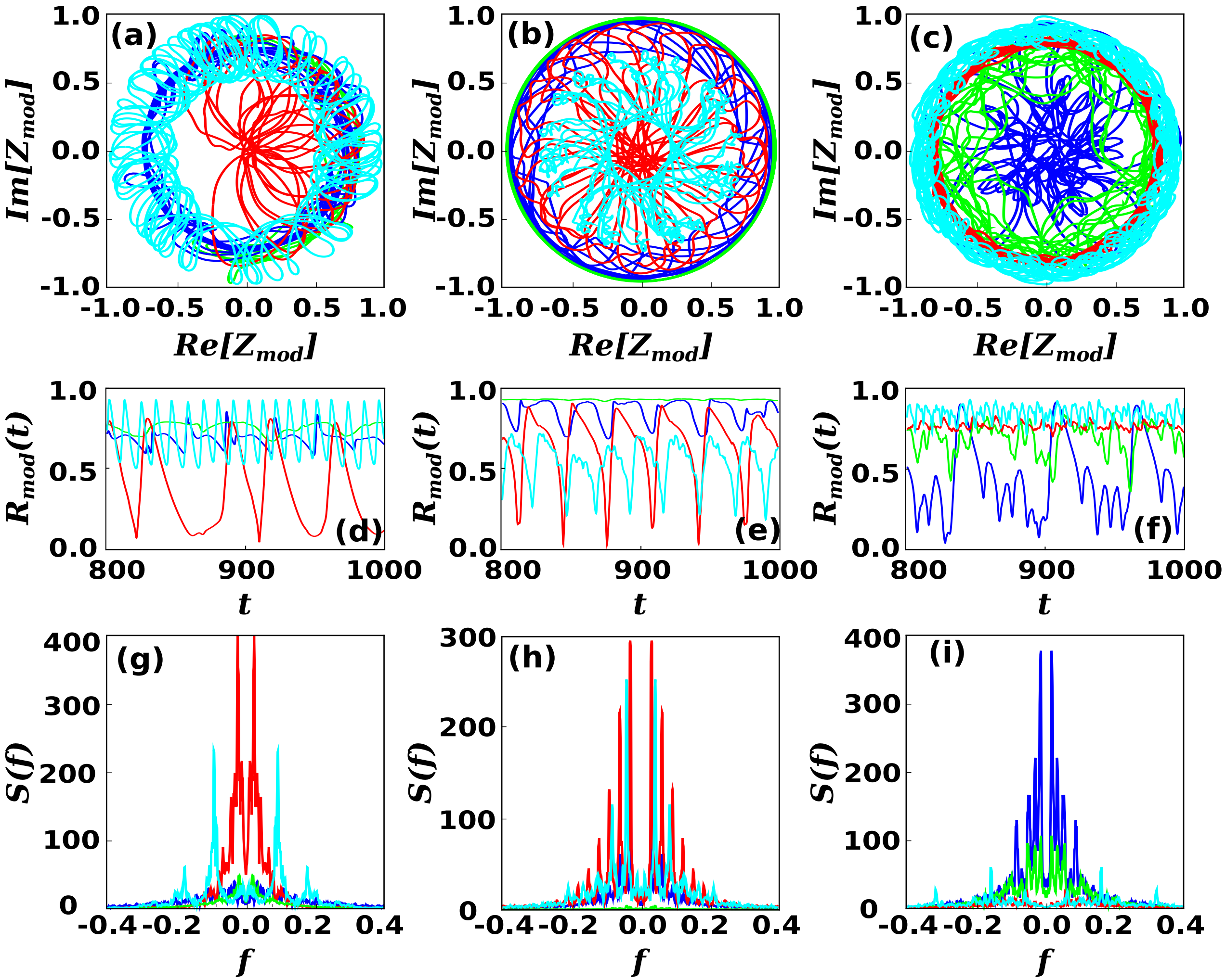

Correlations among communities

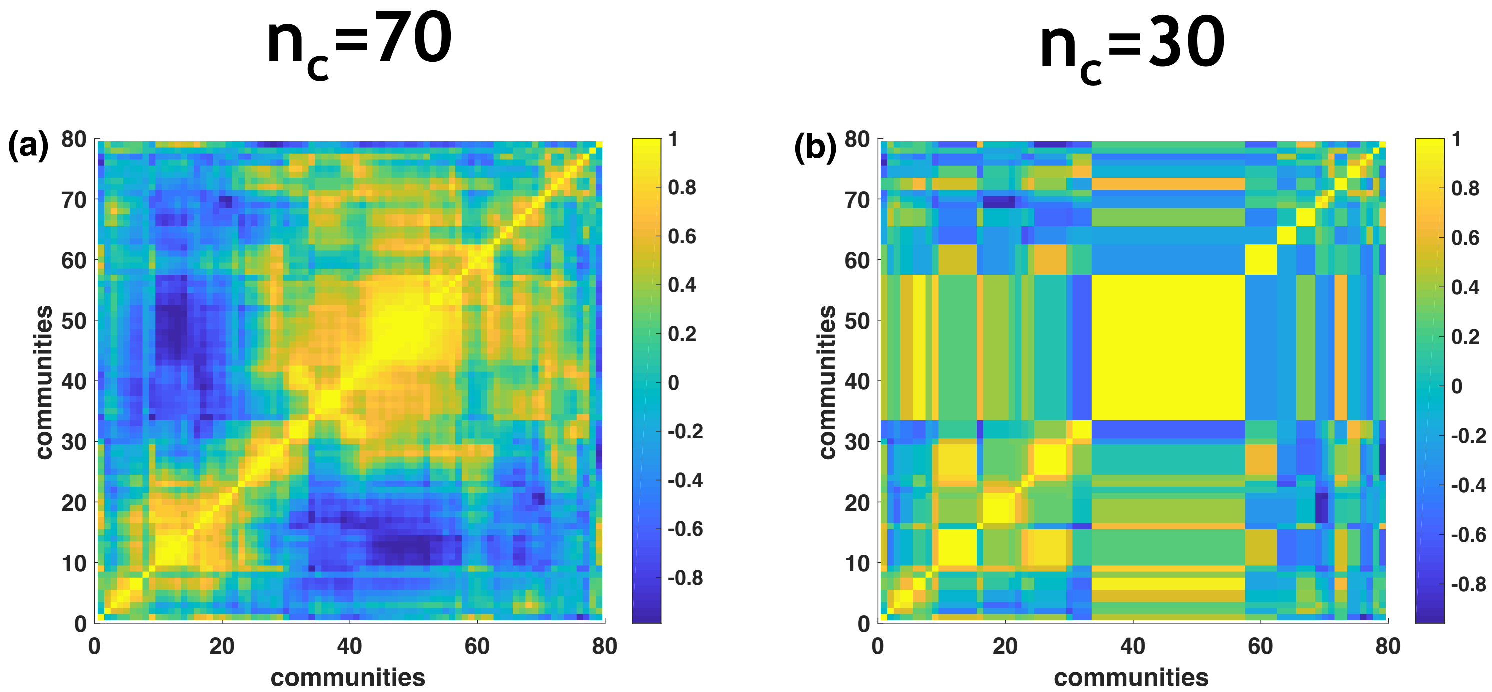

N=1000, D=2, σ=5

Millan et al. Sci. Rep. (2018); Millan et al. PRE (2019)

Percolation on Hyperbolic networks simplicial and cell complexes

Robustness of a network

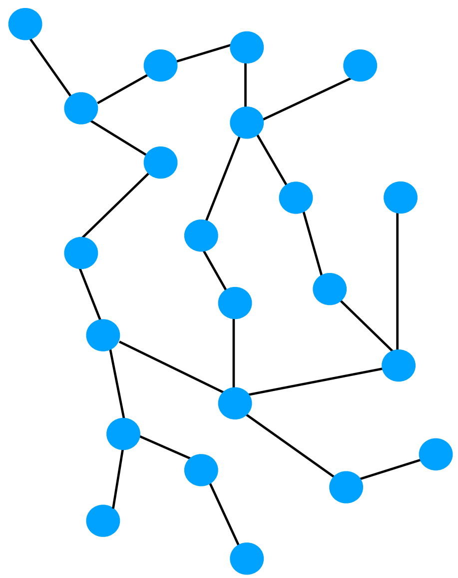

We assume that a fraction 1-p of links is damaged.
We evaluate the robustness of the network by calculating the fraction R of nodes in the giant component after this inflicted damage.

Robustness of a network

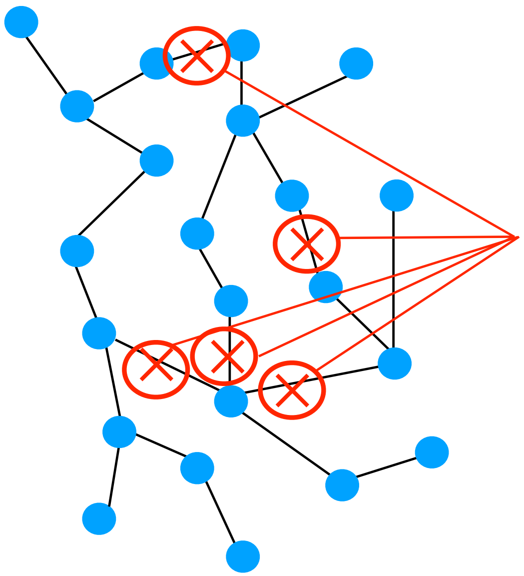

We assume that a fraction 1-p of links is damaged.
We evaluate the robustness of the network by calculating the fraction R of nodes in the giant component after this inflicted damage.

Robustness of a network

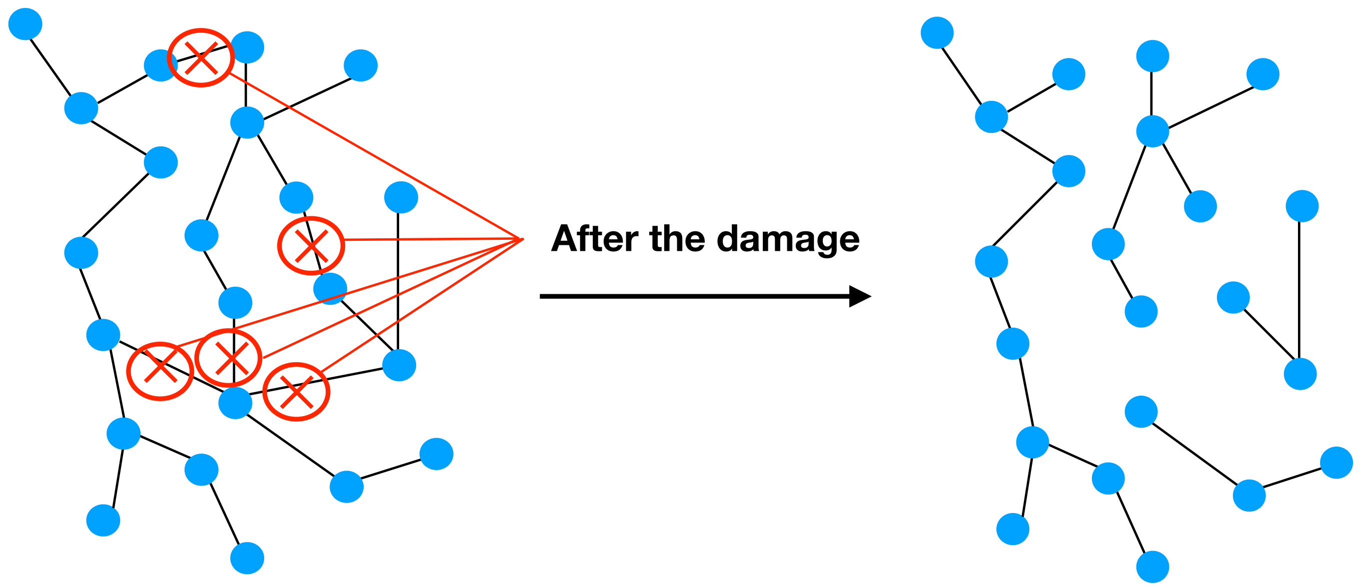

We assume that a fraction 1-p of links is damaged.
We evaluate the robustness of the network by calculating the fraction R of nodes in the giant component after this inflicted damage.

Percolation transition

As links are damaged with probability f=1-p

the fraction R of nodes in the giant component

of an infinite network has a transition from a non-zero to a zero value

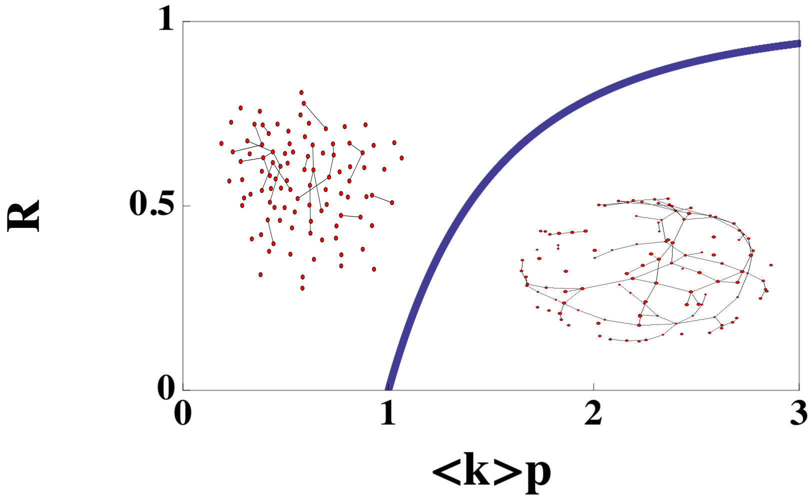

Percolation on a random uncorrelated network

Consider a random uncorrelated network with degree distribution $P(k)$

Percolation displays a single percolation threshold p_c at $p_c = \dfrac{\langle k \rangle}{\langle k(k-1) \rangle}$

For $|p - p_c| \ll 1$

$$R \simeq \begin{cases} a(p-p_c)^{\beta} & \text{for } p > p_c \\ 0 & \text{for } p \leq p_c \end{cases}$$

For $p > p_c$ the giant component is extensive

(contains a finite fraction of nodes)

The transition is continuous

Percolation on a random uncorrelated network

Let us define the generating functions

$$G_0(x) = \sum_k P(k)x^k, \quad G_1(x) = \sum_k \frac{k}{\langle k \rangle} P(k)x^{k-1}$$

The fraction of nodes R in the giant component when links are removed with probability $q = 1 - p$ obeys

$$R = 1 - G_0(1 - pS)$$

with

$$S = 1 - G_1\left(1 - pS\right)$$

Hybrid transitions

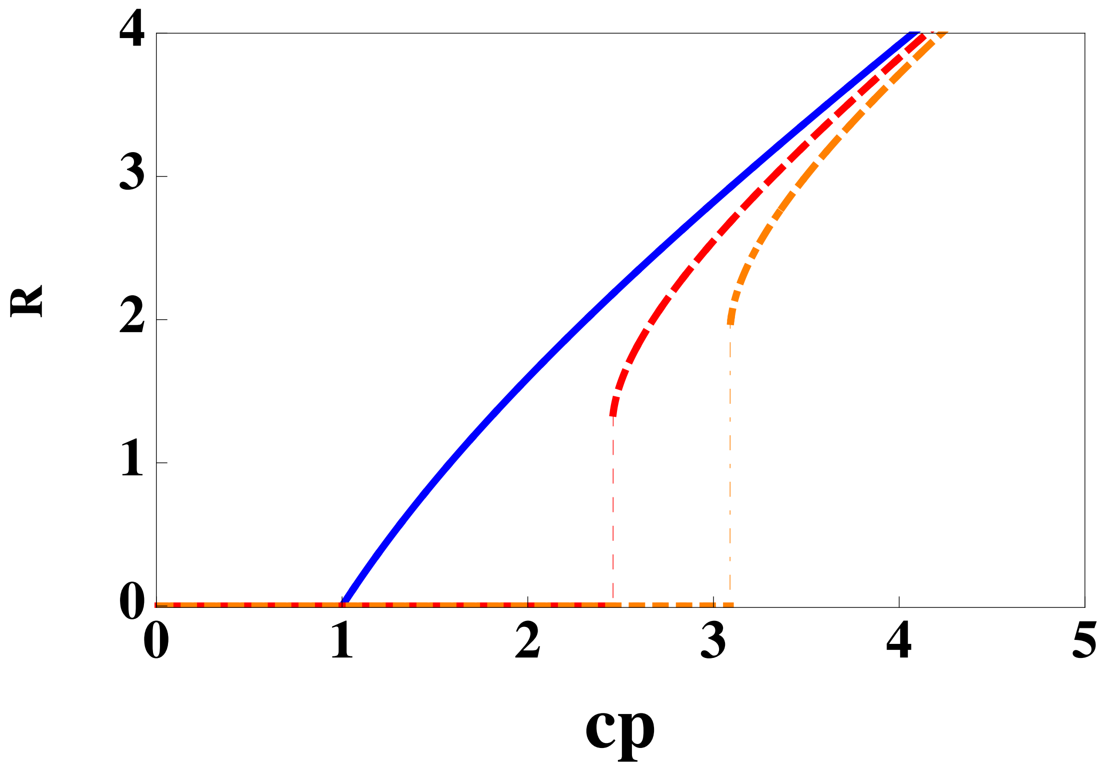

- Generalised percolation problems which involve a cooperative behaviour such a k-core percolation, or interdependent percolation often lead to discontinuous hybrid transition

- Dorogovstev, Goltsev, Mendes, Rev. Mod. Phys. 2008

Critical behavior of hybrid transitions

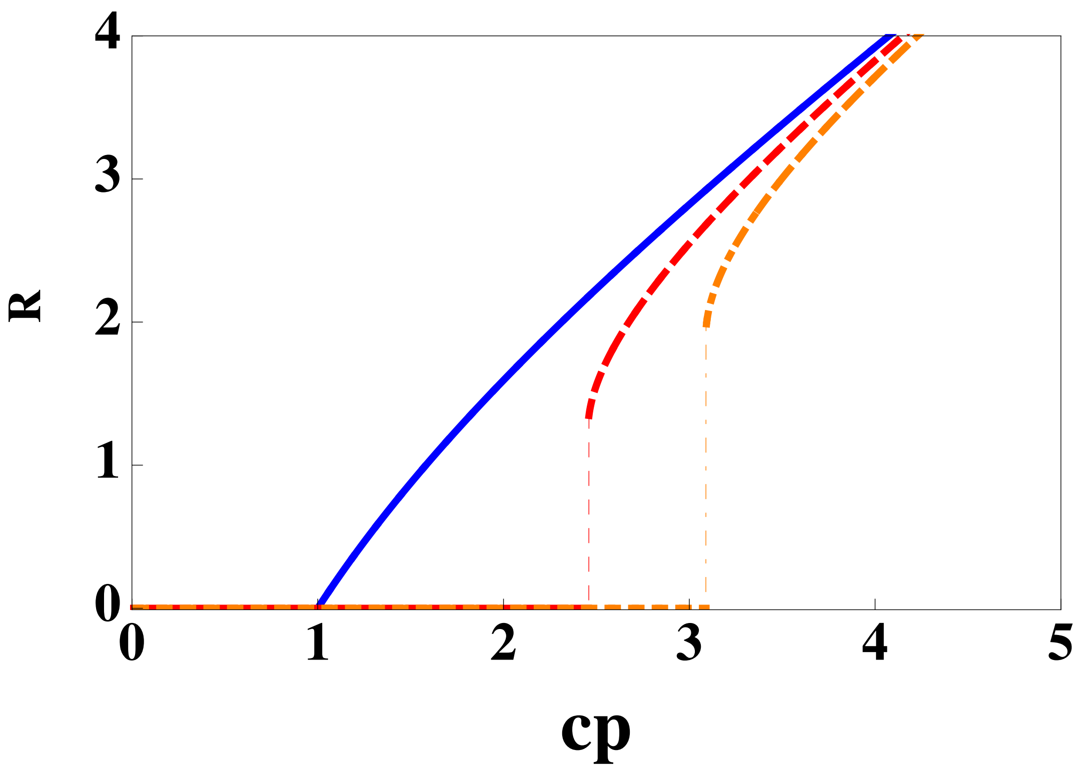

The critical behavior of hybrid transitions is characterized by a discontinuity and a singularity

$$R \simeq \begin{cases} R_c + a(p - p_c)^{\beta} & \text{for } p > p_c \\ 0 & \text{for } p \leq p_c \end{cases}$$

Percolation on
Hyperbolic networks
simplicial and cell complexes

Percolation in hyperbolic networks

Percolation in hyperbolic networks is known to have two percolation thresholds p^l and p^u.

- For $p<p^l$ no infinite cluster exist
- For $p^l<p<p^u$ the maximum cluster is infinite but sub-extensive
- For $p>p^u$ the maximum cluster is extensive

Link Percolation in 2d hyperbolic manifolds

2d Hyperbolic Manifolds

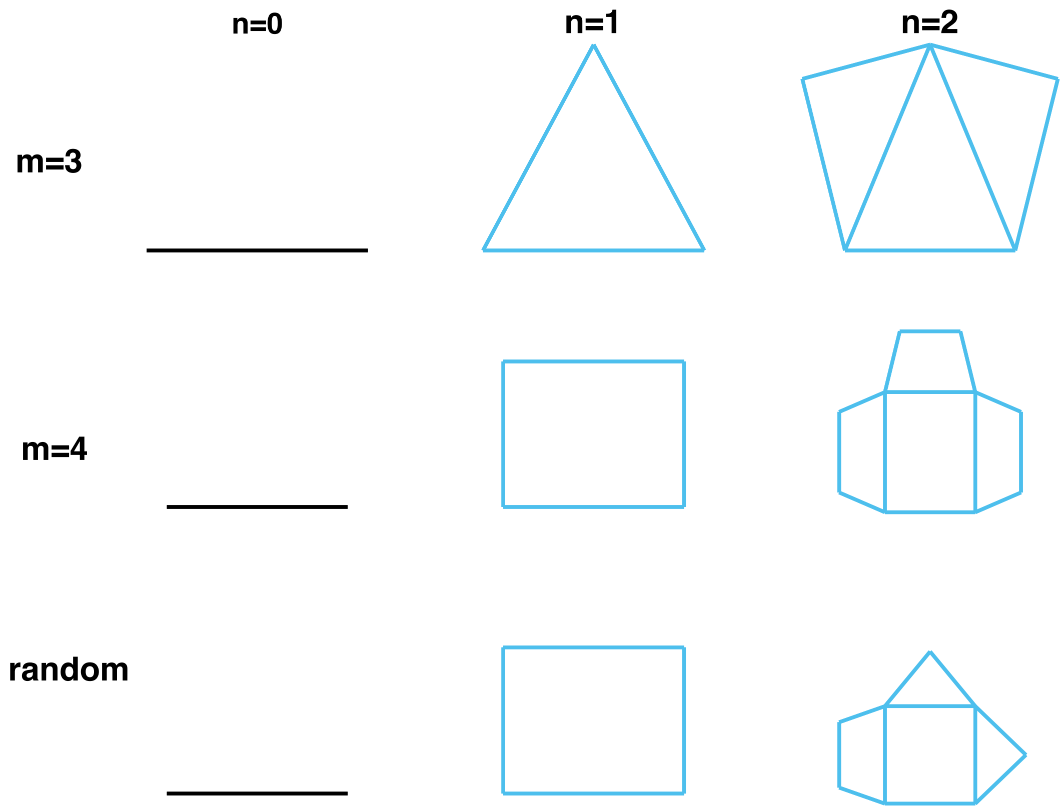

The dual is a tree

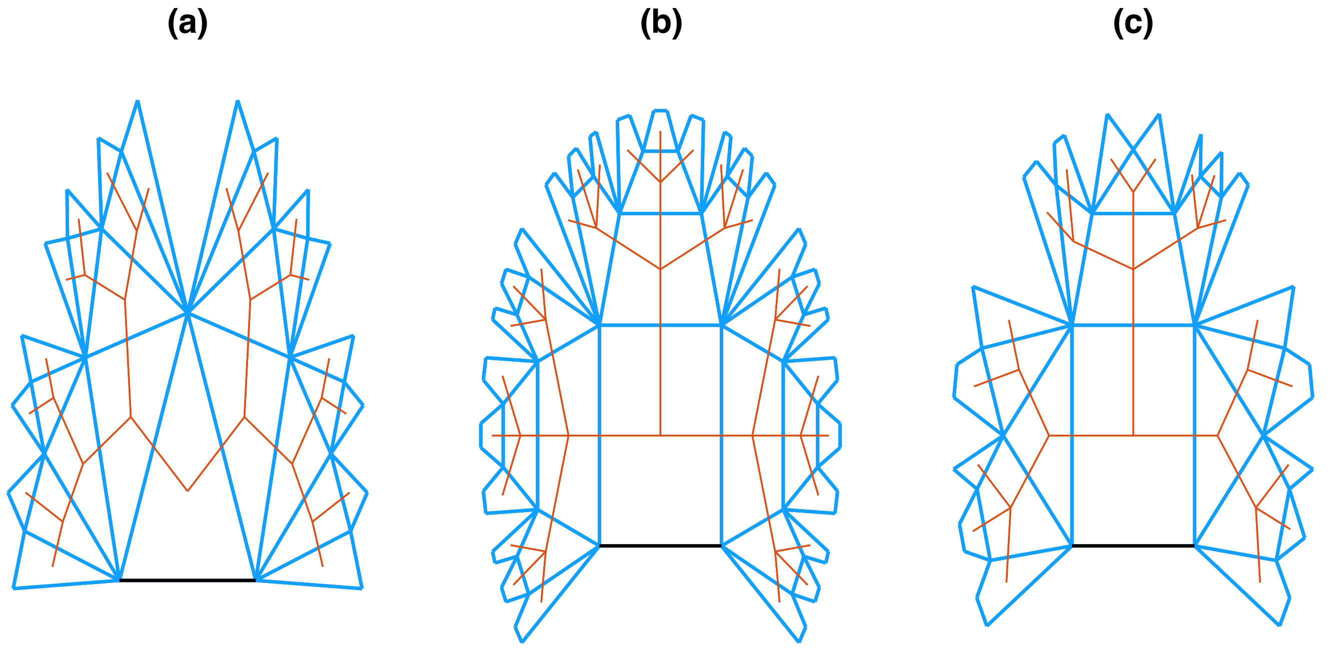

Link percolation in d=2 hyperbolic simplicial complex

The probability T_{n+1} that the two initial nodes are connected at iteration n+1 is given by the RG equation

[Boettcher,Singh, Ziff 2012]

$$T_{n+1} = p + (1-p)T_n^2$$

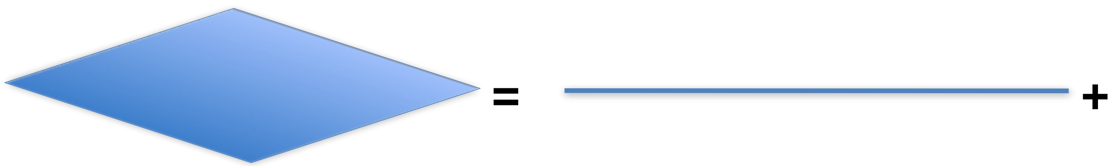

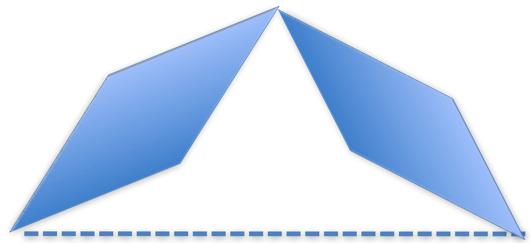

A RG study of the generating functions show that the upper percolation transition Is discontinuous at p=0.5 and non-trivial.

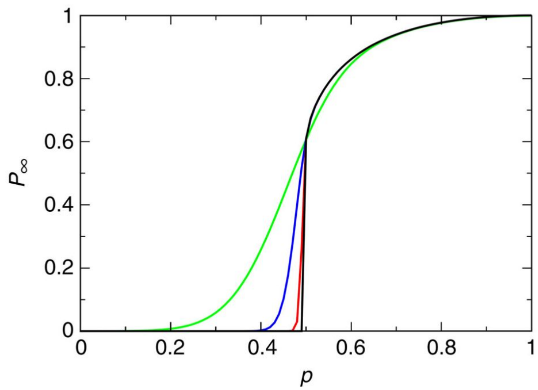

The linking probability

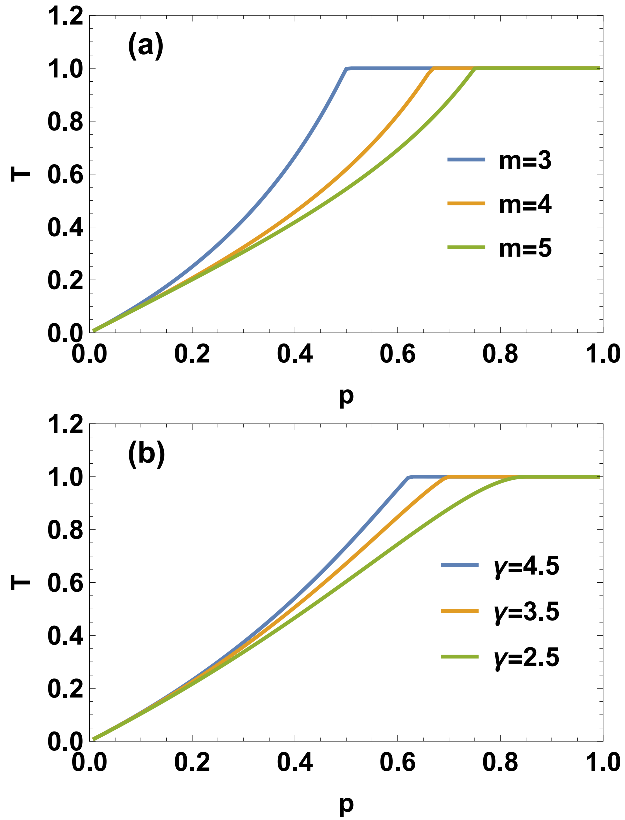

$$T = p + (1-p)\sum_{m=3}^{\infty} q_m T^{m-1}$$

$$p \to 1-p$$
$$T \to 1-S$$
$$q_m \to \frac{k}{\langle k \rangle} P(k)$$

$$S = p\left[1 - \sum_k \frac{k}{\langle k \rangle} P(k)(1-S)^{k-1}\right]$$

[Kryven, Ziff Bianconi 2018]

Upper Percolation Threshold

$$p_c = 1 - \frac{1}{m-1}$$

Fixed m discontinuous phase transition

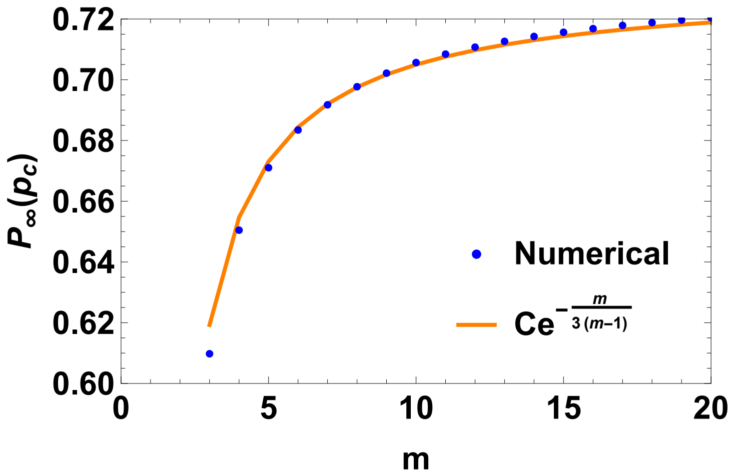

$$P_\infty(p) = \begin{cases} P_\infty(p_c)e^{-h\Delta p \ln(\Delta p/r)} \text{ for } p \geq p_c \\ 0 \text{ for } p < p_c \end{cases}$$

$$P_\infty(p_c) \simeq e^{-\frac{m}{3(m-1)}}$$

[Kryven, Ziff Bianconi 2018]

Critical scaling m=3,4

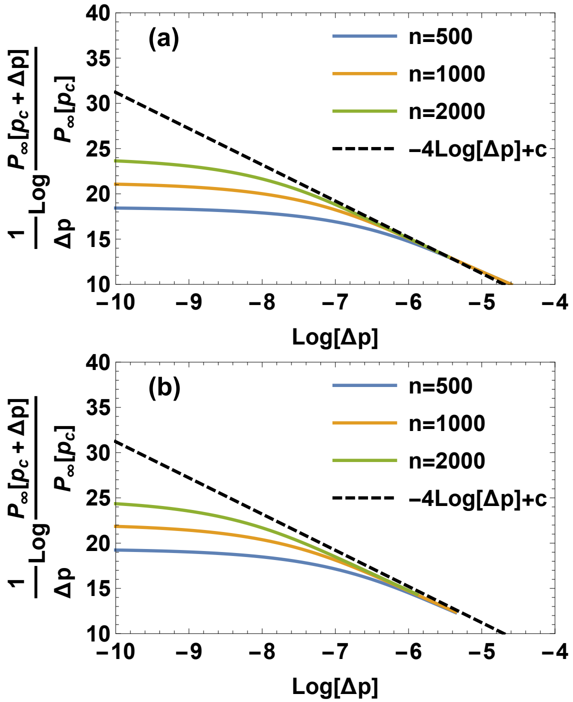

$$P_\infty(p) = \begin{cases} P_\infty(p_c)e^{-h\Delta p \ln(\Delta p/r)} \text{ for } p \geq p_c \\ 0 \text{ for } p < p_c \end{cases}$$

$\frac{dP_\infty}{dp}$ diverges logarithmically with

Δp at $p \to p_c^+$

[Kryven, Ziff Bianconi]

Power-law $q_m = Cm^{-\gamma}$ $m \geq 3$

Upper Percolation Threshold $p_c = 1 - \frac{1}{\langle m - 1 \rangle}$

Range γ	$P_{inf}(p)$ for $p \geq p_c$	
$\gamma > 4$	$P_\infty(p_c) + \alpha_\gamma \Delta p \ln \Delta p$	Discontinuous
$\gamma = 4$	$P_\infty(p_c) + \alpha_\gamma \Delta p [\ln \Delta p]^2$	Discontinuous
$\gamma \in (3,4)$	$P_\infty(p_c) + \alpha_\gamma [\Delta p]^{\gamma-2}$	Discontinuous
$\gamma = 3$	$\alpha_\gamma e^{-C/[\Delta p]}$	Continuous
$\gamma \in (2,3)$	$\alpha_\gamma [\Delta p]^\beta$	Continuous

[Kryven, Ziff Bianconi]

Topological damage

On networks
damage can occur only
on nodes or on links.
On simplicial complexes
topological damage can be directed also
to higher dimensional simplicies,
such as
triangles, tetrahedra etc.

Topological percolation

On d=2 simplicial complexes we distinguish
4 types of topological percolation problems:

Link percolation: Links are removed with probability q=1-p.
Nodes are connected to nodes through intact links

Triangle percolation: Triangles are removed with probability q=1-p.
Links are connected to links through intact triangles.

Node percolation: Nodess are removed with probability q=1-p.
Links are connected to links through intact nodes

Upper link percolation: Links are removed with probability q=1-p.
Triangles are connected to triangles though intact links

On d=3 simplicial complexes we distinguish
6 types of topological percolation problems:

Link percolation, Triangle percolation, tetrahedron percolation

Node percolation, upper link percolation, Upper triangle percolation

[Bianconi and Ziff 2018]

Hyperbolic Simplicial complexes

d=2 HYPERBOLIC SIMPLICIAL COMPLEX

We start from a link.
At each iteration we glue a triangle
to any link added at the previous iteration

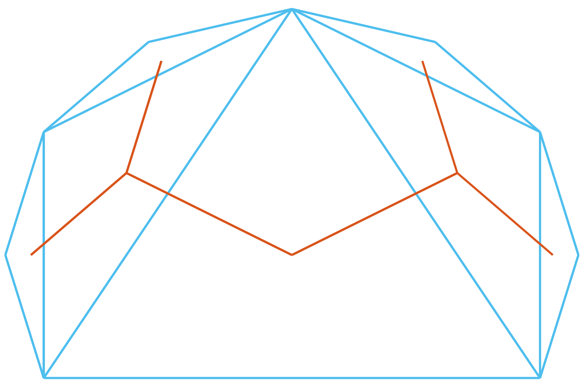

d=3 HYPERBOLIC SIMPLICIAL COMPLEX

We start from a triangle.
At each iteration we glue a tetrahedron
to any triangle added at the previous
iteration

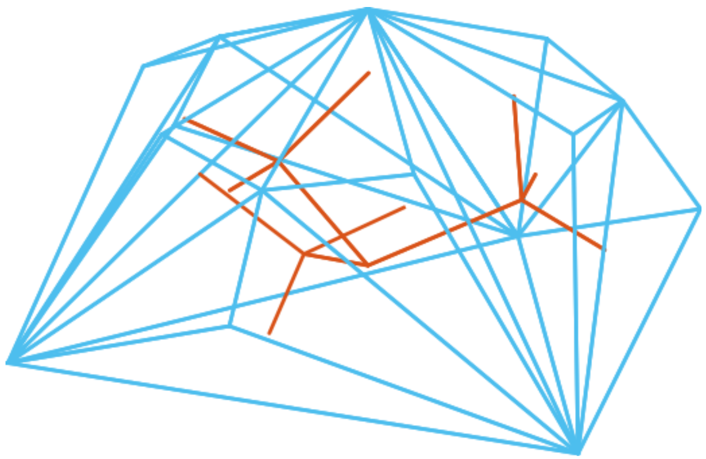

The d=3 Hyperbolic Simplical Complex

At the level of the network skeleton
the d=3 Hyperbolic Simplicial Complex
reduces to the Apollonian network

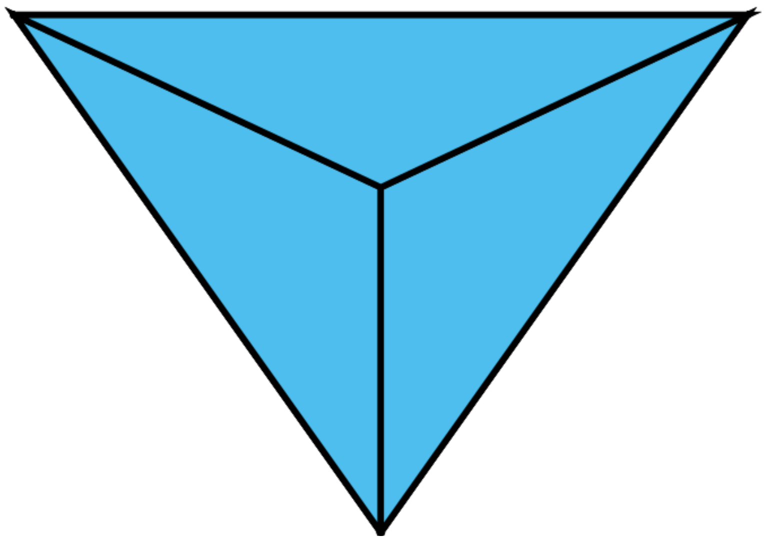

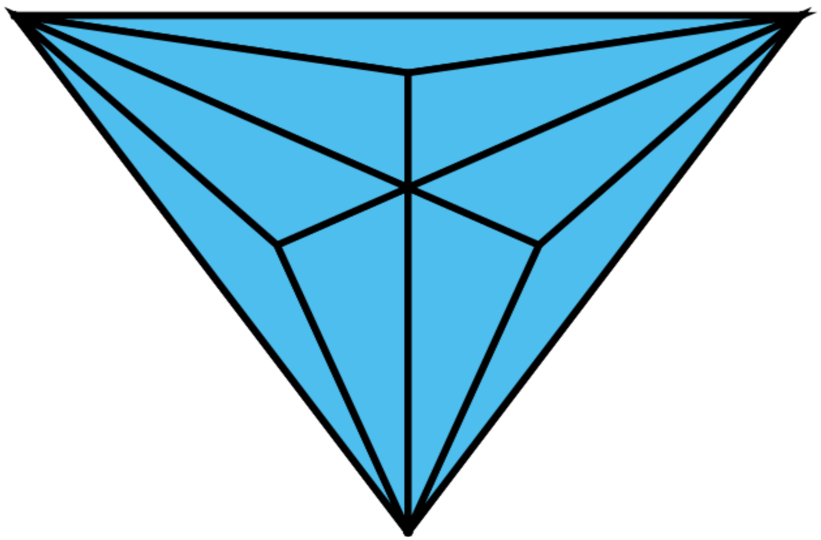

The line graph of the Apollonian network is the Sierpinski gasket

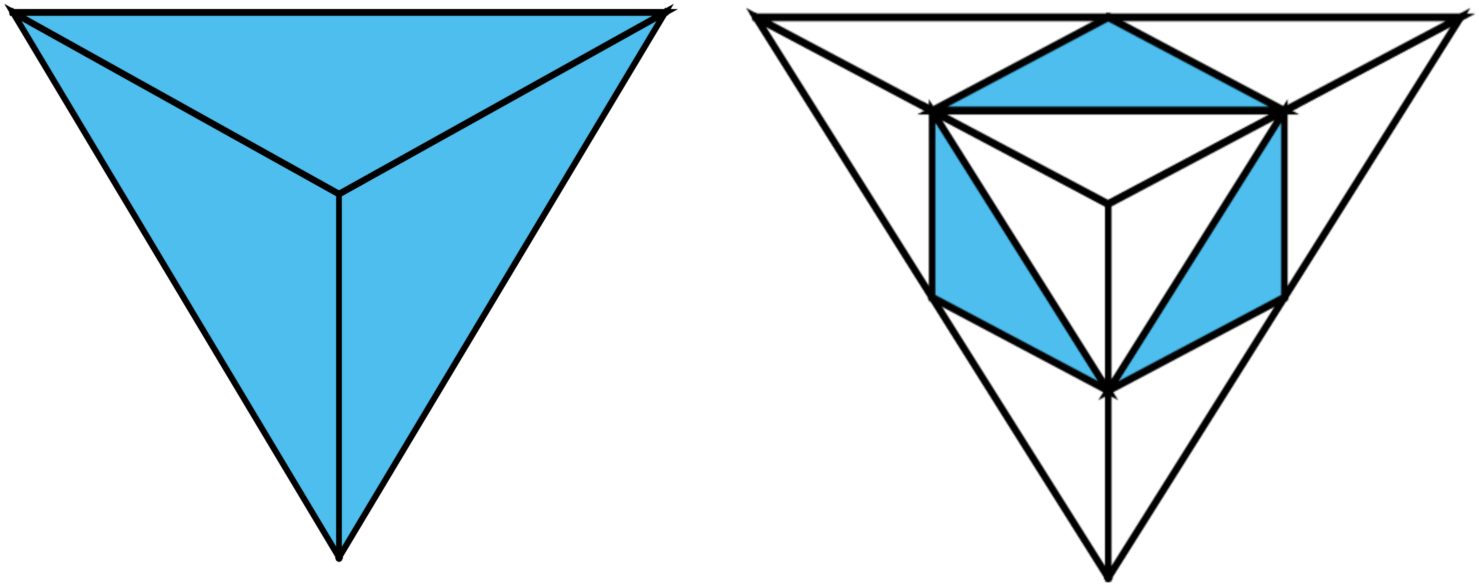

[Bianconi and Ziff 2018]

The line graph of the d=3 Hyperbolic Simplicial Complex
is the multiplex Sierpinski gasket

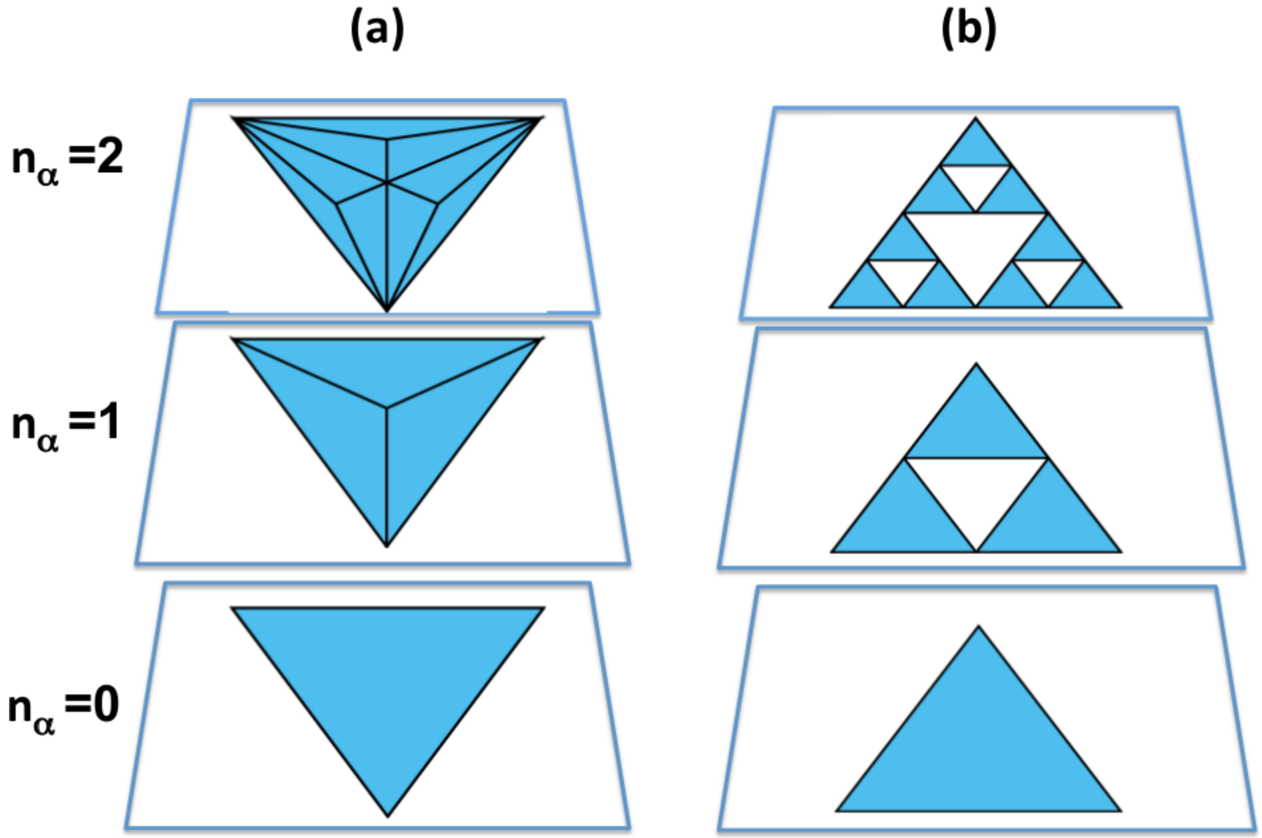

Triangle percolation for the d=3 hyperbolic simplicial complex

The order parameter is the fraction of links
connected to the initial three links through intact triangles

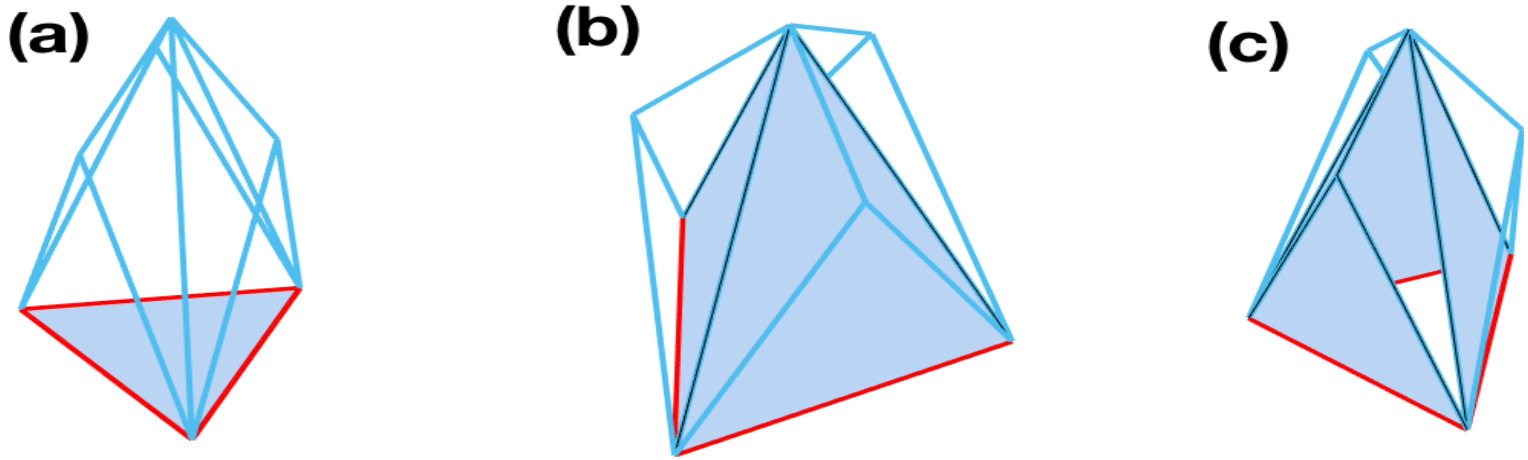

The RG equations

The probability T_{n+1}, S_{n+1}, W_{n+1} that three, two or none of the initial links are connected at iteration n+1 is given by the RG equation

$$
\begin{aligned}
T_{n+1} &= p + (1-p)(T_n^3 + 6T_n^2 S_n + 3T_n S_n^2) \\
S_{n+1} &= (1-p)[T_n^2(S_n + W_n) + T_n S_n(7S_n + 2W_n) + S_n^2(4S_n + W_n)] \\
W_{n+1} &= 1 - T_{n+1} - 3S_{n+1}
\end{aligned}
$$

The RG equations can be written down diagramatically using the multiplex Sierpinski gasket

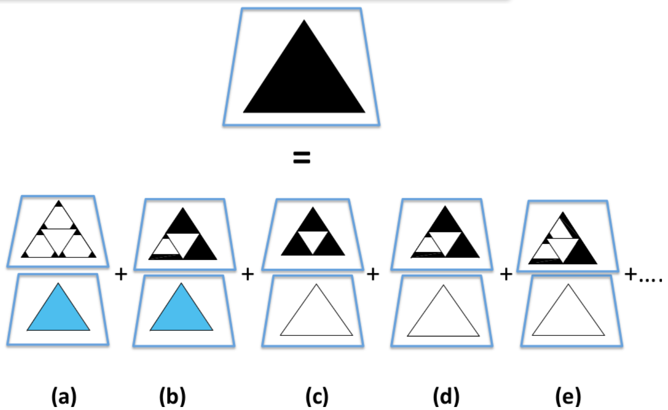

[Bianconi and Ziff 2018]

Berezinskii-Kosterlitz-Thouless transition

Triangle percolation on the d=3 hyperbolic simplicial complex
undergoes a BKT transition
with the order parameter scaling like

$$M_n \propto e^{-A/|p-p_c|^{1/2}}$$

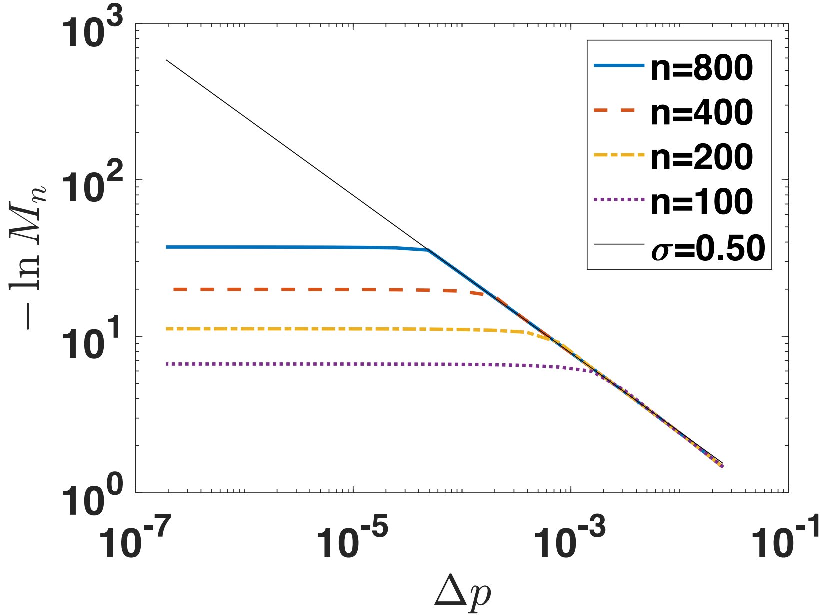

[Bianconi and Ziff 2018]

Topological percolation for d=2 hyperbolic simplicial complex

	p^l	p^u	
$d = 2$			
Link percolation	0	$\frac{1}{2}$	**Discontinuous non-trivial**
Triangle percolation	$\frac{1}{2}$	1	**Discontinuous trivial**
Node percolation	0	1	**Discontinuous trivial**
Upper-link percolation	$\frac{1}{2}$	1	**Discontinuous trivial**

All transitions are discontinuous. Only link percolation is non-trivial

[Bianconi and Ziff 2018]

Topological percolation for d=3 hyperbolic simplicial complex

	p^l	p^u	
$d = 3$			
Link percolation	N/A	0	Continuous SF
Triangle percolation	0	$0.307981\ldots$	Continuous BKT
Tetrahedron percolation	$\frac{1}{3}$	1	Discontinuous trivial
Node percolation	0	1	Discontinuous trivial
Upper-link percolation	0	1	Discontinuous trivial
Upper-triangle percolation	$\frac{1}{3}$	1	Discontinuous trivial

[Bianconi and Ziff 2018]

Comments

Nodes and link percolation
cannot be used to predict
the other topological percolation problems

- *In d=2 Hyperbolic simplicial complex all transitions are discontinuous while in d=3 link and triangle percolation are continuous*
- *Link percolation in d=2 displays a non trivial discontinuous transition while no such transition is observed in d=3*
- *Triangle percolation in d=3 is a BKT transition while no such transition is observed in d=2*

Higher-order structure and dynamics

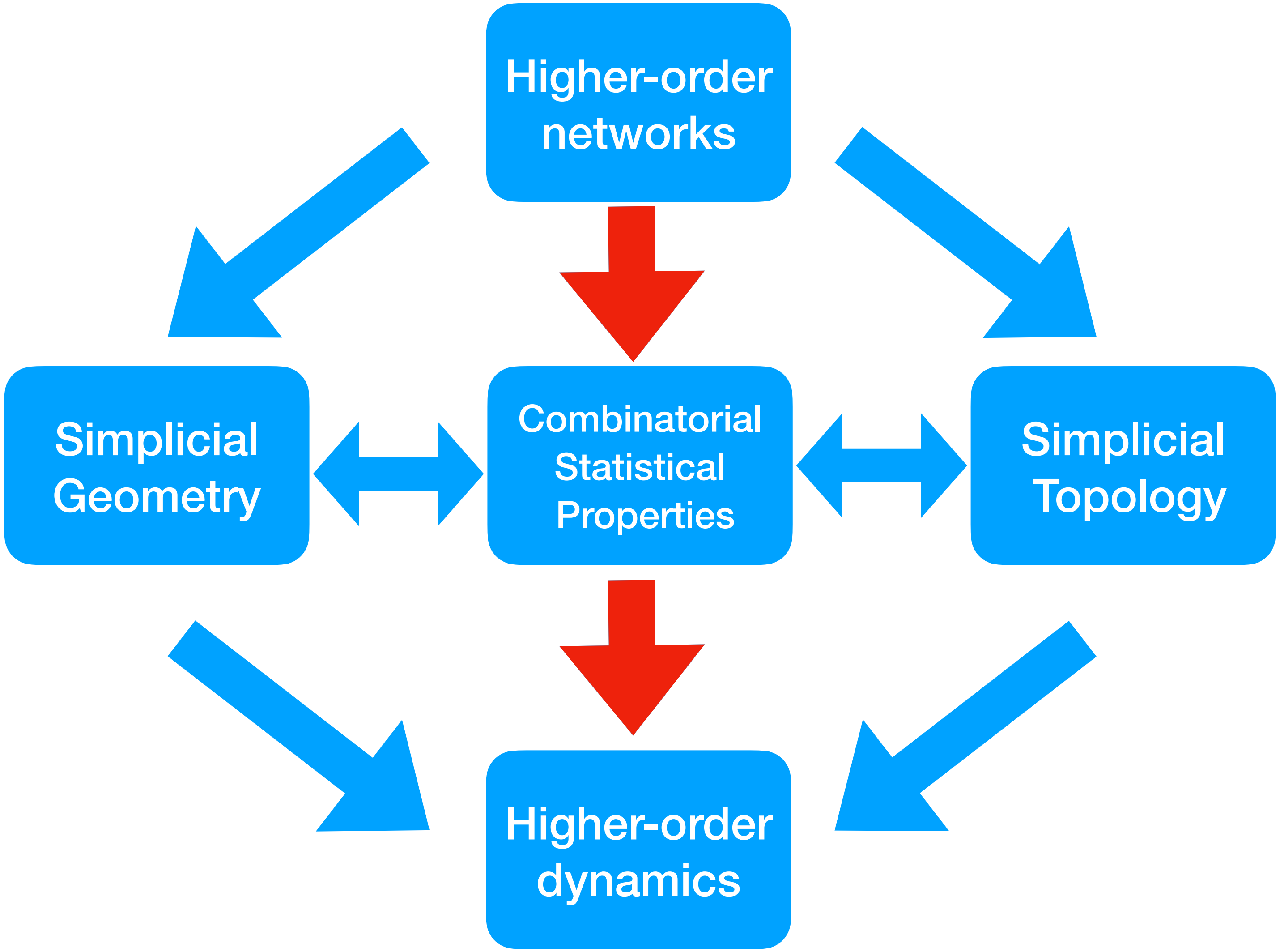

Triadic interactions

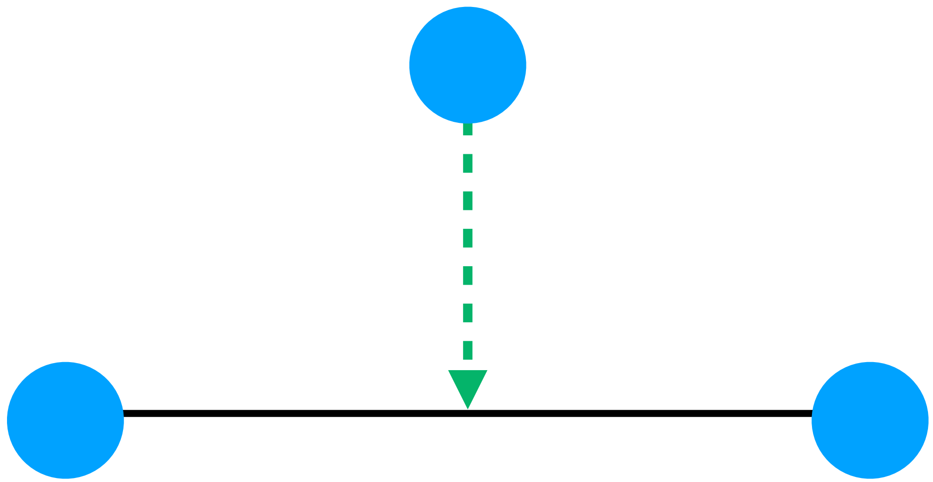

A triadic interaction occurs when a node affects the interaction between other two nodes

Sign of triadic interactions

A triadic interactions can be positive or negative

The presence of a third species can enhance or can inhibit the interaction between two species

The presence of a glia can change the synaptic interactions between two neurons

Robustness of a network

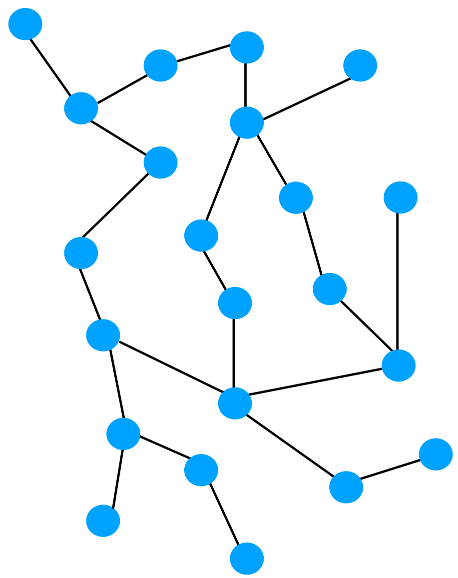

We assume that a fraction 1-p of links is damaged.
We evaluate the robustness of the network by calculating the fraction R of nodes in the giant component after this inflicted damage.

Robustness of a network

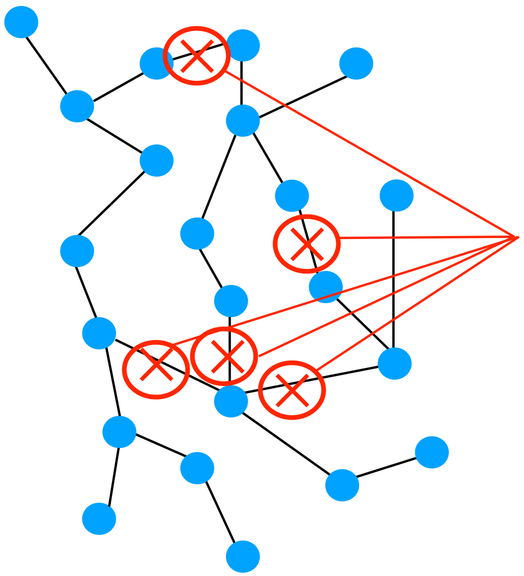

We assume that a fraction 1-p of links is damaged.
We evaluate the robustness of the network by calculating the fraction R of nodes in the giant component after this inflicted damage.

Robustness of a network

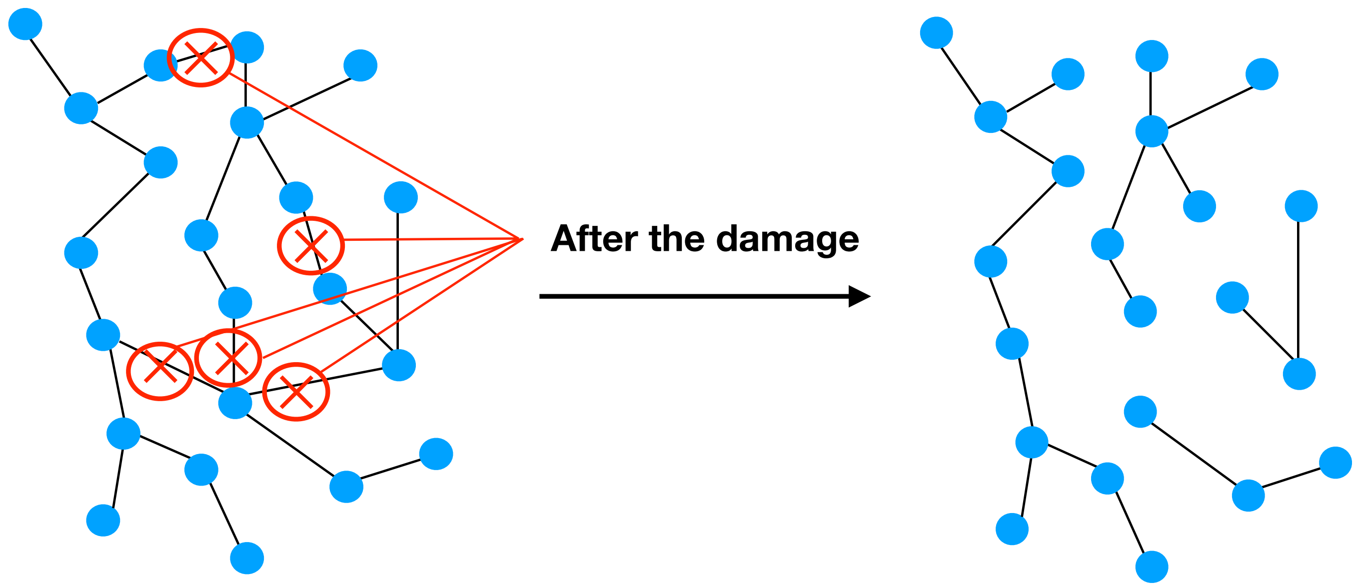

We assume that a fraction 1-p of links is damaged.
We evaluate the robustness of the network by calculating the fraction R of nodes in the giant component after this inflicted damage.

Percolation transition

As links are damaged with probability f=1-p

the fraction R of nodes in the giant component

of an infinite network has a transition from a non-zero to a zero value

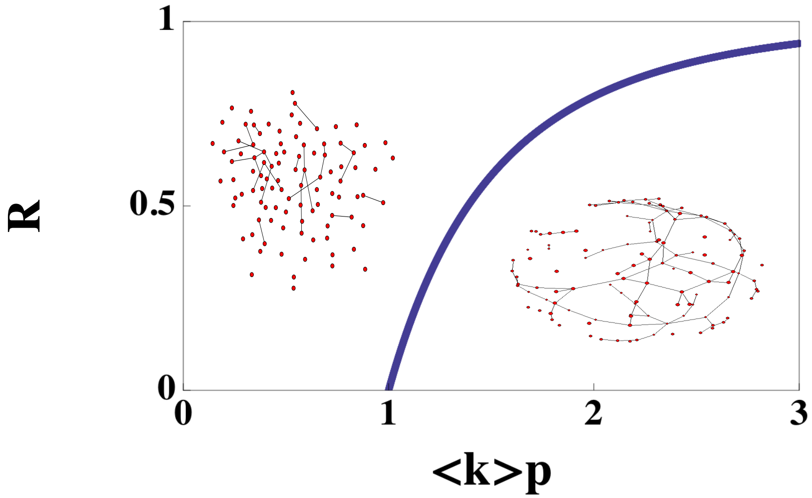

$$S = 1 - G_1\left(1 - pS\right)$$

$$R = 1 - G_0(1 - pS)$$

Higher-order network with triadic interactions

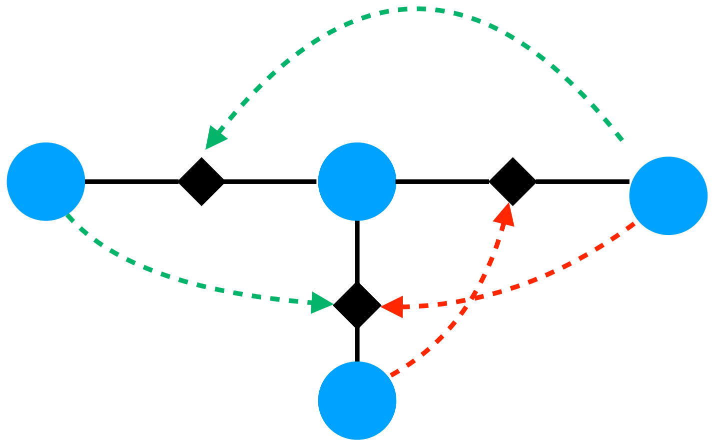

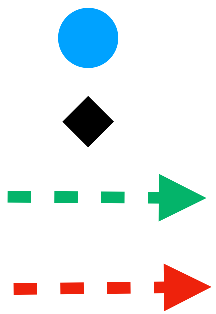

Node

Structural link

Positive regulation

Negative regulation

H. Sun, F. Radicchi, J. Kurths, and G. Bianconi (2020)

Activity of nodes and structural links

Regulatory interactions determine which links are active.

Structural links are active if they are connected to a least a active positive regulator node and they are not connected to any active negative regulator node

Structural interactions determine which nodes are active.

A node is active if it belongs to the giant component of the structural network

Dynamic nature of percolation

- Agorithm:

- Step 1: Evaluate the nodes in the giant component of the structural network. Nodes are active if and only if they belong to the giant component of the network

- Step 2: Deactivate the links that are connected to at least one active negative regulator node or that are not connected to any active positive regulator node. All the other links are damaged with probability $q=1-p$.

- Repeat from Step 1

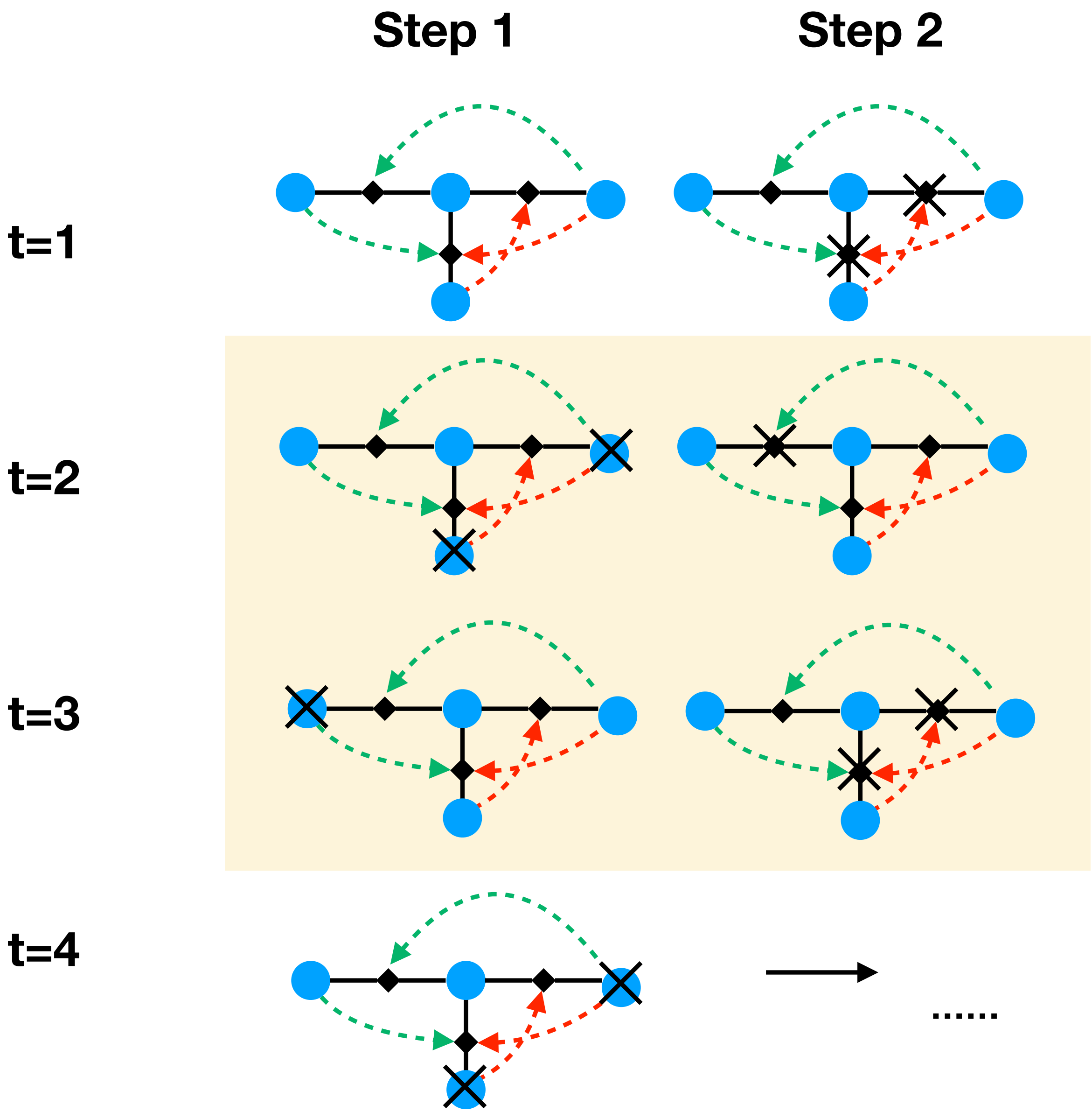
Step 1
Step 2
t=1
t=2
t=3
t=4
......

Theory

Step 1

$$S^{(t)} = 1 - G_1\left(1 - p_L^{(t-1)} S^{(t)}\right)$$

$$R^{(t)} = G_0(1 - p_L^{(t-1)} S^{(t)})$$

Step 2

$$p_L^{(t)} = pG_0\left(1 - R^{(t)}\right)\left[1 - G_0\left(1 - R^{(t)}\right)\right]$$

$$R^{(t)} = f(p^{(t-1)})$$

$$p_L^{(t)} = g(R^{(t)})$$

Blinking of the network

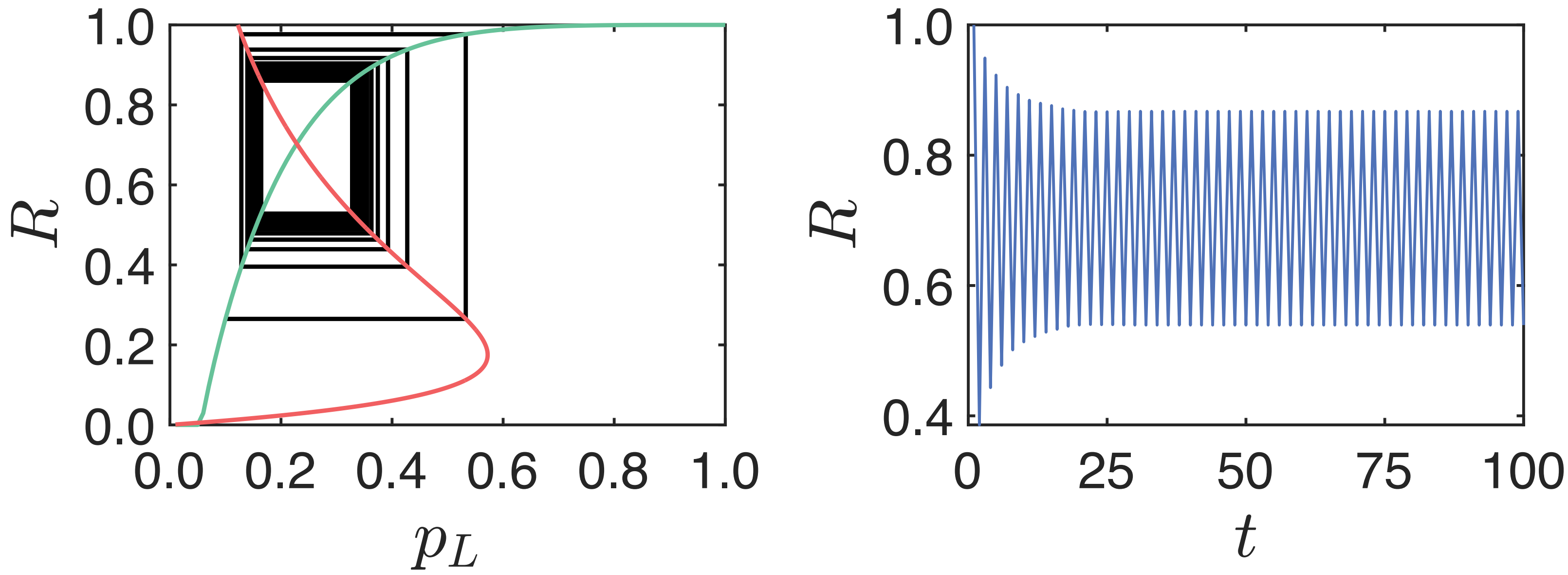

Blinking

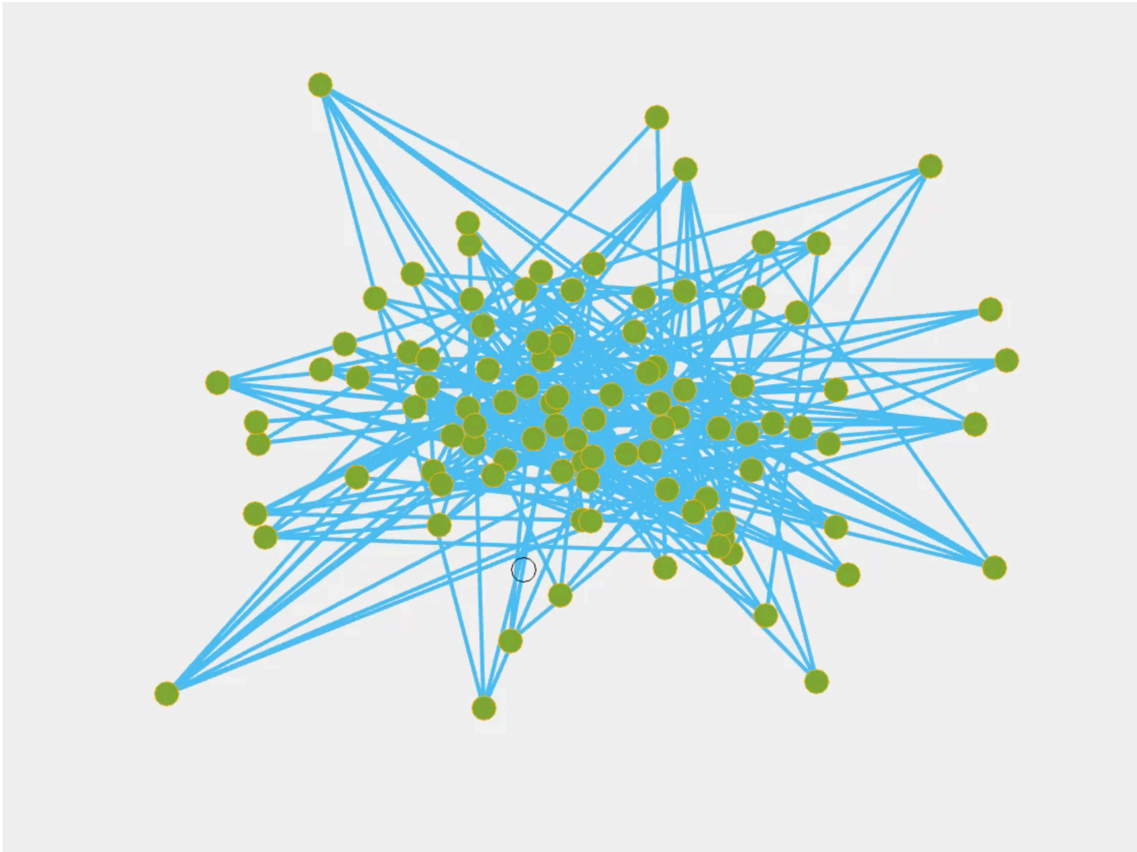

Chaotic pattern of the order parameter of percolation

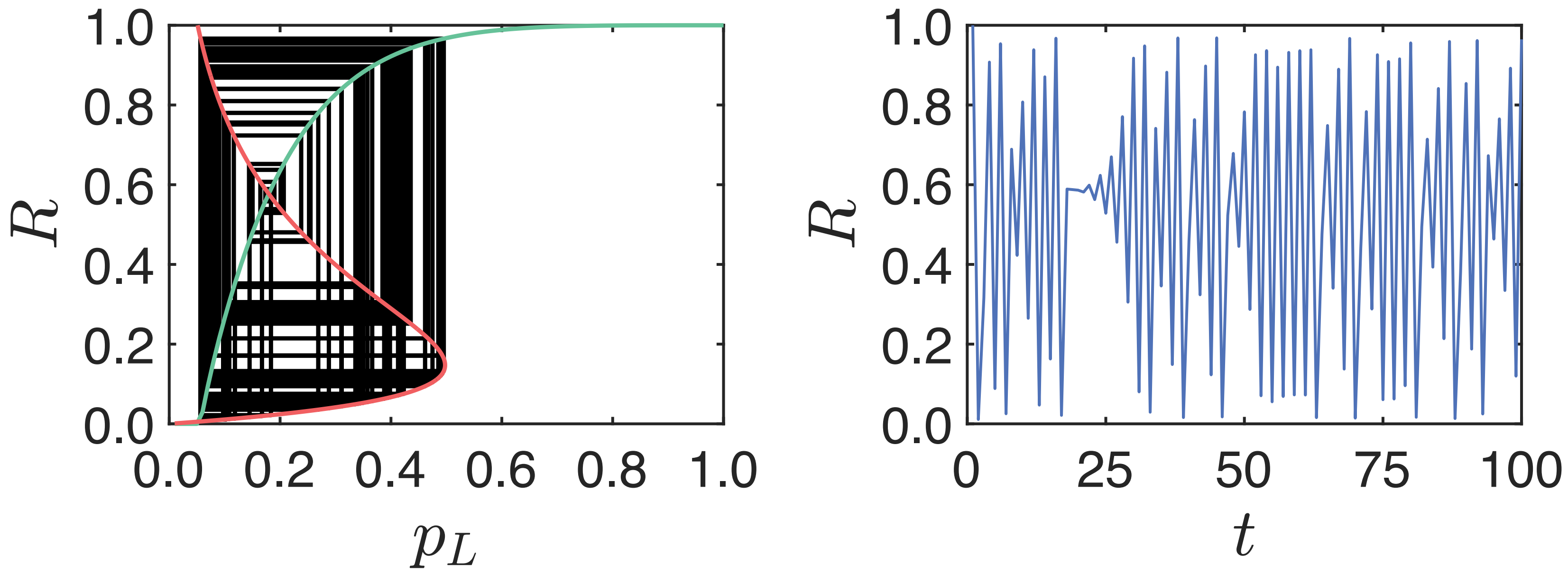

Chaos in connectivity of the network

Route to chaos in scale-free networks

Absence of triadic interactions

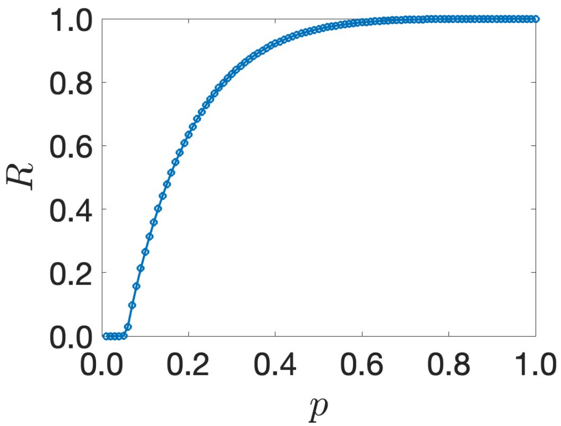

In presence of triadic interactions

Theoretical prediction

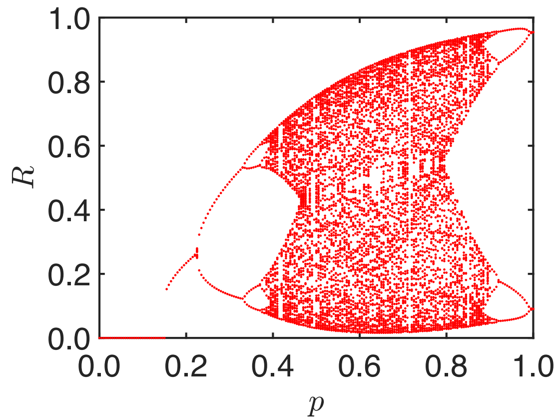

Monte Carlo simulations

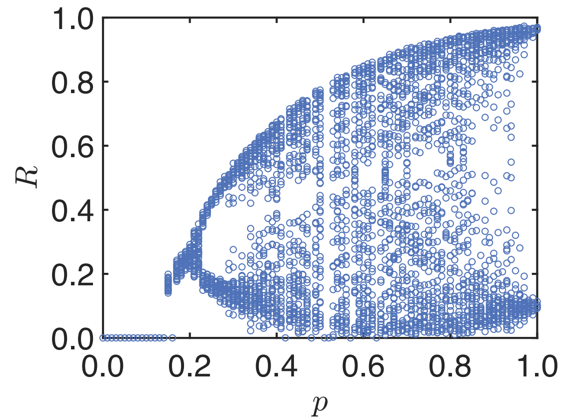

The map of triadic percolation

The map $R^{t+1} = h(R^t)$

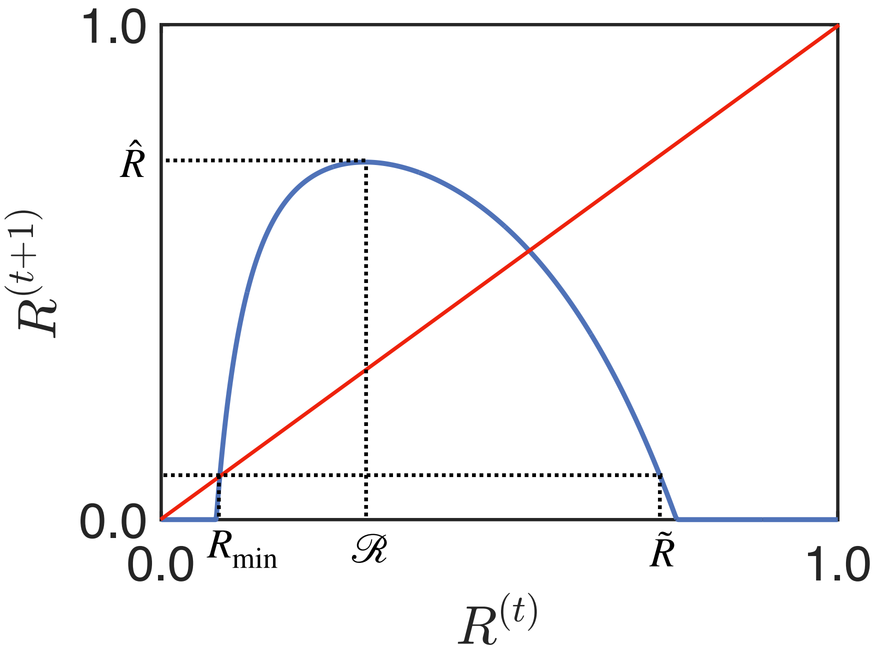

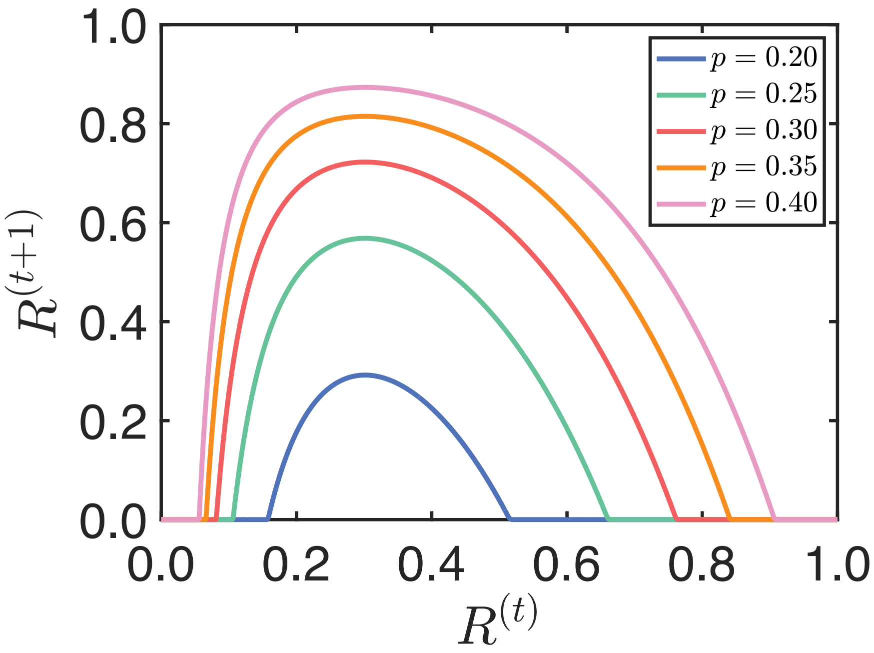

Route to chaos

The map $R^{t+1} = h(R^t)$
is in the universality class of the logistic map

Indeed close to the maximum

for $R \simeq R^\star$ the map displays the quadratic form

$$h(R) \simeq h(R^\star) - \frac{1}{2}h''(R^\star)(R - R^\star)^2$$

which according to

Feigenbaum classic renormalisation group result proves

that the universality class of the map is the same as the one of the logistic map

Blinking and chaos in mouse brain network

Mouse brain network+ random regulatory interactions

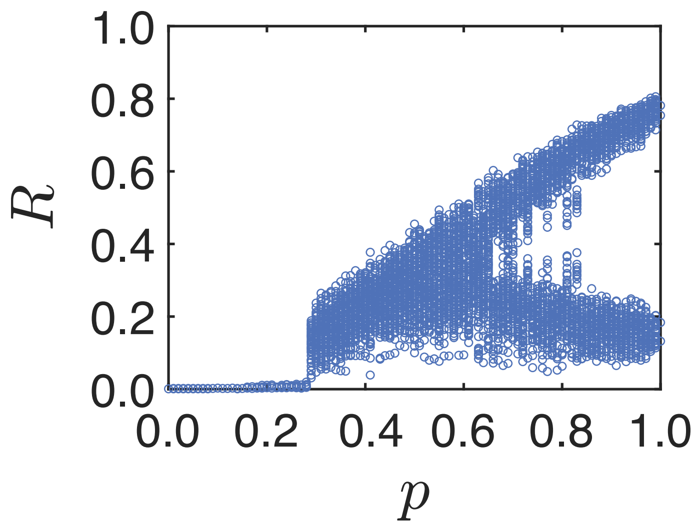

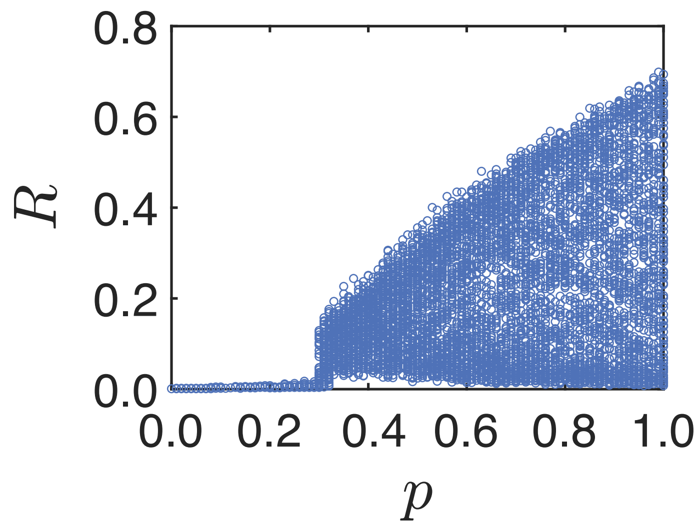

Only positive regulations

The dynamics always reaches a steady state

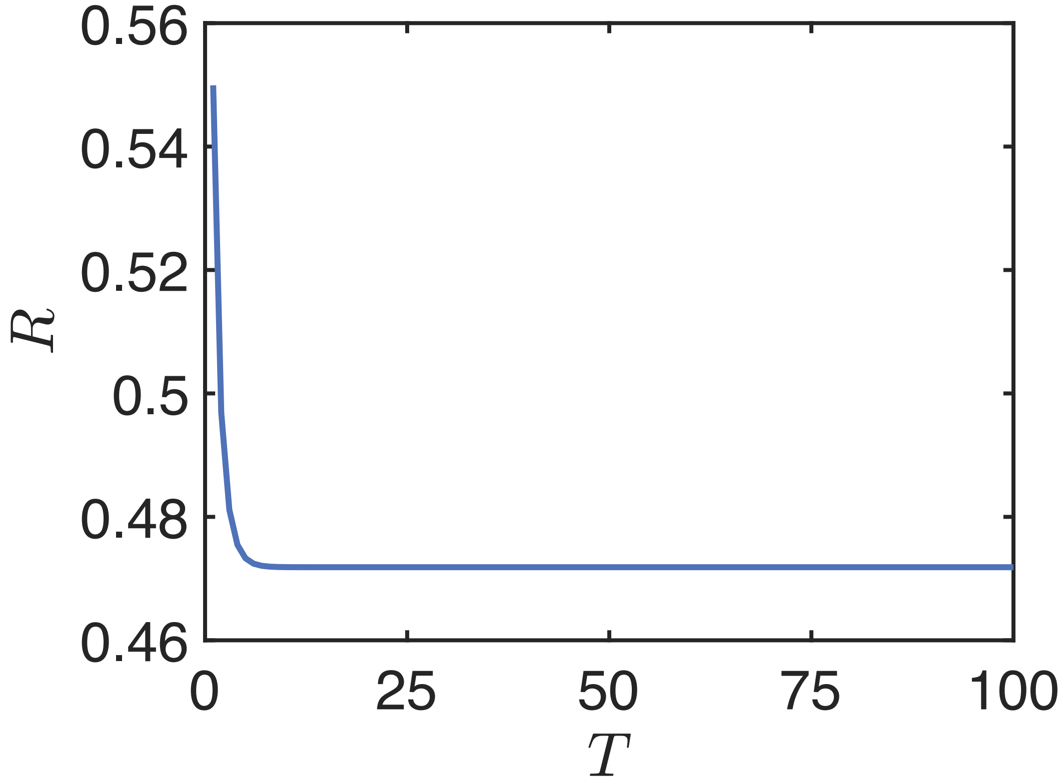

The percolation transition is discontinuous and hybrid

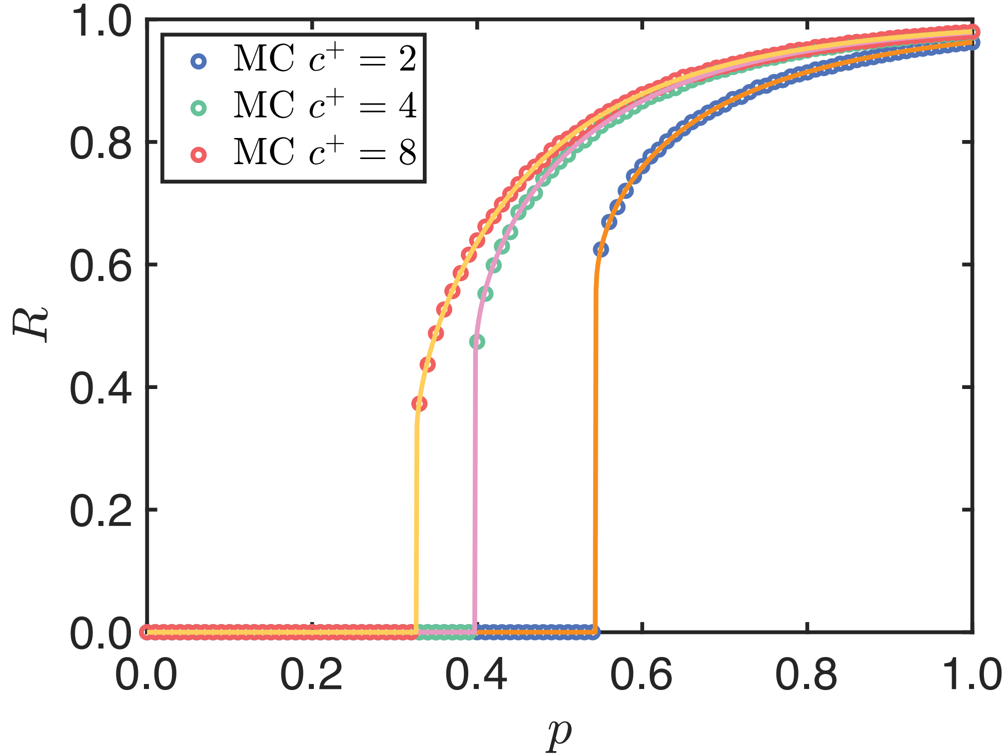

Triadic interactions in more complex settings

Hypergraphs

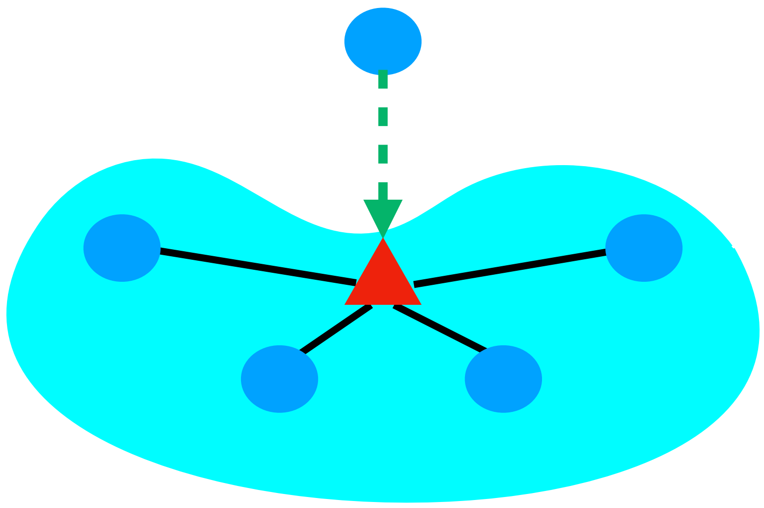

Multiplex nets

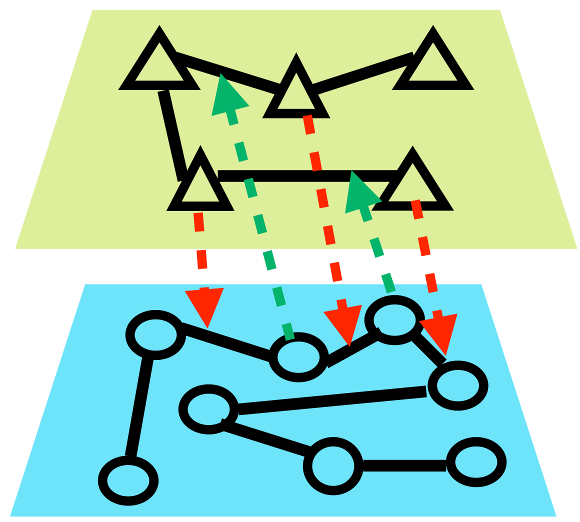

Conclusions

In presence of higher-order interactions the interplay between structure and dynamics is mediated by network topology, and network geometry in addition to network statistical properties

Network geometry can have an important effect on dynamics: for instance a finite spectral dimension can change the stability of the synchronised state of the Kuramoto model
And hyperbolic network geometry can change the critical property of percolation

Higher-order interaction include triadic interactions
Signed triadic interactions inspired by neurone-glia interactions can turn percolation
into a fully-fledged dynamical process.

CODE AVAILABLE AT GITHUB **ginestrab**

Higher-order structure and dynamics